

DIETARY EXPOSURES CONTRIBUTE TO DIFFERENT DISEASES THROUGH THE
MICROENVIRONMENT

Yuanyuan Qin

A dissertation submitted to the faculty at the University of North Carolina at Chapel Hill in partial fulfillment of the requirements for the degree of Doctor of Philosophy in the Department of Nutrition (Biochemistry) in the Gillings School of Global Public Health.

Chapel Hill
2015

Approved by:

Liza Makowski

Melissa Troester

Melinda Beck

Charles Perou

Steven Zeisel

© 2015
Yuanyuan Qin
ALL RIGHTS RESERVED

ABSTRACT

Yuanyuan Qin: Dietary exposures contribute to different diseases through the microenvironment
(Under the direction of Liza Makowski)

Genetic predispositions play an important role in our health, but these are not absolute; lifestyle choices help determine how long and how well we live. The global pandemic of obesity and related diseases is a good example. Lifestyle can contribute to diseases through altering the microenvironment of important tissues including adipose in obesity.

In this dissertation, the consequences of lifestyle components on local and systemic inflammation and hyperinsulinemia were investigated, both of which contribute to risk of diseases such as obesity, insulin resistance, and breast cancer. Using preclinical mouse models, we aimed to uncover mechanisms by which alcohol and obesogenic diet exposures alter the microenvironment in the pathogenesis of adipose and mammary gland dysfunction. We found that binge ethanol exposure followed by burn injury exacerbated the adipose inflammatory response induced by burn alone, with significant elevations in macrophage infiltration and secretion of pro-inflammatory mediators when compared to controls not exposed to binge alcohol intake. It is well established that adipose inflammation contributes to insulin resistance, especially associated with obesity. We discovered that fatty acid transporter 1 (FATP1) predominantly on alternatively activated macrophages contributes to decreased local and systemic inflammation. Macrophage FATP1 overexpression suppressed inflammatory response, while FATP1 knock out exaggerated inflammatory factor expression *in vitro*. Mice

transplanted with *Fatp1*^{-/-} bone marrow and fed an obesogenic diet gained more weight and greater epididymal white adipose accretion, and became hyperglycemic and glucose intolerant. Obesity is a strong risk factor for an aggressive subtype of breast cancer called basal-like breast cancer (BBC) and reducing adiposity is predicted to lower incidence of BBC in human populations. Thus, we made mice obese in early adulthood and induced weight loss by a diet intervention. Mice, which lost weight following an initial weight gain, reversed obesity-driven tumor aggressiveness and mammary gland hyperplasia and ductal carcinoma *in situ* through alterations in kinase activation. The obese microenvironment of mammary glands in adulthood therefore can promote early tumor onset. Importantly the composition of the mammary gland can be reprogrammed with weight loss and restored to a lean phenotype associated with significantly reduced tumor aggressiveness.

To my parents, Yueqing Qin and Yuqin Wu, for their unconditional love and support throughout my graduate studies.

To my mentor, Liza Makowski, for serving as an incredible role model of women in science, guiding me the way to a scientist, trusting my ability and potentials, encouraging and pushing me forward all the time.

To my committee members, for their guidance, support and advice towards my successes as a doctoral student.

To my friends, for their patience, understanding and encouragement.

PREFACE

Chapter 2 of this work was published in *Alcohol Clin Exp Res.* in 2014. The following authors contributed to the work in the following manner. Y. Qin designed, conducted and analyzed majority of the experiments, wrote manuscript, J. L. Hamilton conducted and analyzed gene expression data, M. D. Bird conducted the experiments and analyzed protein expression data, M. M. Chen and A. Zahs provided input on protein expression, E. J. Kovacs designed and conducted the experiments, L. Makowski oversaw studies, provided intellectual input and participated in all aspects of analyzing data and preparation of manuscript.

Chapter 3 of this work is in revision. The following authors contributed to this work: Amy R. Johnson, Yuanyuan Qin, Alex J. Freerman, Megan J. Huang, Alyssa J. Cozzo, Liyang Zhao, Brante P. Sampey, J. Justin Milner, Melinda A. Beck, Blossom A. Damania, Joseph A. Galanko, Matthew L. Edin, Darryl C. Zeldin, Patrick T. Fueger, Brittney Bivins, Andreas Stahl, Liza Makowski. Specific author contributions to this work are as described. A. R. Johnson designed, conducted and analyzed majority of experiments and wrote manuscript. Y. Qin designed, conducted and analyzed majority of experiments and wrote manuscript. A. J. Freerman and M. J. Huang conducted and analyzed gene expression data, J. A. Galanko performed statistical analysis for the data, B. Bivins conducted immunoblot for FATP1 protein expression. A. Stahl provided FATP1^{-/-} mice and provided intellectual input. L. Makowski oversaw all studies and analyses and contributed to the writing of the manuscript.

Chapter 4 of this work has been submitted to Breast Cancer Research and Treatment. The following authors contributed to this work: Yuanyuan Qin, Sneha Sundaram, Luma Essaid, Xing

Chen, Samantha M. Miller, David B. Darr, Joseph Galanko, Stephanie A. Montgomery, Ben Major, Gary L. Johnson, Melissa A. Troester, Liza Makowski. Specific author contributions to this work are as described. Y. Qin designed, conducted and analyzed majority of experiments and wrote manuscript, X. Chen conducted Multiplexed Inhibitor Bead Affinity Chromatography. J. A. Galanko performed statistical analysis for the data, S. A. Montgomery conducted the pathological analysis. L. Makowski oversaw all studies and analyses and contributed to the writing of the manuscript.

All work in this dissertation was supported by the following grants: UNC University Cancer Research Fund, NIH NIAAA AA017376; NIH NIEHS/NCI ES019 472; NIH NIDDK P30DK056350 and P30DK034987, NIH F32HL75970, P30DK056350, Sanofi Global Scholar pre-doctoral fellowship, NIH NIEHS/NCI ES019472, The Mary Kay Foundation, NIH NCI CA180134, University Cancer Research Fund

TABLE OF CONTENTS

LIST OF TABLES	xi
LIST OF FIGURES	xii
LIST OF ABBREVIATIONS.....	xiv
CHAPTER I: INTRODUCTION.....	1
Significance	1
Alcohol consumption in the US	4
Alcohol Metabolism.....	5
Binge Drinking and Trauma.....	5
The Obesity Pandemic	6
Macrophage Subtypes	8
Fatty Acid Transporter Protein 1	10
Breast Cancer.....	13
Risk Factor.....	14
Intrinsic Subtypes Based on Gene Expression.....	15
Basal-like Breast Cancer	16
C3(1)-Tag Mouse Model.....	18
High Fat Diet, Obesity and Breast Cancer.....	19
Weight Loss and Breast Cancer.....	21
The Possible Mechanisms of Obesity-induced Cancer.....	22
Summary	26

CHAPTER II: ADIPOSE INFLAMMATION AND MACROPHAGE INFILTRATION AFTER BINGE ETHANOL AND BURN INJURY.....	27
Overview.....	27
Introduction	28
Results	29
Discussion	34
Materials and methods	40
Tables and Figures	44
CHAPTER III: MACROPHAGE FATTY ACID TRANSPORTER 1 (FATP1) DRIVES ALTERNATIVE MACROPHAGE POLARIZATION AND LIMITS OBESITY-INDUCED INFLAMMATION.....	50
Overview.....	50
Introduction	51
Results	54
Discussion	64
Materials and methods	72
Tables and Figures	82
CHAPTER IV: REMODELING THE MICROENVIRONMENT IN EARLY ADULTHOOD BY WEIGHT LOSS RESTRAINED DIET-INDUCED BASAL-LIKE BREAST CANCER PROGRESSION.....	100
Overview.....	100
Introduction.....	102
Results	104
Discussion	110
Materials and methods	118
Tables and Figures.....	124

CHAPTER V: SYNTHESIS	141
Summary of research findings	141
Direction for future research	142
Public Health Significance.....	144
REFERENCES	145

LIST OF TABLES

Table 3.1: Hematologic analysis of Fatp1 ^{+/+} and Fatp1 ^{-/-} blood.....	96
Table 3.2: Flow cytometric analysis of circulating Fatp1 ^{+/+} and Fatp1 ^{-/-} lymphocytes.....	97
Table 4.1: Adiposity predicts BBC latency in C3(1)-Tag mice.....	136
Table 4.2: Mice with higher body weight have shorter latency.....	137

LIST OF FIGURES

Figure 1.1: Macrophage phenotypes.....	10
Figure 1.2: FATP1 topology model.....	12
Figure 1.3: Progression of breast cancer.....	14
Figure 1.4: C3(1)-Tag Mouse Model.....	19
Figure 1.5: Microenvironment regulates tumor induction and progression.....	23
Figure 2.1: Interleukin-6 (IL-6) levels increase after single and episodic binge ethanol exposure and burn injury.....	44
Figure 2.2: Adipose expression of neutrophil chemokine KC after single and episodic binge ethanol and burn injury.....	46
Figure 2.3: Episodic binge ethanol and burn injury drives crown like structure formation.....	47
Figure 2.4: Adipose chemokine levels of monocyte chemotactic protein-1 (MCP-1) and adiponectin were inversely regulated after single and episodic binge ethanol and burn injury.....	48
Figure 2.5: Single and episodic binge followed by burn injury failed to upregulate pro-inflammatory mediators.....	49
Figure 3.1: FATP1 is predominantly expressed in AAMs and transplant of fatp1 ^{-/-} marrow results in FATP1 deficient macrophages.....	82
Figure 3.2: Deletion of MΦ Fatp1 increased susceptibility to weight gain, glucose intolerance, and increased white fat mass. Lipids are absorbed by small intestinal enterocytes and repackaged into chylomicrons for distribution to peripheral tissues.....	83
Figure 3.3: Lack of MΦ FATP1 increased adipose inflammation, inflammasome priming, and markers of oxidative stress in HFD-fed mice.....	85
Figure 3.4: Fatp1 deletion decreased acyl-CoA synthetase (ACSL) activity and resulted in a metabolic shift from lipid oxidation to glycolysis that resulted in exacerbated CAM and less AAM activation.....	87
Figure 3.5: Lack of FATP1 in CAM-polarized BMDM enhanced Pentose Phosphate Pathway activity.....	89

Figure 3.6: Over-expression of FATP1 in RAW264.7 MΦs induced a substrate switch with enhanced lipid metabolism and reduced glucose metabolism resulting in blunted CAM-activation.....	91
Figure 3.7: Over-expression of FATP1 reduced inflammatory response in RAW264.7 macrophages.....	93
Figure 3.8: FATP1 expression level had no effect on lean body mass, liver weight or brown adipose (BAT) weight.....	98
Figure 3.9: Deletion or over-expression of FATP1 had no effect on cell size or viability.....	99
Figure 4.1: Weight loss protected against HFD-mediated early BBC onset.....	124
Figure 4.2: Body composition predicts latency.....	125
Figure 4.3: Diet did not affect tumor initiation.....	126
Figure 4.4: Pathological changes in the unaffected mammary gland induced by high fat diet were reversed by weight loss.....	127
Figure 4.5: Kinome profiling of unaffected mammary glands revealed dramatic regulation of PKD1-PKC- α -PKA-MEK3 by diet exposure.....	128
Figure 4.6: Protein-Protein interactions of significantly altered kinases in unaffected mammary gland of mice on 60-10% diet compared to mice on 60% diet.....	129
Figure 4.7: Tumor burden and size are not affected by diets.....	131
Figure 4.8: Measures of glucose intolerance were not altered by diet.....	132
Figure 4.9: Kinome profiling reveals significant regulation of pathways by HFD that are reversed with weight loss.....	133

LIST OF ABBREVIATIONS

2-DG	2-deoxyglucose
4-HNE	4-hydroxynonenal
7-AAD	7-aminoactinomycin D
AAM	Alternatively activated macrophages
ABCA1	ATP binding cassette transporter ABCA1
ABCG1	ATP binding cassette transporter ABCG1
ACSL	Acyl-CoA synthetase
ADH	Alcohol dehydrogenase
ADK	Adenosine kinase
AKT	Protein kinase B
ALDH	Aldehyde dehydrogenase
AMPK	5'-AMP-activated protein kinase
ANOVA	Analysis of variance
ATMs	Adipose tissue macrophages
AUC	Area under the curve
BBC	Basal-like breast cancer
BMDM	Bone marrow derived macrophages
BMI	Body mass index
Bmp2K	Bone morphogenetic protein-2-inducible protein kinase
BMT	Bone marrow transplant
CAA	Cancer-associated adipocytes
CAF	Cancer associated fibroblasts
CAM	Classically activated macrophages

CBCS	Carolina Breast Cancer Study
CCR2	C-C chemokine receptor type 2
CD36	Cellular differentiation
CDC	Centers for Disease Control and Prevention
CETP	Cholesterol ester transfer protein
CIS	Carcinoma in situ
CK	Cytokeratin
CLS	Crown-like structures
CO2	Carbon dioxide
CoA	Coenzyme A
CSFR1	Colony stimulating factor 1 receptor
CYP2E1	Cytochrome P4502E1
DAB	Diaminobenzidine
DCIS	Ductal carcinoma in situ
Ddr1	Epithelial discoidin domain-containing receptor 1
DIO	Diet induced obesity
DMEM	Eagle's minimal essential medium
DTH	Delayed-type hypersensitivity
ECAR	Extracellular acidification rates
EGF1R	Epidermal growth factor 1 receptor
EGFR	Epidermal growth factor receptor
ER	Estrogen receptor
ER	Endoplasmic reticulum

ERK	Extracellular signal-regulated kinases
EtOH	Ethanol
eWAT	Epididymal white adipose
FAEE	Fatty acid ethyl ester
Fas	Fatty acids
FAT/CD36	Long-chain fatty acyl coenzyme A
FATP1	Fatty acid transporter 1
FATP1-EV	FATP1 empty vector
FATP1-OE	FATP1 overexpressing
FATPs	Fatty acid transport proteins
FBS	Fetal bovine serum
FFPE	Formalin Fixed Paraffin Embedded
Fn3k	Ketosamine-3-kinase
GEMM	Genetically engineered mouse model
GLUT1	Glucose transporter 1
GLUT1-EV	GLUT1 empty vector
Glut1MΦ ^{-/-}	Macrophage specific Glut1 knock out
GLUT1-OE	GLUT1 over expresser
GSH	Reduced glutathione
GSSG	Oxidized glutathione
GTT	Glucose tolerance test
H&E	Hematoxylin and eosin
HBSS	Hank's buffered saline solution

HEPES	4-(2-hydroxyethyl)-1-piperazineethanesulfonic acid
HER2	Human epidermal growth factor receptor 2
HFD	High fat diet
HGF	Hepatocyte growth factor
HIF1 α	Hypoxia inducible factor 1
HMG-CoA	3-hydroxy—methylglutaryl coenzyme A
i.p.	Intraperitoneal
ICAM	Intercellular adhesion Molecule
ICAM-1	Intercellular Adhesion Molecule 1
IDC	Invasive ductal carcinoma
IFN	Interferon
IFN γ	Interferon gamma
IGF1R	IGF1 receptor
IGFs	Insulin-like growth factors
IHC	Immunohistochemistry
IL-10	Interleukin-10
IL-1 β	Interleukin-1 β
IL-6	Interleukin-6
iNOS	Inducible nitric oxide synthase
INSR	Insulin receptor
Irak1	Interleukin-1 receptor-associated kinase 1
IRS	Insulin receptor substrate
ITT	Insulin tolerance test

JAK	Janus kinase
JNK	C-Jun N-terminal Kinase
Kit	Mast/stem cell growth factor receptor Kit
LCCC	Lineberger Comprehensive Cancer Center
LCFAs	Long chain fatty acids
LFA1	Lymphocyte function-associated anti-gen 1
LFD	Low fat diet
Lfng	Luntatic fringe
LPS	Lipopolysaccharide
LXR	Liver X receptor
MAPK	Mitogen-activated protein kinase
Mark1	Serine/threonine-protein kinase MARK1
MCP-1	Monocyte chemoattractant protein 1
M-CSF	Monocytes colony stimulating factor
MEK3	Specificity mitogen-activated protein kinase kinase 3
MEOS	Microsomal ethanol oxidizing system
MIB	Multiplexed Inhibitor Bead
MMPs	Matrix metalloproteinases
MMTV	Mouse mammary tumor virus
MP1U	Mouse Phase I Unit
MRI	Magnetic resonance imaging
MS	Mass spectrometry
MTT	3-(4,5-dimethylthiazol-2-yl)-2,5-diphenyltetrazolium bromide

MΦ	Macrophage
NAD ⁺	Oxidized nicotinamide adenine dinucleotide
NADH	Reduced nicotinamide adenine dinucleotide
NAF	Normal associated fibroblasts
NF-KB	Nuclear factor kappa-light-chain-enhancer of activated B cells
NLRP3	NOD-like receptor family, pyrin domain containing 3
NO	Nitric oxide
OCR	Oxygen consumption rate
OxLDL	Oxidized low density lipoprotein
PAI-1	Plasminogen activator inhibitor-1
PBS	Phosphate buffered saline
PI3K	Phosphatidylinositol-4,5-bisphosphate 3-kinase
Pik3c3	Phosphatidylinositol 3-kinase catalytic subunit type 3
PPARs	Peroxisome proliferator-activated receptor
PPP	Pentose Phosphate Pathway
PR	Progesterone receptor
Prkaa2	5'-AMP-activated protein kinase catalytic subunit alpha-2
Prkca	Protein kinase C alpha type
Prkd1	Serine/threonine-protein kinase D1
PTEN	Phosphatase and tensin homolog
qPCR	Quantitative PCR
RIPA	Radioimmunoprecipitation assay buffer
ROS	Reactive oxygen species

RPMI	Roswell Park Memorial Institute medium
Salk-1	Soluble serine/threonine-protein kinase receptor R3
SAM	S-adenosylmethionine
SDS	Sodium dodecyl sulfate
SMC	Smooth muscle cells
SR-A	Scavenger Receptor Class A Type I/II
SREBP	Steroid receptor element binding protein
SREBP1	Sterol regulatory element binding protein 1
STAT3	Signal transducer and activator of transcription 3
STRING	Search Tool for the Retrieval of Interacting Genes/Proteins
SV40	Simian virus 40
T2D	Type 2 diabetes
TAG	Triacylglyceride
Tag	T antigen
TCGA	Cancer Genome Atlas
TGF α	Transforming growth factor alpha
TLR4	Toll-like receptor 4
TLRs	Toll-like receptors
TNBC	Triple-negative breast cancer
TNF- α	Tumor necrosis factor- α
ULK3	Unc-51 like kinase 3
VCAM	Vascular cells adhesion molecule
VEGF	Vascular endothelial growth factor

VEGFA	Vascular endothelial growth factor A
VLCFAs	Very long chain fatty acids
WD	Western Diet
WHO	World Health Organization
WHR	Waist hip ratio

CHAPTER I: INTRODUCTION

Significance

Lifestyle plays a very important role in both the health of individuals and the public. Obesity-related diseases like cardiovascular heart disease, stroke, type 2 diabetes and certain types of cancer are the major causes of death in the US that have modifiable risk factors, making them potentially preventable diseases¹. Our genetic predisposition, which was once considered to be a determining factor for many diseases, may not be as important as we thought it was. Take cancers as an example. The study of cohorts of twins from Sweden, Denmark and Finland found that inherited genetic factors make a minor contribution to susceptibility to most types of cancers². The majority of cancers is considered preventable and could be avoided by adopting healthy lifestyle practices and avoiding unhealthy environmental factors³. In addition, diet can potentially modify genetic effects on diseases (the gene–environment interaction)⁴.

One of the leading causes of preventable death in the US is excessive alcohol consumption⁵. Binge drinking is the most common form of excessive alcohol consumption. In the US, approximately half of trauma-related patients were under the influence of alcohol at admission, and the majority of these patients engaged in binge drinking⁶⁻⁸. Ethanol exposure is a significant problem especially prior to burn injury because it dramatically elevates systemic and tissue-specific inflammatory responses^{9,10}, increases susceptibility to infections, and is associated with poorer outcomes including longer hospital stays and increased mortality¹¹. However, it was

unknown if adipose tissue, an important organ in whole body metabolism, contributed to the inflammatory status after alcohol consumption and injury. Thus, part of this thesis aimed at discovering the underlying causes of systemic inflammation with alcohol exposure and focused on alterations to the adipose microenvironment.

Why is adipose tissue such an important organ to study as a contributing factor in many preventable diseases? More than one-third of U.S. adults (35%) are obese, and another one-third are overweight¹². Obesity is considered to be a low-level chronic inflammatory condition that contributes to insulin resistance, type 2 diabetes, cardiovascular disease, cancer, and many other diseases^{13,14}. It has been indicated that the infiltration of macrophages into adipose plays an important role in the inflammatory status associated with obesity¹⁵⁻¹⁷. Different phenotypes of macrophages contribute in varied ways to disease. Generally, classically activated macrophages (CAM), also called M1 macrophages, are found in adipose tissue of obese individuals, contributing to inflammation; while alternatively activated macrophages (AAM), also known as M2 macrophages, are found dispersed in lean adipose tissue maintaining tissue function and homeostasis¹⁸. Importantly, M1 macrophages rely upon glucose as their main fuel, while M2 macrophages primarily use fatty acids¹⁹⁻²¹. With the recent knowledge that substrate metabolism is different in CAM versus AAM, the concept of metabolic reprogramming has arisen, wherein metabolism may drive the inflammatory response. Considering the important role of fatty acids and lipid metabolism in AAM, fatty acid transport proteins (FATPs) could be central in macrophage-mediated inflammation and obesity²²⁻²⁷. While it was unknown whether manipulating FATPs could affect macrophage biology and the inflammatory response of adipose tissue and the whole body, it may be important in understanding the contribution of FATPs to obesity and related diseases.

A disease tightly linked to obesity and often inflammation is breast cancer. Breast cancer alone is estimated to account for 29% (226,870) of all new cancer cases among women in the US in 2012, and it is the leading cause of cancer death among women ages 20 to 59 years²⁸. An important advancement in the field of breast cancer research is recent stratification of breast cancer to different intrinsic subtypes based on gene expression profiles²⁹. One of the subtypes called basal-like breast cancer (BBC) is highly aggressive with poor survival. Because it is triple negative for ER (estrogen receptor), PR (progesterone receptor) and HER2 (human epidermal growth factor receptor 2), it currently has no targeted therapy. Importantly, it is also more prevalent in premenopausal African-American women³⁰.

Obesity is a well-known risk factor for BBC, although the mechanism of the relationship between obesity and BBC is not well known. Therefore, obesity could be an intervention target for breast cancer, especially in BBC prevention. Based on the Carolina Breast Cancer Study (CBCS), Milikan et al. estimated that up to 68% of BBC could be prevented by promoting breastfeeding and reducing abdominal adiposity³¹. It has not been proven, though, whether reducing weight would decrease the risk of BBC in women. Weight loss may protect against BBC onset and/or progress by modulating the microenvironment of the mammary glands³². The mechanisms need to be further explored and are investigated in this thesis.

Thus, burn injury after ethanol, insulin resistance, and basal-like breast cancer are all regulated by the alteration of the adipose microenvironment. In recent years, attention has increasingly been drawn to the microenvironment. Cancer is a good example. Zamboni's group reported that the tumor microenvironment of triple-negative breast cancer affected nanoparticle drug delivery and therapeutic outcomes³³. The data presented in this dissertation demonstrate that lifestyle-related factors like alcohol intake, high fat diet and obesity could contribute to

disease onset and progress by regulating growth factors, kinases, cytokines, chemokines and possibly through other unknown pathways in the microenvironment. Therefore, our findings contribute to a growing body of evidence that the microenvironment (i.e. cellular composition, metabolism, and activation of specific kinase signaling cascades) in specific tissues contributes greatly to local and systemic pathologies.

Alcohol Consumption in the US

The Alcohol-Related Disease Impact report from the Centers for Disease Control and Prevention of the United States indicated that excessive alcohol use led to approximately 88,000 deaths and 2.5 million years of potential life lost each year from 2006 – 2010. Furthermore, excessive drinking accounted for 1 in 10 deaths among adults aged 20-64 years³⁴. The economic costs of excessive alcohol consumption in 2006 were estimated at \$223.5 billion, or \$1.90 a drink³⁵. In the United States, a drink is defined as 0.6 ounces (14.0 grams) of pure alcohol. Based on Dietary Guidelines for American 2010, a drink can be 12-ounces of beer (5% alcohol content), 8-ounces of malt liquor (7% alcohol content), 5-ounces of wine (12% alcohol content), or 1.5-ounces of 80-proof (40% alcohol content) distilled spirit or liquor (e.g., gin, rum, vodka, whiskey). Excessive alcohol consumption is the third leading cause of preventable death in the US³⁴. Excessive drinking includes binge drinking, heavy drinking, and any drinking by pregnant women or people younger than 21 years old according to the National Institute on Alcohol Abuse and Alcoholism. Binge drinking is defined as consuming 4 or more drinks for women or 5 or more drinks for men on one occasion. Heavy drinking is defined as consuming 8 or more drinks per week for women or 15 or more drinks per week for men. Most people who drink excessively are not alcoholics or alcohol dependent³⁶. Alcoholism or alcohol dependence

syndrome is also known as alcohol use disorder (AUD). Individuals must meet certain number of criteria in the Diagnostic and Statistical Manual of Mental Disorders (DSM) to be diagnosed with an mild, moderate or severe AUD³⁷.

Alcohol Metabolism

Alcohol metabolism takes places primarily in the liver by three enzymatic pathways. The main pathway, which is responsible for most ethanol oxidation, is through alcohol dehydrogenase (ADH) – aldehyde dehydrogenase (ALDH). The second pathway is the microsomal ethanol oxidizing system (MEOS) catalyzed by cytochrome P4502E1 (CYP2E1). CYP2E1 has been reported to be expressed in hepatocytes, Kupffer cells and adipocytes³⁸. The third pathway for ethanol elimination is a nonoxidative pathway catalyzed by fatty acid ethyl ester (FAEE) synthase, resulting in the formation of fatty acid ethyl esters³⁹. Importantly, besides in the liver, alcohol exposure involves changes in other organ systems, including intestinal barrier function, the innate immune system, and, as we and one other group has demonstrated, adipose tissue⁴⁰.

Binge Drinking and Trauma

Binge drinking is the most common form of excessive drinking in the US. Alcohol consumption is a major risk factor for all types of injuries, such as falls, fires, drowning, assaults, suicides, and motor vehicle collisions^{41,42}. Around half of all alcohol-related deaths are due to injuries. Among alcohol-related incidents, injuries resulting from motor vehicle collisions are the leading cause of death^{34,43}. Alcohol has been reported to cause changes in the physiological response following trauma, leading to increased complications and mortality⁴⁴⁻⁴⁶. Half of the

patients with burn-related injuries in the US have alcohol in their system at the time of admission, and the vast majority of those subjects are binge drinkers rather than chronic alcoholics⁸.

Burn injuries induce dramatic insulin resistance, hyperlipidemia, hyperglycemia and hepatosteatosis in patients, greatly contributing to elevated morbidity and mortality⁴⁷⁻⁴⁹. Insulin resistance in liver, skeletal muscle and adipose tissue can persist even 3 weeks after a burn injury^{49,50}. Burn injuries also drive systemic inflammation with elevations in pro-inflammatory cytokines and suppressed cell-mediated immunity, leading to multi-organ dysfunction⁵¹. Ethanol exacerbates burn-induced inflammation systemically and in the lung and adipose tissue^{52,53}, and impairs the immune response, thus increasing a patient's susceptibility to infection⁹. Clinical and laboratory studies have demonstrated that ethanol exposure prior to traumatic injury, such as a burn, markedly elevates systemic and tissue-specific inflammatory responses^{9,10} and is associated with poorer outcomes¹¹. It is well established that alcohol increases the dysregulated inflammatory and immune response caused by burns in animal models and human patients, but most of the previous focus has been on the lung and susceptibility to infection⁹. To date there were no studies examining the role of adipose tissue in contributing to the inflammatory response and insulin resistance associated with alcohol and burn trauma.

The Obesity Pandemic

The World Health Organization (WHO) defines overweight and obesity as excessive fat accumulation that is a risk factor to human health. A crude yet convenient population measure of obesity is the body mass index (BMI): a person's weight (in kilograms) divided by the square of his or her height (in meters)⁵⁴.

$$\text{BMI} = \text{Weight (kg)} / \text{Height}^2 (\text{m}^2)$$

$$= \text{Weight (lb)} / \text{Height}^2 (\text{in}^2) * 703$$

In Western countries, a person with a BMI of 30 or more is considered obese, and a person with a BMI greater than or equal to 25 is considered overweight. Overweight and obesity are risk factors for many diseases, including diabetes, cardiovascular diseases and many types of cancers. The fundamental cause of obesity and overweight is an energy imbalance between calorie intake and calorie expenditure. Globally, there has been an increase in intake of energy-dense foods that are high in fat and sugar, and a decrease in physical activity due to the increasingly sedentary lifestyle of work, changing modes of transportation, and increasing urbanization⁵⁵. Once considered a problem only in developed countries, overweight and obesity are now on the rise in developing countries. Recently the WHO estimated that in 2014, more than 1.9 billion adults were overweight globally. Of these, over 600 million were obese. Overall, around 39% of adults (38% of men and 40% of women) were overweight, and 13% of the world's adult population (11% of men and 15% of women) was obese in 2014⁵⁴. The worldwide prevalence of obesity more than doubled between 1980 and 2014⁵⁴. The situation in the United States is even worse. More than one-third of U.S. adults (35%) and approximately 17% (or 12.7 million) of children and adolescents were obese as reported by Ogden et al. in 2014¹². Some of obesity-related diseases like heart disease, stroke, type 2 diabetes and certain types of cancer are the leading causes of preventable death in the US (CDC guideline)⁵⁶. Obesity also brings an economic burden. The estimated annual medical cost of obesity in the U.S. was \$147 billion U.S. dollars, and the medical costs for people who are obese were \$1,429 higher than those of normal weight in 2008⁵⁷.

Macrophage Subtypes

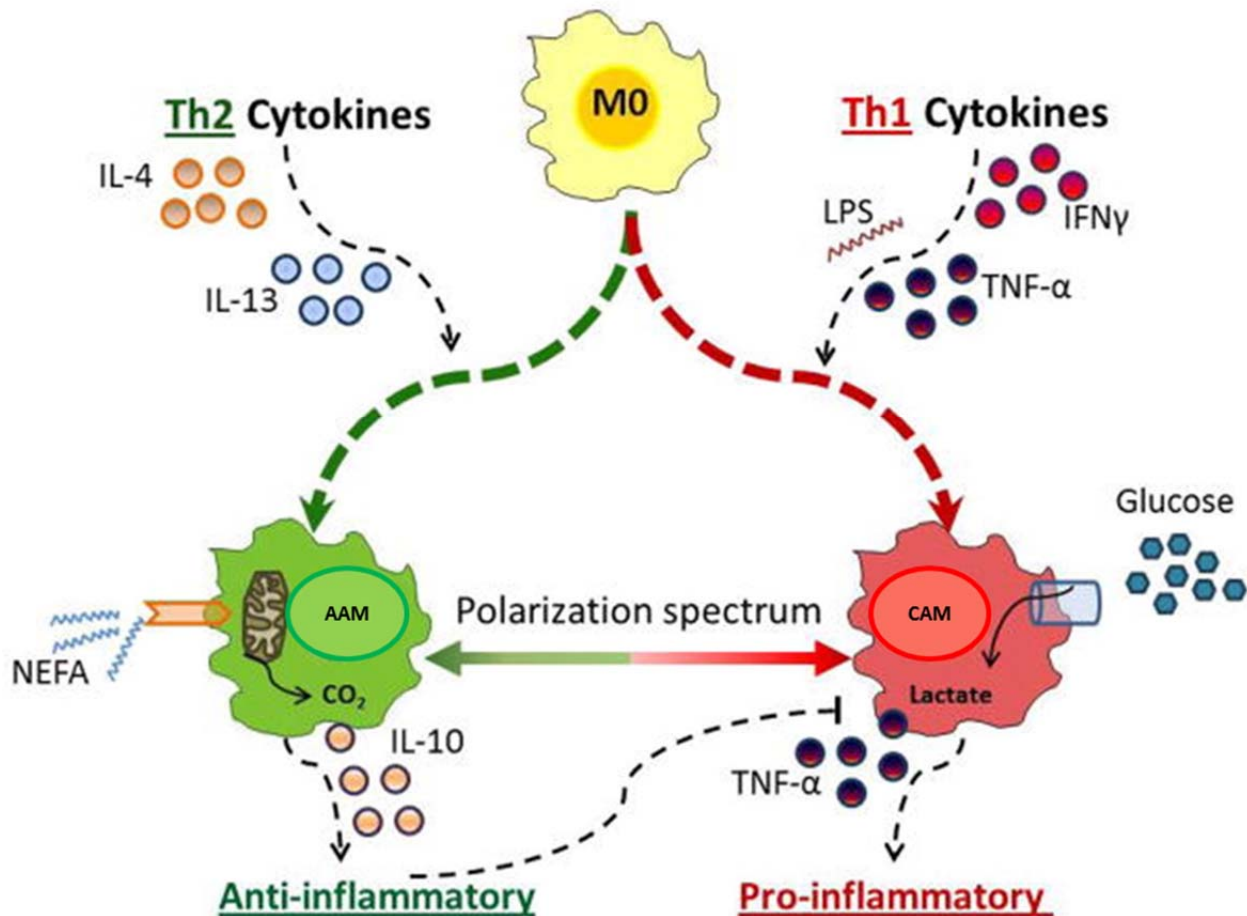
The currently accepted understanding of obesity as low-level chronic inflammation that contributes to insulin resistance, type 2 diabetes, cardiovascular disease, cancer and many other diseases emerged in the early 1990s^{13,14}. Although the mechanism is not fully understood, it has been indicated that the infiltration of macrophages into adipose tissue plays an important role in the inflammatory changes seen in obesity¹⁵⁻¹⁷.

Macrophages are important immune cells which reside in many tissues of the body, like microglia, Kupffer cells, osteoclasts, etc. Macrophages clear pathogens and apoptotic cells, and produce immune effector molecules⁵⁸. They have a central role in protecting the host but also hinder the resolution of inflammation, which is a hallmark of numerous diseases, including atherosclerosis, obesity, tumor, asthma, etc.⁵⁹. When there is tissue damage or infection, the precursors, monocytes, are rapidly recruited from the circulation to the tissue and differentiate into tissue macrophages⁶⁰. Macrophages are remarkably plastic and can change their functional phenotypes depending on the environmental cues⁵⁸.

There is a spectrum of macrophages in adipose tissue. The phenotype of the macrophage can affect the inflammatory status in the microenvironment of adipose tissue, which is integral to obesity and diabetes. Generally, CAMs are found in obese adipose tissue, forming crown-like structures surrounding dying adipocytes, while AAMs are dispersed in lean adipose tissue maintaining tissue function¹⁸. Importantly, CAMs utilize glucose, while AAMs primarily use fatty acids¹⁹⁻²¹ (**Figure 1.1**). Other activated immune cells like T cells have been reported to exhibit a similar Warburg-like metabolism^{20,61-65}. Most cancer cells predominantly rely on aerobic glycolysis which is an ineffective way to produce ATP, while normal cells rely on mitochondrial oxidative phosphorylation with a relatively low rate of glycolysis^{66,67}.

CAMs are a prominent source of pro-inflammatory cytokines such as iNOS, TNF α , MCP1 and IL6. In contrast, AAMs are involved in tissue remodeling and repair^{68,69}. Considering the important role of fatty acids and lipid metabolism in regulating macrophage biology, fatty acid transport proteins could be central in macrophage-mediated inflammation and obesity through metabolic reprogramming²²⁻²⁷.

Figure 1.1 Macrophage phenotypes



Adapted from Johnson AR, 2012

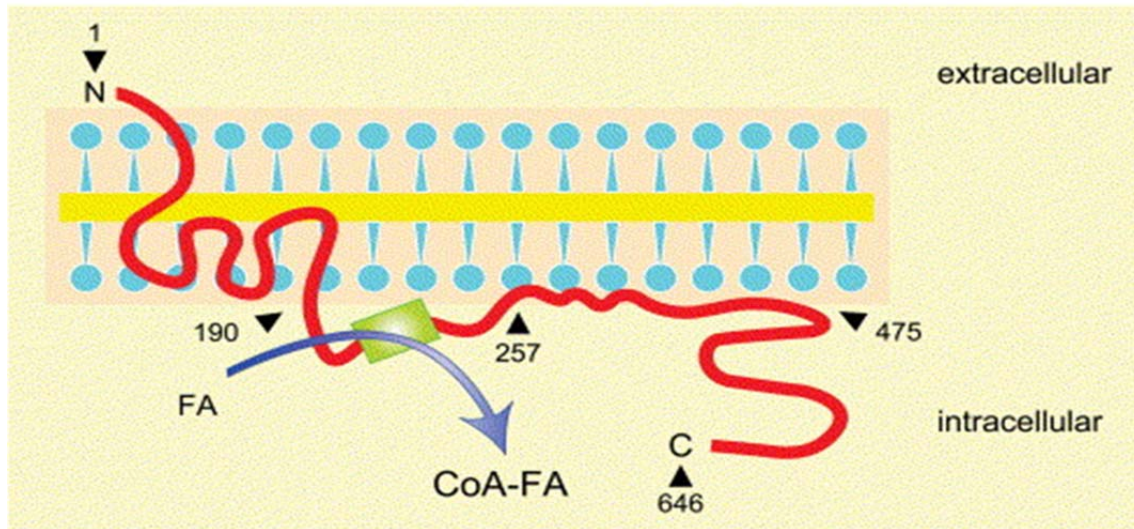
Figure 1.1. Macrophage polarization. Macrophages can be generally categorized as classically activated macrophage (CAMs) and alternatively activated macrophages (AAMs). CAMs are pro-inflammatory and polarized from precursor M0 macrophages via components of bacteria such as lipopolysaccharide (LPS) and type 1 T-helper (Th1) inflammatory cytokines interferon γ (IFN γ) and TNF α . AAMs are activated by type 2 (Th2) cytokines IL-4 and IL-1, involved in remodeling, tissue repair and maintenance of insulin sensitivity and considered anti-inflammatory. There is plasticity along the macrophage polarization spectrum.

Fatty Acid Transporter 1

The fatty acid transport protein (FATP) family consists of six members in humans and mice and is expressed in tissues with high levels of fatty acid uptake and active lipid metabolism, like adipose tissue, heart and skeletal muscle⁷⁰⁻⁷³. We have found that FATP1 and FATP4 are the

main FATPs expressed in macrophages, with macrophage FATP1 expressed at mRNA concentrations as high as those in the total adipose tissue. FATPs have been shown to be fatty acyl-CoA synthetases with an affinity for long chain fatty acids (LCFAs) and very long chain fatty acids (VLCFAs)^{74,75}. Acyl-CoA synthetases are enzymes that add a CoA to the fatty acid (**Figure 1.2**). Purified FATP-1 exhibited substrate specificity for fatty acids 16-24 carbons in length, while uptake of fatty acids shorter than 10 carbon atoms is unaffected by FATP expression^{70,74,76}. The majority of FATP1 is found on intracellular structures like the endoplasmic reticulum (ER) and mitochondria⁷⁷⁻⁷⁹. Insulin can induce translocation of FATP1 from an intracellular compartment to the plasma membrane, but doesn't change FATP1 protein expression in adipocytes⁸⁰. Adiponectin can increase FATP1 expression in skeletal muscle but not adipose tissue or liver⁸¹. TNF α is a negative regulator of FATP1 expression both in the liver and adipocytes^{80,82}. Fatty acids and their derivatives are ligands for PPARs, and a PPAR binding site has been identified in the murine FATP1 promoter⁸³, so a positive feedback loop might regulate expression of FATP1^{84,85}. A particular member of the nuclear receptor family, the TR4 orphan nuclear receptor facilitates lipid accumulation in 3T3-L1 adipocytes by activating FATP1 gene expression⁸⁶. To date, there have been no reports of FATP1 function in macrophages.

Figure 1.2 FATP1 topology model



Jurgen Pohl. 2004

Figure 1.2. FATP1 is a transmembrane protein. A short segment of the N-terminus is located in the extracellular side of the membrane bilayer while the C-terminus faces the cytoplasm. Amino acid residues 1–190 of FATP1 are transmembrane domains. Amino acid residues 190–257 are in the cytoplasmic side and contain the AMP-binding motif (rectangle) that has acyl CoA-synthetase activity. Amino acid residues 258–475 are also associated with the inner leaflet of the plasma membrane.

Whole body FATP1 deletion protected mice from fat-induced insulin resistance and intramuscular accumulation of fatty acyl-coA without alteration in adiposity⁸⁷. Insulin-stimulated fatty acid uptake was completely abolished in adipocytes and greatly reduced in skeletal muscle of the FATP1 knockout mouse following a high-fat diet, while basal LCFA uptake by both tissues was unaffected⁸⁸. In the same mouse model, lipids were redistributed from adipose tissue and muscle to the liver, leading to a complete protection from diet-induced obesity and insulin resistance⁸⁸. FATP1 overexpression in human muscle cells led to enhanced palmitate and oleate uptake and the incorporation into triacylglycerides (TAG)⁸⁹. A recent study indicated that FATP1, together with DGAT1, is part of a TAG synthesis complex that facilitates lipid droplet expansion in *Caenorhabditis elegans*⁷⁸. However, some *in vivo* and *in vitro* studies also suggested

FATP1 channeled FA to oxidation by activating AMP-activated protein kinase (AMPK)⁹⁰⁻⁹².

Therefore, it is likely that FATP1 can transport LCFA to both lipid storage and lipid oxidation depending upon the cells, growth factors and tissues.

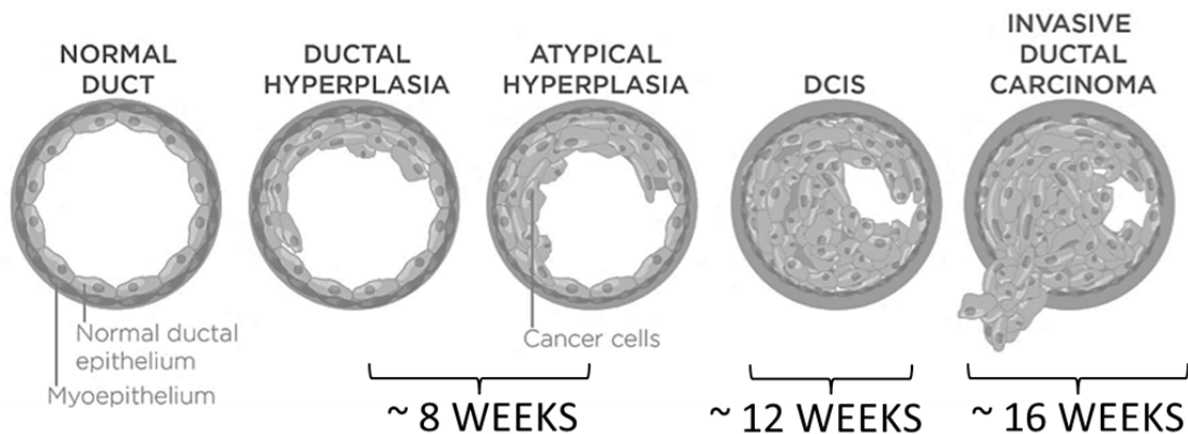
The role of FATP1 in insulin resistance is likely to be tissue-specific based on where and how fatty acids are stored. An increased FATP1-mediated fatty acid uptake into adipose tissue is beneficial for protecting muscle from harmful triacylglycerol accumulation, a phenomenon called “lipotoxicity”, while an increase in FATP1-mediated fatty acid uptake into muscle will contribute to insulin resistance. Macrophages can have extensive fatty acid metabolism, TG and cholesterol ester storage, especially AAMs or lipid-laden foam cells. Foam cells are fat-laden macrophages involved in fatty streak formation in atherosclerosis⁹³. However, how FATP1 affects macrophage biology and the inflammatory response is unknown but may be important in understanding cell-specific contributions to obesity, inflammation and insulin resistance. Our research showed that when fed a high fat diet (HFD), mice with specific FATP1^{-/-} macrophages are glucose intolerant, had greater weight gain, larger fat pads, and an increased inflammatory response in epididymal adipose tissue and systemically when compared to control mice on HFD.

Breast Cancer

Breast cancer is the most common cancer in women in the world and 2nd in cancer deaths in the US⁹⁴. Breast cancer can be divided into two main groups: the sarcomas and the carcinomas. Sarcomas are rare cancers that arise from the stromal components of the breast⁹⁵. These stromal cells include myofibroblasts and endothelial cells and cancers arising from these cells are phyllodes tumors and angiosarcoma, respectively⁹⁶. Sarcomas account for less than 1% of primary breast cancers⁹⁷, while carcinomas comprise the majority of all breast cancers.

Carcinomas are cancers that arise from the epithelial component of the breast, which consists of the cells that line the lobules (milk glands) and milk ducts (thin tubes that carry milk from the lobules of the breast to the nipple). Ductal carcinoma is the most common type of breast cancer. Lobular carcinoma begins in the lobules of the breast, and ductal carcinoma originates from the milk duct. Generally ductal carcinoma can progress from atypical ductal hyperplasia (ADH) to ductal carcinoma *in situ* (DCIS, meaning within the ducts), and then to invasive ductal carcinoma (IDC) where the tumor invades the stroma surrounding the ducts⁹⁸ (**Figure 1.3**). Breast cancer occurs in both men and women, but male breast cancer is rare⁹⁹.

Figure 1.3 Progression of breast cancer



Adapted from Kopans DB, 1989

Figure 1.3. Breast cancer progression in C3(1)-Tag mouse model. Ductal carcinoma progresses from atypical ductal hyperplasia (ADH) to ductal carcinoma *in situ* (DCIS) and to invasive ductal carcinoma (IDC). For C(3)1-Tag mice, at 8 weeks old, females developed ADH; at 12 weeks DCIS appeared; around 16 weeks femal mice developed tumors and DCIS became IDC.

Risk factors

The strongest risk factor for breast cancer is age¹⁰⁰. A woman's risk of developing breast cancer increases as she gets older. Other risk factors of developing breast cancer include

inherited changes in certain genes, like Brca1 and Brca2, a family history of breast cancer, geographical location (developed country), higher breast density, menarche at early age (before age 11), menopause at older age (after age 54), a first full-term pregnancy after age 30, never having been pregnant, obesity, excessive alcohol consumption and low socioeconomic status¹⁰¹. There is high lifetime risk of developing breast cancer for women in the US. Approximately 12.3% of women will be diagnosed with breast cancer at some point during their lifetime, according to Cancer Statistics (2012) based on incidence data from the National Cancer Institute, the Centers for Disease Control and Prevention, and the North American Association of Central Cancer Registries¹⁰². The number of new cases of breast cancer was 124.6 per 100,000 women per year, and the number of deaths was 22.2 per 100,000 women per year in the US, using age-adjusted data based on 2007-2011 cases and deaths¹⁰². In 2011, there were an estimated 2,899,726 women living with breast cancer in the United States¹⁰².

Intrinsic subtypes based on gene expression

Breast cancer is not a single disease. Instead it is composed of a spectrum of tumor subtypes with distinct cellular origins, somatic changes, and etiologies¹⁰³. In 2000, Perou's group used a semi-unsupervised approach to identify breast cancer subtypes in a population of 40 patients with locally advanced disease treated with neoadjuvant chemotherapy¹⁰⁴. They identified 496 genes, termed the intrinsic gene set, which showed little variance within repeated tumor sample, but high variance across different tumors, and then used this gene set for subtype discovery. Among these breast cancers, patterns of expression of these genes divided the tumors into five subtypes, which are called "intrinsic subtypes", because the gene list that defines them reflects intrinsic properties of breast cancers rather than selected clinical behavior¹⁰⁴. These 6

intrinsic subtypes include luminal A, luminal B, her2-enriched, basal-like, claudin-low and normal-like breast cancers¹⁰⁵. These subtypes have been consistently identified in independent datasets using multiple different methods¹⁰⁶⁻¹⁰⁸. They are conserved across ethnic groups, and are present in preneoplasia^{109,110}. Importantly, the intrinsic subtypes of breast cancer can predict patient relapse, overall survival, and response to endocrine and chemotherapy regimens^{111,112}.

Basal-like breast cancer

In clinical studies, there is a group of breast tumors known as “triple-negative” due to their typical immunohistochemical (IHC) staining that is negative for ER, PR, and HER2, which are commonly scored for predictive markers in breast cancer clinics¹¹³. About 80% of triple-negative breast cancer (TNBC) is basal-like¹⁰⁶. Likewise, a majority of basal-like breast cancers are triple-negative; about 25% of basal-like tumors are not triple-negative¹¹⁴. The basal-like subtype is characterized by low expression of the luminal genes and the HER2 gene cluster, high expression of the proliferation cluster, and high expression of genes called the basal cluster¹⁰⁶. The basal gene cluster includes basal epithelial cytokeratins (CK) such as CK5, 6, 14, and 17; epidermal growth factor receptor (EGFR); c-Kit; Vimentin; P-Cadherin; Fascin; Caveolins 1 and 2; and aB-crystallin¹⁰⁶. Importantly, it was the expression of cytokeratins 5, 6, 14, and 17 that gave rise to the term “basal-like,” as these are typically cytokeratins that are expressed within basal epithelial cells of the skin and airways¹⁰³.

Several genetic risk factors for developing basal-like tumors have been identified. One of the most interesting links is between the basal-like subtype and BRCA1 mutation carriers¹¹⁵⁻¹¹⁷. Specifically, if a woman is a BRCA1 mutation carrier and develops breast cancer, over 80% of the time her cancer is the basal-like subtype¹⁰³. Although BRCA1 mutation carriers usually

develop basal-like breast cancer, most basal-like breast cancers are sporadic, and the BRCA1 gene and protein appear intact in these tumors¹¹⁸. Other known genetic defects in basal-like tumors include a high P53 mutation rate^{119,120} and loss of RB1 function^{121,122}. P53 and Rb are two tumor suppressor genes. Loss or mutation of P53 and/or Rb results in increased cell proliferation that is manifested by the high expression of the “proliferation signature”¹²³. Another notable association is between the basal-like subtype, race, and age. Several population-based studies have suggested that the basal-like subtype is prevalent in young women with breast cancer, especially in the African-American population^{120,124,125}¹²⁶. In the Carolina Breast Cancer Study, which is a population-based, case-control study of environmental and molecular determinants of breast cancer risk that oversampled African American and premenopausal women^{120,127}, basal-like breast cancer was the most common among premenopausal African-American women (27%) and least common among postmenopausal non African-American women (9%)³¹. Interestingly, this over-representation of basal-like cancers is even more prevalent in Africans in Nigeria¹²⁸. These findings suggest that there may be a genetic predisposition of Africans to basal-like tumors. The frequency of MYBL2 alleles has been found to be increased in basal-like cases versus controls¹²⁹. In the Cancer Genome Atlas (TCGA) study, when tumors from different organs were analyzed based on their gene expression, basal-like breast tumors fell into their own category, indicating that basal-like breast cancer is distinct from other breast cancer subtypes¹³⁰.

There are life history risk factors for developing basal-like cancers, including multiple pregnancies (≥ 3), no lactation, and having a high waist/hip ratio (a more accurate indicator of obesity compared to BMI)³¹. Notably, pregnancy is a protective factor for luminal breast cancer.

This indicates that basal-like and luminal subtypes require different prevention strategies based on different risks.

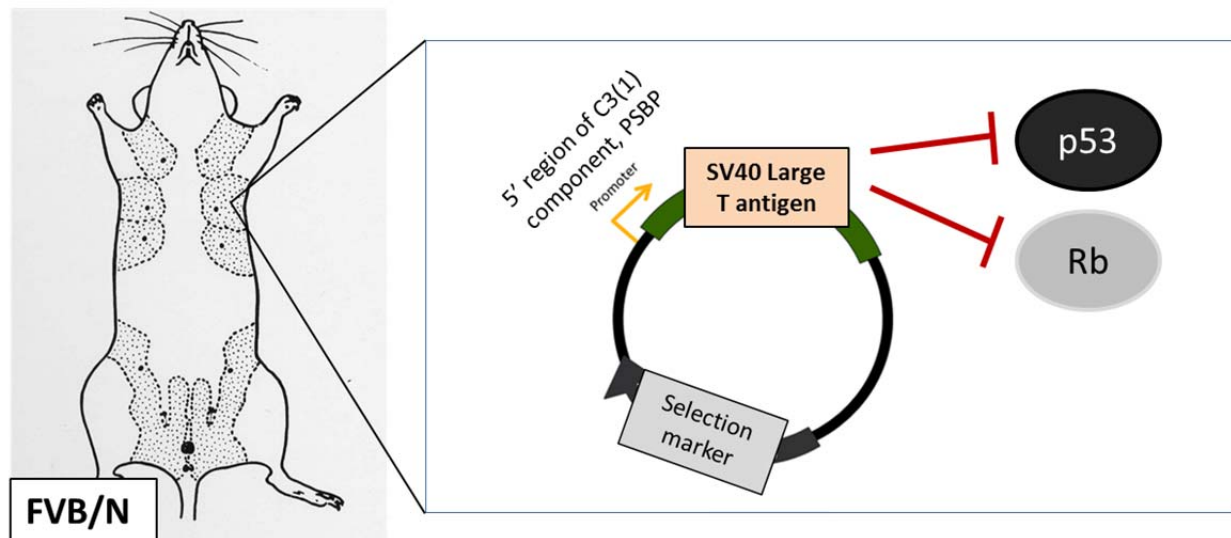
C3(1)-Tag Mouse Model

The C3(1)-Tag mouse model was created on FVB/N background in Jeffery Green's lab at NCI. It was originally created for the study of prostate cancer. C3(1)-Tag mice express simian virus large T antigen (Tag) under the 5' region of prostate steroid binding protein. SV 40 Tag can inactivate p53 and Rb, which are tumor suppressor genes, by directly or indirectly binding to them¹³¹. Researchers found that male C3(1)-Tag mice develop prostate cancer, while female ones develop breast cancer¹³². Green's lab reported that, at 8 weeks old, C(3)1-Tag mice developed atypical hyperplasia of ductal epithelium; at 12 weeks ductal carcinoma in situ (DCIS) appeared; at 16 weeks female mice developed tumors and DCIS became invasive ductal carcinoma (IDC)^{132,133}. The SV40 Tag used in the C3(1)-Tag model inactivates p53 and RB, which also occurs in human basal-like tumors because these tumors are known to harbor p53 mutations¹³⁴ (**Figure 1.3&1.4**). Hershkowitz et al. demonstrated that tumors from C3(1)-Tag mice¹³² display characteristics consistent with human basal-like breast tumors including BRCA1-deficiency, TP53 mutant/deficiency, and high expression of Keratin 5, 17, and P-Cadherin¹³⁵. Thus, for basal-like breast cancer, the C3(1)-Tag mouse is representative of human tumors.

Using genetically engineered modified mouse models (GEMM) such as the C3(1)-Tag mouse is advantageous because the timeline of tumor progression is clearly established in this mouse model and it allowed us to investigate basal-like breast carcinogenesis, namely to understand the role of obesity in promoting tumorigenesis and decreasing tumor latency. In contrast to xenograft models (which often have altered tissue composition due to clearing of the

fat pad and/or altered immune function), the C3(1)-Tag mouse has an intact stroma and requires no chemical treatment to initiate tumors.

Figure 1.4 C3(1)-Tag Mouse Model



Adapted from Murphy ED, 1966

Figure 1.4. C3(1)-Tag mouse model. C3(1)-Tag mice are on FVB/N background and express simian virus 40 (SV40) large T antigen (Tag) under the 5' region of prostate steroid binding protein (PSBP). SV 40 Tag can lead to cancer onset by inactivating p53 and Rb, which are 2 tumor suppressor genes, by directly or indirectly binding to them.

High Fat Diet, Obesity and Breast Cancer

Obesity is associated with increased risk of cancers, including breast cancer. Increased body weight was associated with increased death rates for all cancers in a prospective cohort study of U.S. adults¹³⁶. Considering the high prevalence of obesity (35.7%) and overweight (68.8%) in the US¹³⁷, targeting obesity could be an effective intervention for cancer prevention. Adulthood is an important window of susceptibility for obesity-induced breast cancer¹³⁸. Early epidemiologic studies indicated that obesity did not increase breast cancer risk among premenopausal women, but did increase risk in postmenopausal women by around 50%¹³⁹. Indeed, weight gain during adult life increases the risk of breast cancer among postmenopausal

women in the prospective Nurses' Health Study. However, recent advances in technology have shed light on breast cancer biology¹³⁰ and specifically on obesity-induced risk. It has been established that breast cancer has multiple subtypes²⁹. Breast cancer can be classified based upon different intrinsic subtypes each with distinctive gene expression profiles as discussed above²⁹. This genomic-based classification is now being used to better understand breast cancer and can predict prognosis based on each subtype¹⁴⁰. Therefore, early epidemiologic studies (that were not stratified based on subtype or only examined ER status) which suggested that obesity is only a risk factor in post-menopausal women, were actually based on populations heavily represented by the most prevalent breast cancer: Luminal A. Luminal A is a subtype that affects mainly older Caucasian women. In the case of BBC, several epidemiologic studies have demonstrated that obesity as measured by BMI or waist hip ratio (WHR) is associated with risk of BBC in both young (pre-menopausal) and older (post-menopausal) women^{31,141,142}. The prevalence of BBC is about 12.3–36.7% of all breast cancer cases¹⁴³. The mechanism defining the relationship between obesity and BBC is not well known and is the subject of my studies. Of all the subtypes of breast cancer, BBC is a severe clinical problem because there are no targeted therapies, driving us to investigate potential modifiers of risk.

Studies in preclinical models demonstrate that obesity is associated with shortened mammary tumor latency^{144,145}. Soner et al. found a connection between body weight and mammary tumor incidence and development in MMTV (mouse mammary tumor virus)-TGF α mice¹⁴⁶. MMTV-HER2/Neu mice fed on a diet with 45% of calories from fat for a year starting at 4 weeks old had increased body weight, fat mass, and increased mammary tumor numbers compared to mice fed a LFD (10% calories from fat)¹⁴⁷. Dunlap et al. reported that C57BL/6 mice receiving a xenograft fed a HFD (60% calories from fat) for 14 weeks have increased tumor

progression of claudin-low breast cancer compared to mice fed a control diet (10% calories from fat)¹⁴⁸. Obesity induced by HFD was also found to promote mammary tumor progression in C57BL/6 mice with MMTV-Wnt-1 tumor cell xenografts¹⁴⁹. Prior to our recent publications, no studies examined the effects of obesity on BBC using murine models. We previously reported that obesity significantly decreased BBC latency in C3(1)-Tag mice¹⁵⁰.

Weight Loss and Breast Cancer

The WHO suggested that body weight and physical inactivity together account for approximately one-fifth to one-third of the most common cancers, including breast cancer¹⁵¹. It may be possible to decrease the risk of breast cancer by exercising and maintaining a healthy weight¹⁵²⁻¹⁵⁴. Michels et al. reported that weight loss of 5 kg or more since age 18, maintained for at least 4 years, was related to lower incidence of premenopausal breast cancer when compared to maintaining a stable weight¹⁵⁵. In the Iowa Women's Health Study based on 34,000 women, maintaining $\geq 5\%$ weight loss reduced post-menopausal breast cancer risk by approximately 25%¹⁵⁶. A prospective cohort study within the Nurses' Health Study indicated that weight loss after menopause is associated with a decreased risk of breast cancer¹⁵⁷. Furthermore, weight loss of 10% or more reduces breast cancer risk in postmenopausal overweight and obese women¹⁵⁸. Based on Carolina Breast Cancer Study, it has been estimated that up to 68% of BBC could be prevented by promoting breastfeeding and reducing abdominal adiposity³¹. However, it hasn't been proved whether reducing weight in adulthood would decrease the risk of BBC in experimental models. Weight loss in animal models is commonly induced by calorie restriction. Caloric restriction is defined as the consumption of fewer calories without malnutrition¹⁵⁹. Calorie restriction protects against the development of different types of cancers including breast

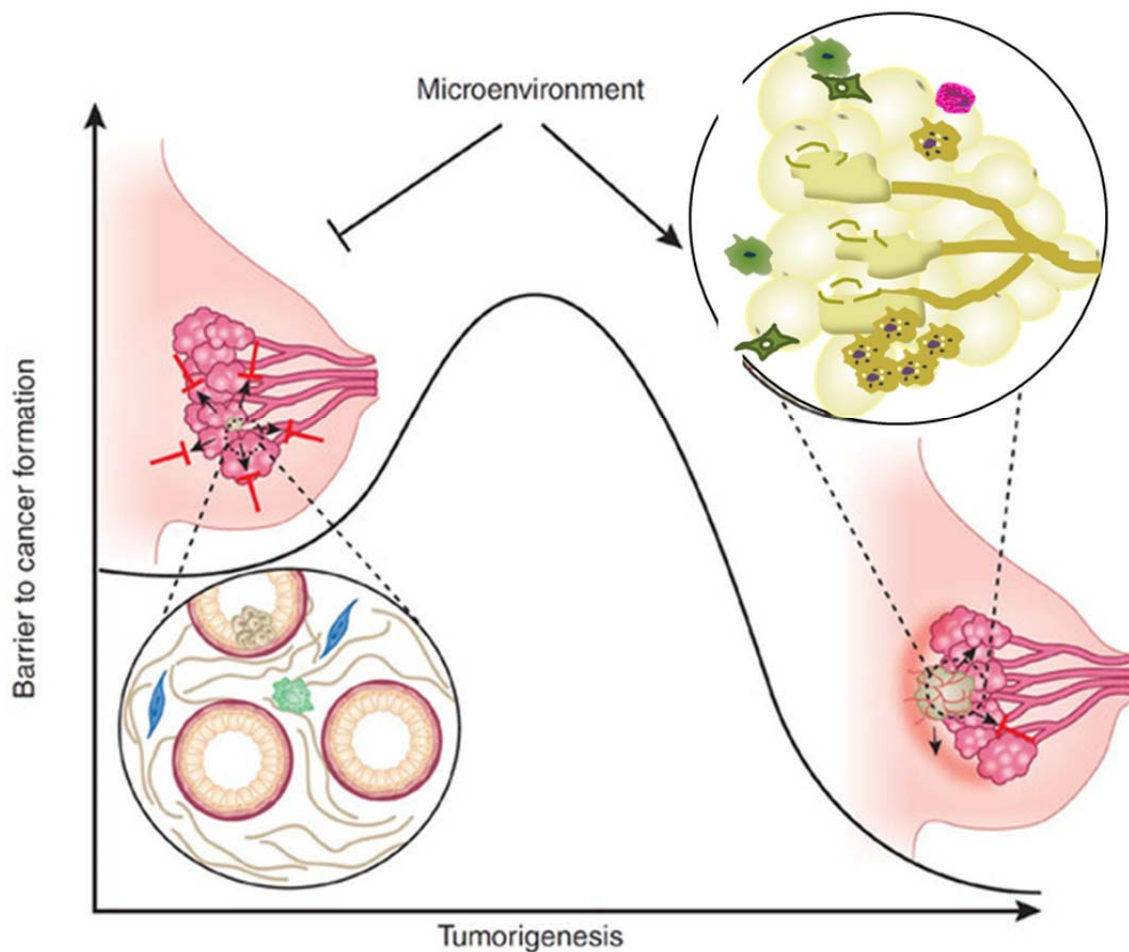
cancers in various animal models¹⁵⁷. A meta-analysis of experimental mouse models also suggested that energy restriction decreased tumorigenesis in the mammary gland¹⁶⁰. Cleary et al. reported that intermittent calorie restriction-refeeding provided a moderate protective effect against mammary tumor development in MMTV-neu transgenic mice, which is an animal model of luminal breast cancer¹⁶¹. Caloric restriction using a murine xenograft model of BBC demonstrated reduced tumor growth¹⁴⁸. None of these studies examined weight loss in a BBC with a GEMM model. Green et al. demonstrated the protective benefits of exercise on BBC tumor progression, potentially through a significant exercise-induced weight loss, but the effects of exercise versus weight loss were not investigated¹⁶². Our group previously showed that in C3(1)-Tag mice made obese from weaning that were then induced to lose weight demonstrated a decrease in tumor progression that correlated with weight loss¹⁶³. In sum, human and murine models demonstrate that high fat diet induced obesity is a strong but modifiable risk factor for breast cancer, although the protective effects and mechanisms of weight loss specifically on BBC must be further investigated.

The Possible Mechanisms of Obesity-induced Cancer

There are many hypotheses about how obesity is linked to cancer including hormonal promotion, alterations to the microenvironment, and release of growth factors¹³. Since BBC is triple negative (estrogen receptor, progesterone receptor, and HER2-negative), it is likely that obesity-induced production of estrogen through aromatase is not a strong driver of tumor onset. Indeed, our recent work in C3(1)-Tag mice has demonstrated no obesity-induced alterations in systemic estrogen levels or mammary gland concentrations of aromatase¹⁵⁰. The role of the microenvironment or the “seed and soil” theory, where cancer cells (the seeds) are modulated by

the stroma (the soil) is a likely hypothesis that may contribute to carcinogenesis. The microenvironment surrounding a tumor has been realized to play an important role in tumor onset and progression³². When the microenvironment is normal, it can suppress tumorigenesis. However, changes in the microenvironment can also promote tumorigenesis and progression³² (Figure 1.5).

Figure 1.5 Microenvironment regulates tumor induction and progression



Modulated from Bissell MJ 2011; Sundaram S 2013.

Figure 1.5. The role of microenvironment in tumor progression. Normal tissue homeostasis and architecture inhibit progression of cancer. Disruption in the microenvironment (e.g. obesity) can promote tumorigenesis and progression.

The metabolites, growth factors, hormones and modifications of extracellular matrix in this microenvironment have critical effects on tumor cells. In fact, multiple reports from the Troester lab have demonstrated that BBC is characterized by unique epithelial-stroma interactions, which likely play a role in the etiology¹⁶⁴. There were numerous alterations in the gene expression profiles in the microenvironment of breast tumors compared to normal breast tissues¹⁶⁵. BBCs are more likely to recur locally than non-BBC cancers¹⁶⁶, even after mastectomy with clean margins, suggesting a local field defect¹⁶⁷ that may arise from epithelial or stromal alterations in the microenvironment.

Stroma-derived growth factors and metabolites are strongly relevant to obesity-induced cancer onset by modifying the extracellular matrix or angiogenic factors provided by the stroma. Hepatocyte growth factor (HGF) is a good example. High expression of cMet, the receptor of HGF, is significantly correlated with BBC in mouse and humans¹⁶⁸. Our previous studies have shown that obesity upregulates HGF and cMet expression in the normal mammary gland of C3(1)-Tag mice, and this upregulation of HGF/cMet is correlated with a shortened latency¹⁵⁰. Likewise, after life-long obesity, weight loss also decreased HGF/cMet expression in normal mammary glands¹⁶³. cMet signature in 87% of BBC tumors and patients predicted worse outcomes¹⁶⁹. In a mutant mouse deficient for luntatic fringe (Lfng), a sugar transferase, the Perou lab demonstrated induction of BBC with amplification of the cMet locus and elevated cMet signaling¹⁷⁰.

Furthermore, we and other research groups have demonstrated that obesity is associated with low-grade adipose inflammation in adipose tissue^{18,23,171}. In the mammary gland, ours and Dannenberg's labs have reported that macrophage infiltration occurs in the normal mammary gland of human subjects¹⁷²⁻¹⁷⁴. We have also found increased macrophage infiltration in

mammary glands of obese C3(1)-Tag mice (manuscript in prep). In addition to HGF release from immune cells like monocytes and macrophages, inflammatory cytokines release from activated macrophages contribute to breast cancer onset and development^{175,176}.

Obesity can also disturb the microenvironment by reprogramming the kinome, or activating and interrupting growth factor/receptor signaling, such as leptin and other mediators^{13,18}. Leptin is a hormone produced by adipocytes in proportion to adiposity. A meta-analysis of case-control studies reported that women with breast cancer have elevated plasma leptin levels. High leptin receptor mRNA expression in breast cancer tissue was also established to predict poor prognosis in patients with high serum leptin levels. Therefore leptin may play a central role at the interface of obesity and breast cancer and may act through several pathways¹³. One way that leptin may drive BBC is that leptin promoted the survival of cancer stem cells (CSCs) *in vivo*¹⁷⁷, and leptin signaling is required to maintain CSC-like properties in triple negative breast cancer cells, which was shown to mediate tumor recurrence and metastasis in orthotopically transplanted mice. Leptin signaling also induces breast tumor cell growth through activation of the JAK-STAT and PI3K signaling pathway in both human and mouse cell lines. Leptin receptor deficiency in MMTV-PyMT mice was shown to attenuate tumor growth and metastasis through increasing mitochondrial respiration capacity in tumor cells and deactivating the downstream ERK and STAT3 pathways. About one fourth of all kinases may be involved in oncogenesis. Protein kinases regulate cell proliferation, survival, and metabolism and can contribute to tumor progression.

Taken together, in many ways, the microenvironment of breast tumors may be modified by obesity. Therefore, based on published literature and findings from our lab, it is likely that the microenvironment plays a strong etiologic role in BBC.

Summary

In modern society, lifestyle related factors might play a more important role in diseases compared to the genetic background. There is compelling evidence that the microenvironment can regulate disease onset and progress. This dissertation details evidence that the life style alters the microenvironment, which reflects and contributes to systemic inflammation, obesity, glucose intolerance, and basal-like breast cancer. This dissertation also addresses the gap in knowledge among obesity and cancer studies, which may shed light on mechanisms of how the microenvironment is regulated by lifestyle factors and leads to different diseases. Considering the high prevalence of obesity in the US and the high rate of alcohol consumption (87.6% of adults), our studies will have a significant potential to develop prevention strategies for these public health issues, like breast cancer and inflammation-related diseases.

Hypothesis: Lifestyle-related factors like alcohol consumption and high fat diet contribute to varied diseases including obesity and breast cancer through altering the microenvironment.

The hypothesis is tested in 3 different studies, which will be described in details below.

CHAPTER II: ADIPOSE INFLAMMATION AND MACROPHAGE INFILTRATION AFTER BINGE ETHANOL AND BURN INJURY.

Qin Y, Hamilton JL, Bird MD, Chen MM, Ramirez L, Zahs A, Kovacs EJ, Makowski L.

Overview

Ethanol (EtOH) exposure prior to traumatic injury, such as a burn, elevates systemic and local inflammatory responses and increases morbidity and mortality. Adipose is a large tissue mass that is often inflamed during obesity or other stresses, which disturbs metabolic homeostasis. To date, there has been little investigation into the inflammatory response of adipose tissue after combined EtOH exposure and burn injury. Two EtOH exposure regimens were utilized to examine the role of inflammation in adipose tissue after EtOH and burn injury. Mice were either given a single or episodic binge exposure to EtOH or saline followed by scald (burn) or sham injury 30 minutes later. Twenty-four hours post injury, serum and adipose tissue were collected for assessment of inflammatory mediators. Single binge EtOH alone induced no inflammation in adipose when compared with sham vehicle-treated mice. However, single binge EtOH followed by burn injury induced significant elevations in mRNA and protein concentrations of pro-inflammatory mediators interleukin-6 (IL-6), KC, and monocyte chemoattractant protein 1 (MCP-1) compared with either insult alone or sham vehicle group. Additionally, EtOH exposure and burn injury significantly blunted inducible nitric oxide synthase (iNOS), indicating a complex inflammatory response. Episodic binge EtOH exposure followed by burn injury exacerbated the postburn adipose inflammatory response. The magnitude of the episodic binge

induced inflammatory parameters postburn were 2- to 5-fold greater than the response detected after a single exposure of EtOH, indicating EtOH-induced potentiation of burn-induced inflammatory response. Finally, inflammatory loci and crown-like structures in adipose were significantly increased by episodic binge EtOH and burn injury. This is the first report of binge and burn-induced crown-like structure formation. Evidence presented herein suggests an important role for alcohol and burn as an additional mediator of adipose inflammation in postburn injury, a common complication in burn patients.

Introduction

Burn-induced hyperglycemia, hepatosteatosis, and insulin resistance are common complications observed in the burn patient population and are associated with poor outcomes, contributing significantly to morbidity and mortality^{47,48}. Insulin resistance in liver, skeletal muscle, and adipose can persist even 3 weeks after burn injury^{49,50,178}. Burn injury also drives systemic inflammation with elevations in pro-inflammatory cytokines and suppressed cell-mediated immunity, leading to multi-organ dysfunction¹⁷⁹. One mechanism of systemic insulin resistance may be through adipose dysfunction and inflammation¹⁸⁰. Macrophages are known to infiltrate adipose during states of metabolic stress, such as in obesity, and contribute to inflammation, uncontrolled lipolysis, as well as local and systemic insulin resistance¹⁸⁰.

Clinical and laboratory studies have demonstrated that ethanol exposure prior to traumatic injury, such as a burn, markedly elevates systemic and tissue-specific inflammatory responses^{9,10} and is associated with poorer outcomes¹¹. In the United States, half of the patients with burn-related injuries have alcohol in their system at the time of admission and the vast majority of those subjects are binge drinkers rather than chronic alcoholics⁸. It is well-established that alcohol increases the dysregulated inflammatory and immune response caused by burn in

animal models and patients (reviewed in⁹). We and others have shown previously that neutrophils infiltrate the gut, lung, and site of injury after the combined insult¹⁸¹⁻¹⁸⁶. While the primary role of neutrophils is to clear pathogens, they often cause damage due to production of enzymes such as elastase, reactive oxygen species, and pro-inflammatory cytokines including IL-6, IL-1 β , and tumor necrosis factor alpha (TNF α). Serum cytokines IL-6 and TNF α and tissue levels of KC and IL-6, are elevated in response to the dual insult of ethanol and burn injury compared to either injury alone^{182,186}.

Chronic ethanol has been shown to drive macrophage infiltration into adipose tissue and it is associated with reduced fat mass due to upregulated lipolysis^{187,188}. To date, it is not known how ethanol exposure combined with burn injury affects the adipose microenvironment. Using an established murine model of binge ethanol exposure and burn injury, we demonstrated that the combined insults drove systemic and adipose inflammation 24 hours post-injury. Furthermore, we found that employing an episodic multi-day binge ethanol exposure paradigm followed by burn injury potentiated adipose inflammation and induced macrophage infiltration, indicating that binge, and especially episodic binge ethanol exposure, followed by burn drives adipose inflammation that could contribute to systemic inflammation.

Results

Single and episodic binge and burn injury drive inflammation in adipose tissue

In our previous work, we demonstrated that serum IL-6 was higher at 24 hours after combined ethanol exposure and 15% total body surface area scald compared to either insult alone¹⁸⁹. To determine if adipose tissue might contribute to the elevated systemic inflammation seen after ethanol and burn injury, we examined the expression of IL-6 and other inflammatory mediators in adipose tissue. As shown in **Figure 2.1A**, IL-6 mRNA levels were not altered by

ethanol exposure alone and increased 4-fold with burn injury compared to sham mice. IL-6 mRNA was significantly upregulated after the combined insult when compared to all other groups ($P < 0.001$). Likewise, the adipose tissue level of IL-6 protein was unchanged after ethanol exposure alone, and was 6-fold higher in adipose tissue from burn vehicle mice compared to sham mice (**Figure 2.1B**). Ethanol exposure doubled the burn-induced elevation in adipose IL-6 protein (**Figure 2.1B**, $P < 0.05$ burn ethanol vs. sham groups).

Further studies were conducted to determine if a more severe alcohol exposure paradigm, such as a multi-day episodic binge prior to burn would drive adipose inflammation when compared to a single binge followed by burn. To accomplish this, mice were given ethanol (or saline) for 3 days, rested 2-4 days, and exposed again for 3 days prior to burn or sham injury. Ethanol alone did not modulate IL-6 mRNA or protein expression (**Figure 2.1C&D**). After episodic binge ethanol exposure and burn, adipose tissue IL-6 mRNA levels were 18-, 42- and 12-fold higher than sham vehicle, sham alcohol and burn vehicle, respectively, (**Figure 2.1C**, $P < 0.001$ all groups versus burn ethanol). Significant interactions existed between burn and ethanol in single binge treatment and in episodic binge for IL-6 mRNA expressions. No significant interactions were found in single and episodic binge for IL-6 protein expression. Moreover, adipose levels of IL-6 protein reached 110 pg/mg, a value which is approximately 2 times that of burn alone and 8-fold that of sham groups (**Figure 2.1D**, $P < 0.05$). Of note, IL-6 protein levels in adipose tissue were 3 times greater in tissue obtained from episodic binge and burn injury mice compared to tissue from mice exposed to a single binge and burn (**Figure 2.1B** compared to **Figure 2.1D**).

The presence of neutrophils in adipose tissue after either ethanol exposure or burn injury alone, or the combined insult was investigated, as was previously observed in gut and lung^{182,189}.

Like IL-6, levels of the neutrophil chemokine KC were not increased after a single binge ethanol exposure, however, burn alone (in the absence of ethanol exposure) elevated KC mRNA and protein by approximately 5-fold, although this did not reach significance (**Figures 2.2A&B**). A statistically significant interaction between single binge and burn existed in the mRNA expression of KC ($p<0.05$), but this was lost at the protein level. Combined binge ethanol and burn exposure significantly elevated expression of KC 8-fold at the mRNA level compared to all other groups (**Figure 2.2A**, $P<0.01$), while ethanol plus burn increased KC protein levels 50% over burn alone (**Figure 2.2B**, $P<0.05$ versus sham groups). Based upon elevations in neutrophil chemokine, we next examined if there was neutrophil infiltration into adipose tissue in response to ethanol exposure and burn injury by measuring expression of elastase, an enzyme enriched in neutrophils and demonstrated to correlate with neutrophil infiltration into adipose ¹⁹⁰. There were no significant changes in adipose tissue mRNA levels of neutrophil elastase following any treatment (**Figure 2.2C**). Although burn elevated KC mRNA levels compared to sham in episodic binge treatment, there were no statistically significant alterations between groups (**Figure 2.2D**). In contrast, while adipose tissue KC protein levels were not altered by ethanol alone, KC protein levels were nearly 4 times higher after burn alone compared to sham ethanol mice and were elevated 4-fold in ethanol plus burn injured mice compared to both sham groups ($P<0.05$, **Figure 2.2E**). There were no statistically significant interactions between burn and episodic binge in KC mRNA or protein expression. Relative to sham vehicle mice, mRNA levels of elastase were not significantly elevated after episodic binge exposure (**Figure 2.2F**). Burn alone was not different than sham vehicle, but was reduced to 40% the level of sham episodic binge (**Figure 2.2F**, $P<0.05$). However, episodic binge ethanol and burn injury dramatically blunted elastase expression 83% compared to sham vehicle ($P<0.01$) or by 89% versus sham

ethanol treated mice ($P < 0.001$, **Figure 2.2F**). This latter observation in episodic binge exposure differs from the adipose response to single ethanol exposure with and without injury where no significant differences were detected (**Figure 2.2C&2.2F**). No interaction was found in elastase mRNA expression in single binge, but there was a significant interaction ($p < 0.05$) between burn and ethanol in episodic binge.

Macrophage infiltration is evident in adipose tissue after episodic binge exposure and burn injury

We next sought to examine if macrophages were responsible for the observed elevations in adipose IL-6 levels by investigating the degree of macrophage infiltration into adipose tissue after episodic binge ethanol exposure and burn injury. We and others have demonstrated that the formation of crown-like structures is a well-documented measure of adipose tissue inflammation that correlates with insulin resistance^{23,180,188}. Immunohistochemical (IHC) analysis was used to quantitate the number of F4/80-positive (F4/80+) crown-like structures. Representative images are shown in **Figure 2.3A**. No crown-like structures were detected in sham vehicle mice (**Figure 2.3B**). Mice exposed to ethanol or burn injury alone had detectable crown-like structures, but these measures did not reach statistical significance compared to sham vehicle mice (**Figures 3B**). However, the combined injury of episodic ethanol exposure and burn yielded a significant 2.5- and 4-fold increase in the crown-like structures compared to sham episodic binge, and burn vehicle, respectively (**Figure 2.3B**, $P < 0.01$ both vehicle groups vs. burn ethanol, $P < 0.05$ sham ethanol vs. burn ethanol). Sham ethanol treated adipose samples displayed an 8-fold elevation in F4/80+ inflammatory loci compared to sham vehicle (**Figure 2.3C**, $P < 0.05$). There was a significant 12-fold increase in inflammatory loci in adipose tissue from burn vehicle, and a 16-fold increase from episodic binge and burn mice, over that of sham vehicle mice (**Figure 2.3C**,

P<0.01 sham vehicle vs. burn vehicle and P<0.001 sham vehicle vs. burn ethanol). No interaction between burn and ethanol was found in episodic binge with the numbers of crown-like structures or inflammatory loci.

The expression of monocyte chemokine MCP-1 was next examined because it is a pro-inflammatory mediator demonstrated to be necessary and sufficient to drive macrophage infiltration into adipose tissue and induce crown-like structure formation¹⁸⁰. In the absence of burn injury, mRNA and protein levels of MCP-1 were not altered by single binge ethanol alone (**Figure 2.4A&B**). The ethanol plus burn group displayed significant 5-fold increases in MCP-1 mRNA expression compared to both vehicle groups (**Figure 2.4A**, P<0.05). Burn injury alone doubled MCP-1 protein content in adipose versus sham vehicle (**Figure 2.4B**). MCP-1 protein was significantly increased in ethanol plus burn injured mice compared to sham treated groups (**Figure 2.4B**, P<0.01 sham vehicle versus burn ethanol, P<0.05 sham ethanol versus burn ethanol). Adiponectin is an anti-inflammatory adipokine that promotes insulin sensitivity¹⁸⁰. Nagy et al. demonstrated down regulation of adiponectin mRNA associated with chronic ethanol-induced adipose inflammation¹⁸⁸. Single binge and burn significantly blunted adiponectin mRNA expression by 75% (**Figure 2.4C**, sham vehicle (P<0.001) or burn vehicle (P<0.05 vs. burn ethanol). Episodic binge did not change MCP-1 mRNA expression in mice, nor were levels significantly upregulated after burn (**Figure 2.4D**). MCP-1 protein levels were elevated more than 2-fold in mice exposed to episodic binge plus burn injury versus sham vehicle controls, although this increase was not statistically significant (**Figure 2.4E**). Importantly, MCP-1 protein levels were nearly 3 times as high in adipose tissue obtained from mice with episodic binge alcohol exposure prior to burn relative to single ethanol exposure plus burn injury (**Figure 2.4B** compared to **Figure 2.4E**). Episodic binge did not modulate

adiponectin levels (**Figure 2.4F**). No significant interactions between burn and ethanol were found in MCP-1 or adiponectin mRNA or protein expression with single or episodic binge treatment.

Protein levels of other pro-inflammatory ($\text{TNF}\alpha$, IL-1 β) or anti-inflammatory (IL-10) cytokines were not significantly different between each treatment group in single binge and burn studies (**Figure 2.5 A-C**). Interestingly, inducible nitric oxide synthases (iNOS) mRNA was not altered by ethanol exposure alone, but was significantly suppressed by 75% in both burn groups when compared to respective sham treated groups with greatest attenuation due to the combination of ethanol and burn (**Figure 2.5D**, $P < 0.001$ burn treated groups vs. sham treated groups). Episodic binge followed by burn did not significantly change protein levels of $\text{TNF}\alpha$, IL-1 β and IL-10 (**Figures 2.5 E- G**). Similar to acute binge exposure and burn injury, the adipose iNOS mRNA level was not significantly altered by episodic ethanol, and was reduced by burn injury regardless of ethanol exposure. Compared to sham ethanol, burn ethanol iNOS mRNA was blunted 54% (**Figure 2.5H**, $P < 0.05$). There were no significant interactions between burn and ethanol in any of the cytokines with single or episodic binge treatment.

Discussion

Half of burn patients admitted to the hospital consumed alcohol prior to sustaining their injuries^{8,191,192}. The vast majority of inebriated burn patients is not chronic alcohol abusers, but rather binge drinkers. Recent evidence suggests that binge drinking is on the rise with 1 in 6 Americans reporting an average of four binge drinking episodes per month. Thus, gaining a better understanding about the effects of episodic binge alcohol exposure on post burn morbidity and mortality is of immediate public health relevance. Burn injury induces dramatic insulin resistance, hyperlipidemia, and hyperglycemia, contributing to elevated morbidity and

mortality^{47,49}. Ethanol exacerbates burn-induced inflammation and impairs the immune response, thus increasing a patient's susceptibility to infection⁹.

Previous work by our lab has demonstrated that IL-6 is elevated in serum, lungs and gut of animals exposed to ethanol and burn^{182,186}. We provide evidence herein that cytokines and chemokines are also elevated in adipose tissue suggesting that this tissue may be an additional source of circulating inflammatory mediators. Adipose tissue plays a critical role in maintaining systemic metabolic homeostasis, and adipose inflammation leads to metabolic dysregulation characterized by insulin resistance, hyperlipidemia and hyperglycemia – all of which commonly occur in burn patients. We set out to examine the role of adipose inflammation in response to the combined insult of ethanol exposure and burn injury. We have demonstrated that mice *singly or episodically* exposed to ethanol alone did not mount a dramatic inflammatory response in adipose tissue in the absence of a secondary insult such as burn. However, in mice administered a single ethanol binge and burn injury, there was a dramatic elevation in the pro-inflammatory response in adipose tissue indicated by elevations of cytokine and chemokines IL-6, KC, and MCP-1, along with a blunting of adiponectin, an anti-inflammatory adipokine. IL-6 is primarily secreted by macrophages and T cells to stimulate the immune response, e.g. during infection and after burn⁹, and elevated serum IL-6 in injured patients is correlated with negative outcomes¹⁹³. While we detected elevations in KC, we found that there was no change in neutrophil elastase in adipose tissue after single binge ethanol exposure, burn injury, or the combined insults. It is likely that 24 hours post-injury may not be the correct time point for the neutrophil composition of adipose to be dramatically regulated, unlike the neutrophil response in lung, skin, or gut. Furthermore, Nagy et al. reported down regulation of the anti-inflammatory adipokine adiponectin in chronic ethanol-induced adipose inflammation, while Xu et al. showed that

increasing adiponectin improves alcoholic fatty liver disease^{188,194}. We demonstrate dramatic blunting of adiponectin after single binge and burn, which may aid in driving the pro-inflammatory milieu. Finally, iNOS was down-regulated by single binge ethanol and burn injury. Interestingly, Syapin et al. have demonstrated that iNOS is inhibited by ethanol in glial cells¹⁹⁵. In other tissues, burn has been shown to elevate iNOS expression or have no effect^{196,197}. Hence, iNOS regulation by ethanol and burn in adipose needs further investigation. Taken together, our data support the findings that adipose tissue may be a source of some circulating cytokines after single binge ethanol and burn injury.

Binge drinking is not usually a single acute event; binge drinkers tend to consume alcohol in multiple binge episodes. Using an episodic binge model, we demonstrated that burn-induced inflammation was markedly elevated in mice given multiple exposures to binge levels of ethanol and that this occurred to a greater extent than following a single binge exposure. Similar to single binge, after episodic binge and subsequent burn, IL-6 and KC were elevated compared to either insult alone or sham vehicle controls. Despite elevations in KC protein in combined injury, neutrophil elastase mRNA level was dramatically reduced in burn ethanol groups relative to either insult alone. This was a surprising finding because other insults such as a 3 day exposure to high fat diet have been shown to induce neutrophil infiltration into adipose tissue^{190,198}, which persisted for up to 90 days¹⁹⁰. Perhaps a more detailed study of episodic binge and burn injury over a time course might capture neutrophil infiltration in response to high levels of KC. Even with dramatic increases in IL-6, KC, and MCP-1 associated with episodic binge ethanol exposure, iNOS was blunted similar to a single binge. It is evident that while some production of pro-inflammatory cytokines or chemokines occurs in response to burn and ethanol, some immunosuppression is concurrent. Future studies will include examining the role of IL-6 in

adipose inflammation as it has been shown to be both pro-inflammatory and anti-inflammatory in binge and burn injured animals, and may mediate some of the divergent effects demonstrated.

Finally, we report for the first time that F4/80+ macrophages were detected in adipose crown-like structures and inflammatory loci resulting from episodic binge ethanol exposure and burn injury, likely due to elevations in MCP-1. MCP-1 and its receptor CCR2 have been shown to mediate macrophage infiltration into adipose tissue in response to obesity¹⁸⁰, and these infiltrating macrophages often surround dying adipocytes forming crown-like structures¹⁸⁰. Kang et al. have demonstrated infiltration of macrophages and production of pro-inflammatory cytokines, IL-6, MCP-1 and TNF α , in adipose tissue after chronic ethanol exposure for 4 weeks¹⁸⁸. Our data demonstrate that macrophage infiltration occurs within days after burn and ethanol exposure.

From our studies it is evident that burn injury primarily drives inflammation in adipose tissue, and ethanol exposure prior to burn potentiates this response. The dramatic increase in magnitude of response between single and episodic binge exposure suggests that the driving factor in the inflammatory response is the frequency of the ethanol exposure, since the burn injury and time of sacrifice is identical in each group. Our findings support the relevance of adipose inflammatory response to ethanol and burn insult that warrants further investigation. Like ethanol, obesity is also associated with a prolonged increase in pro-inflammatory mediators, such as IL-6 and MCP-1, an impaired immune response, and an increased susceptibility to bacterial infection^{180,199}. Work from our group and others over the past decade has linked adipose inflammation to obesity and insulin resistance^{22,23,180}.

One mechanism linking both obesity-induced inflammation and ethanol exposure that could drive insulin resistance is an increase in gut permeability, resulting in bacterial

translocation into tissues to induce both organ-specific and systemic inflammation. We have previously reported on increased gut permeability and bacterial translocation in ethanol and burn models^{183,186,200,201}. In humans and murine models, elevated morbidity and mortality result after burn injury due to inflammation secondary to intestinal permeability and septicemia^{183,186,201-203}, which is often followed by an exaggerated alcohol-induced suppression of immune function through a lower delayed-type hypersensitivity (DTH) response and blunted lymphocyte proliferation²⁰³⁻²⁰⁶. At 6 and 24 hours post ethanol plus burn injury, gut permeability is compromised, which could account for elevated leukocyte infiltration, and IL-1 β and IL-6 in mice exposed to ethanol then burn as compared to either insult alone^{183,186}. Gut bacteria also regulate obesity susceptibility and systemic inflammation in response to high fat diet²⁰⁷. Additionally, we have previously demonstrated the dependence of toll-like receptor 4 (TLR4, but not TLR2) in ethanol and burn-induced lung pathology and pro-inflammatory response¹⁸⁹. TLR4 has also been shown to be necessary for obesity-induced inflammation²⁰⁸. Elevated gut permeability and bacterial translocation after the combined insult of ethanol and burn may be responsible for the rise in lipopolysaccharide (LPS, endotoxin) burden and a TLR4 dependent inflammatory response in adipose, similar to obesity.

A second mechanism regulating ethanol and burn-induced alterations in adipose inflammation is lipolysis and adipocyte apoptosis, which would release free fatty acids into the local microenvironment and circulation. In humans, chronic alcohol use correlated with reduced fat mass²⁰⁹. Burn injury also results in loss of fat mass through apoptotic cell loss²¹⁰. Duffy et al. (2009) demonstrated that insulin and glucose are elevated in patients post-burn compared to healthy controls, with burn-induced increases in cytokine release from adipose tissue macrophages and circulating monocytes, which could interfere with insulin signaling²¹¹. In

rodents, single binge and burn drive a transient microvesicular steatosis, while chronic alcohol exposure also leads to reduced fat mass and adipocyte size, along with an increase in hepatosteatosis and induction of systemic insulin resistance^{187,212}. It has been shown that alcohol-driven lipolysis is not catecholamine-mediated²¹³. Ethanol has been shown to increase levels of phosphatase and tensin homolog (*PTEN*) and suppressor of cytokine signaling (*SOCS3*), which are important negative regulators of insulin signaling in both liver and adipose and can lead to elevated lipolysis and cytotoxicity^{187,214}. It is possible that saturated free fatty acids liberated by lipolysis, which are known to signal through TLRs during obesity-induced inflammation and insulin resistance²¹⁵, may mediate a pro-inflammatory response after ethanol and burn exposure. Additionally, reduction in fat mass through apoptosis or lipolysis contributes to reduced insulin sensitivity because fat is redistributed from adipose to other metabolically sensitive tissues, such as the liver where hepatosteatosis ensues¹⁸⁰. Liver IL-6 and other pro-inflammatory mediators increase with ethanol and/or burn exposure^{182,216}. Emanuele et al. demonstrated single and/or combined injury increased hepatic ICAM-1, IL-1 β , TNF α , and nuclear NF-KB²¹⁷ which can lead to insulin resistance. Indeed, we have previously reported that insulin administration to rodents after ethanol and burn, improves liver inflammation and microvesicular steatosis, demonstrating further evidence of links between metabolic homeostasis and inflammatory response²¹⁷.

Finally, a third mechanism linking ethanol intake to exacerbated inflammation is oxidative stress resulting from alcohol metabolism. Besides alcohol dehydrogenase (ADH), ethanol can also be metabolized through the microsomal ethanol oxidizing system (MEOS) by cytochrome P4502E1 (CYP2E1), which has been shown to lead to increased oxidative stress⁴⁰. CYP2E1 is mainly expressed in the liver, but also found in the white adipose tissues²¹⁸. Sebastian et al. demonstrated that CYP2E1 protein levels in adipose tissue were increased after

chronic ethanol feeding²¹⁹. In our study, we failed to find a significant increase in mRNA or protein expression of CYP2E1 in adipose tissue of episodic binge, burned mice, or the combined exposure (data not shown). This may be due to the type or length of exposure, as our treatment was shorter with either a one-dose single binge or episodic binge constituting a total of 6 days of ethanol exposure.

Taken together, we report for the first time that there is an inflammatory response in adipose tissue after the combined insult of ethanol and burn injury, and that this response is augmented after episodic binge relative to a single ethanol exposure. While binge drinking leads to unintentional injuries such as falls, crashes and burns, it may also lead to more insidious tissue inflammation as comorbidity with obesity leading to insulin resistance. Future studies in lean versus obese rodents could yield further mechanistic insight into burn and ethanol-induced effects on local and systemic inflammation.

Methods

Mice. Male C57BL/6 mice, 8 to 10 weeks old, were obtained from Jackson Laboratories (Bar Harbor, ME). They were housed in cages with food and water available *ad libitum* at the Loyola University Medical Center Animal Facility in rooms that were temperature and humidity controlled on a 12-h light-dark cycle. All animal studies described here were performed according to the Animal Welfare Act and the Guide for the Care and Use of Laboratory Animals, National Institutes of Health and were approved by the Loyola University IACUC. Before each experiment, mice were weighed and those weighing 22 to 27 grams were used in the studies.

Murine model of ethanol exposure and burn injury. The murine model of a single binge ethanol exposure and burn injury was employed as described previously^{205,220} with minor modifications¹⁸⁹. Briefly, mice were given 1) either a single binge dose of 150 μ l of 20% (v/v)

ethanol solution (1.12 g/kg) intraperitoneally (i.p.) that resulted in a blood ethanol level of 150 mg/dl at 30 minutes or saline vehicle²²¹ or 2) for episodic binge exposure, mice were given the same dose of ethanol (or saline) daily for 3 days consecutively, rested for 2-4 days (rest time did not alter outcome, data not shown), and then given 3 additional daily exposures. Thirty minutes after ethanol exposure (or the last ethanol exposure in the case of the episodic binge paradigm), mice were anesthetized with 100 mg/kg of Ketamine and 10 mg/kg of Xylazine (Webster Veterinary, Sterling, MA), their dorsum shaved, and placed in a plastic template exposing 15% of the total body surface area of their back²²⁰ and subjected to a scald injury in a 90 to 92°C water bath for 8 seconds. As a control, sham animals were anesthetized, shaved, and immersed in room temperature water. The scald injury resulted in an insensate, full-thickness burn injury of approximately 15% total body surface area¹⁸¹. To compensate for fluid loss and prevent circulatory shock, all animals received 1 mL of body temperature saline i.p. immediately after burn injury and were allowed to recover on warming pads. No other therapeutic intervention was provided as administration of anti-inflammatory or analgesic medication may introduce confounding factors into the assessment of inflammatory responses. Twenty-four hours after burn injury, mice were sacrificed using carbon dioxide (CO₂) inhalation and cervical dislocation. Blood was collected for serum isolation and measurement of cytokines. Epididymal white adipose tissue was removed. Tissue was either snap frozen in liquid nitrogen and stored at -80°C for mRNA isolation or immunologic analysis or fixed in paraformaldehyde, paraffin-embedded, and sectioned for immunohistochemistry.

RNA isolation and analysis. QIAzol Lysis Reagent was used to isolate mRNA from adipose tissue with DNase treatment (RNeasy Lipid Tissue Mini Kit mRNA; Qiagen, Valencia, CA). For quantitative PCR (qPCR) analysis, cDNA was synthesized using an iScript cDNA synthesis

kit (Bio-Rad, Hercules, CA). Real-time qPCR was completed using TaqMan Assay on Demand primers/probe sets (Applied Biosystems, Carlsbad, CA) as previously described²³. qPCR reactions were run using an Applied Biosystems thermocycler and SDS 2.4 software (Applied Biosystems, Carlsbad, CA).

Quantification of IL-6 in serum. Blood was obtained by cardiac puncture after sacrifice. Serum IL-6 levels were determined by multiplex according to manufacture instructions (Invitrogen, Carlsbad, CA), as previously described¹⁸⁹.

Analysis of cytokine and chemokine protein levels. Adipose tissue was homogenized in 1 mL of BioPlex Cell Lysis Buffer according to manufacturer's protocol (BioRad, Hercules, CA). Homogenates were then filtered and analyzed for IL-6, MCP-1, KC, TNF α , IL-10 and IL-1 β protein levels by multiplex (BioRad, Hercules, CA) and normalized to the total amount of protein in adipose tissue homogenate as described¹⁸⁹.

Immunohistochemistry (IHC) examination of episodic binge exposed and burn-injured adipose. Paraffin-embedded tissues were sectioned at 5 microns and mounted for histological staining. Briefly, immunohistochemistry was carried out using anti-F4/80 primary antibody (Abcam ab562), similar to Sampey et al.²³. All histological sections were digitally scanned on the Aperio ScanScope CS Ultra-Resolution Digital Scanner and analyzed by ScanScope Image Analysis Toolbox software (Aperio Inc., Vista, CA). Representative images for adipose tissue from each treatment group were selected. To determine the inflammatory state of the adipose tissue, ten randomly selected 10 \times fields per study animal were quantified for number of crown-like structures and inflammatory loci including F4/80+ macrophage staining. N= 4-7 mice per group.

Statistical Analysis. Data are shown as means \pm SEM. Analysis was performed using two-way analysis of variance (ANOVA). Post hoc comparisons were made with the Tukey post hoc test

using JMP (SAS Institute, Cary, NC) and significant interactions are described. $P < 0.05$ was considered significant.

Figures and Tables

Figure 2.1

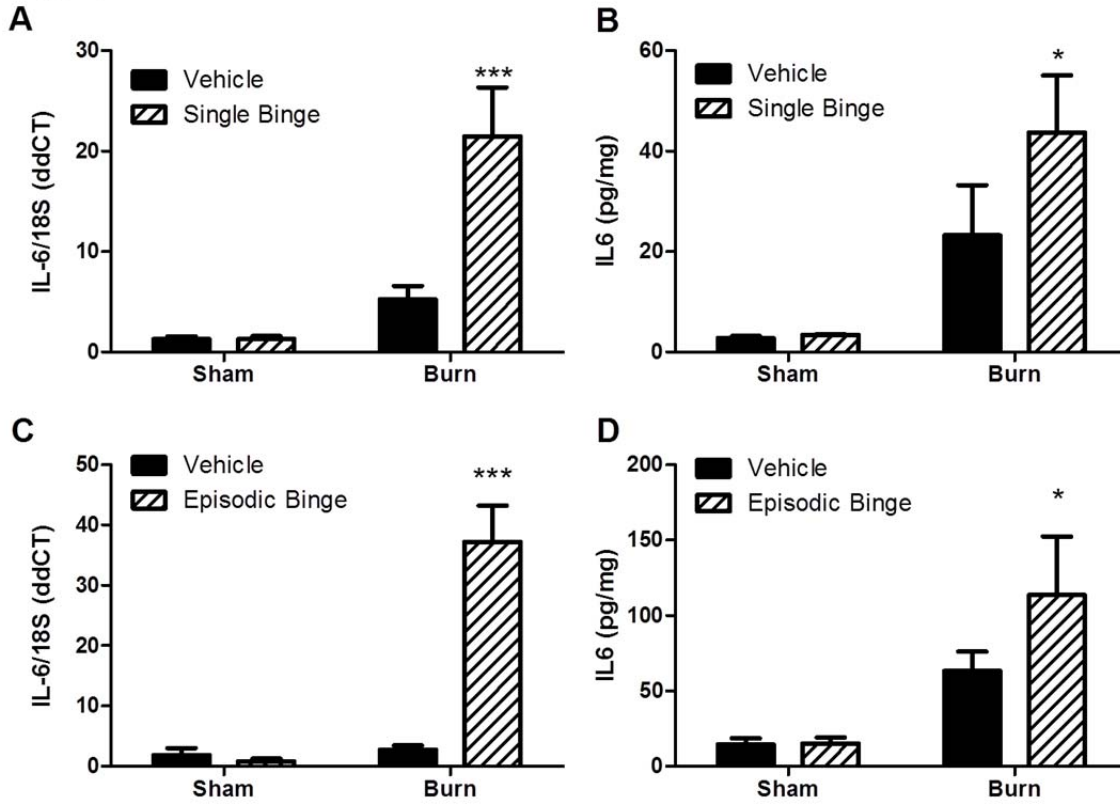


Figure 2.1. Interleukin-6 (IL-6) levels increase after single and episodic binge ethanol exposure and burn injury. Mice received single binge (A-B), episodic binge (C-D), or vehicle control. Thirty minutes after ethanol, mice were either subjected to burn or sham injury, sacrificed 24 hours later, and adipose tissue was isolated, as described in methods. A. IL-6 mRNA was measured by quantitative (q)PCR and normalized to 18S. N=16, 16, 18 and 19 for sham vehicle, sham ethanol, burn vehicle and burn ethanol, respectively. There was a significant interaction between burn and ethanol ($p < 0.05$). *** $P < 0.001$ versus (vs.) all groups. B. Whole adipose tissue was homogenized and IL-6 protein levels were determined and normalized to the total amount of protein in the homogenate. N=4, 3, 5 and 5 for sham vehicle, sham ethanol, burn vehicle and burn ethanol, respectively. No significant interaction was found between burn and ethanol. * $P < 0.05$ vs. sham groups. C. After episodic binge and burn, IL-6 mRNA was measured by qPCR and normalized to 18S. N=7, 4, 7 and 10 for sham vehicle, sham ethanol, burn vehicle and burn ethanol, respectively. There was a significant interaction between burn and ethanol ($p < 0.05$). *** $P < 0.001$ vs. all groups. D. IL-6 protein levels were detected after episodic binge in adipose tissue and were normalized to total protein as above. N=7, 5, 12 and 10 for sham vehicle, sham ethanol, burn vehicle and burn ethanol, respectively. There was no significant interaction between burn and ethanol in episodic binge treatment. * $P < 0.05$ vs. sham groups.

Figure 2.2

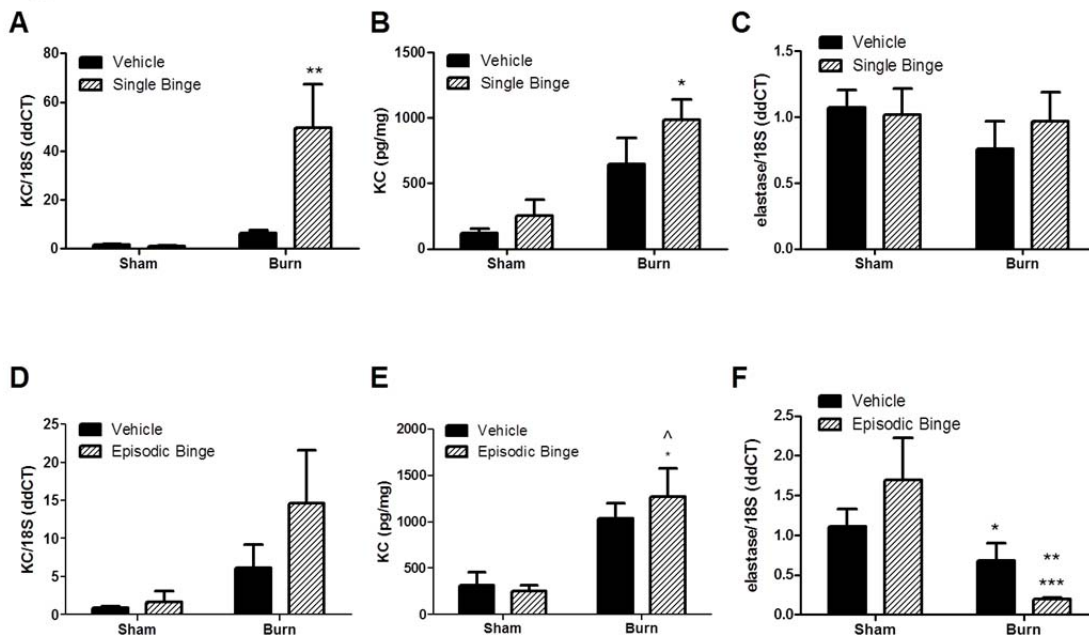


Figure 2.2. Adipose expression of neutrophil chemokine KC after single and episodic binge ethanol and burn injury. Mice received single (A-C) or episodic binge (D-F), or vehicle control and burn, as described above. A. Adipose tissue KC mRNA levels were measured by qPCR and normalized to 18S. N=20, 20, 27 and 21 for sham vehicle, sham ethanol, burn vehicle and burn ethanol, respectively. There was a significant interaction between burn and ethanol ($p < 0.05$). ** $P < 0.01$ vs. all other groups. B. Whole adipose tissue homogenate levels of KC protein were determined and normalized to the total protein. N=4, 3, 5 and 4 for sham vehicle, sham ethanol, burn vehicle and burn ethanol, respectively. No significant interaction was found between burn and ethanol. * $P < 0.05$ vs. sham groups. C. Neutrophil elastase mRNA level was quantified by qPCR in adipose tissue and normalized to 18S. N=12, 11, 16 and 15 for sham vehicle, sham ethanol, burn vehicle and burn ethanol, respectively. There was no significant interaction between burn and ethanol. D. After episodic binge and burn, adipose tissue KC mRNA levels were measured by qPCR and normalized to 18S. N=6, 4, 7 and 8 for sham vehicle, sham ethanol, burn vehicle and burn ethanol, respectively. E. Whole adipose tissue KC protein levels were determined and normalized to total protein. N=7, 5, 12 and 10 for sham vehicle, sham ethanol, burn vehicle and burn ethanol, respectively. There was no interaction between burn and ethanol ($p < 0.05$) in episodic binge treatment. * $P < 0.05$ vs. sham vehicle. ^ $P < 0.05$ vs. sham ethanol group. F. Neutrophil marker elastase mRNA level was quantified after episodic binge or burn by qPCR in adipose tissue. N=7, 4, 7 and 13 for sham vehicle, sham ethanol, burn vehicle and burn ethanol, respectively. There was a significant interaction between burn and ethanol ($p < 0.05$). * $P < 0.05$ vs. sham ethanol. ** $P < 0.001$ vs. sham vehicle. *** $P < 0.001$ vs. sham ethanol.

Figure 2.3

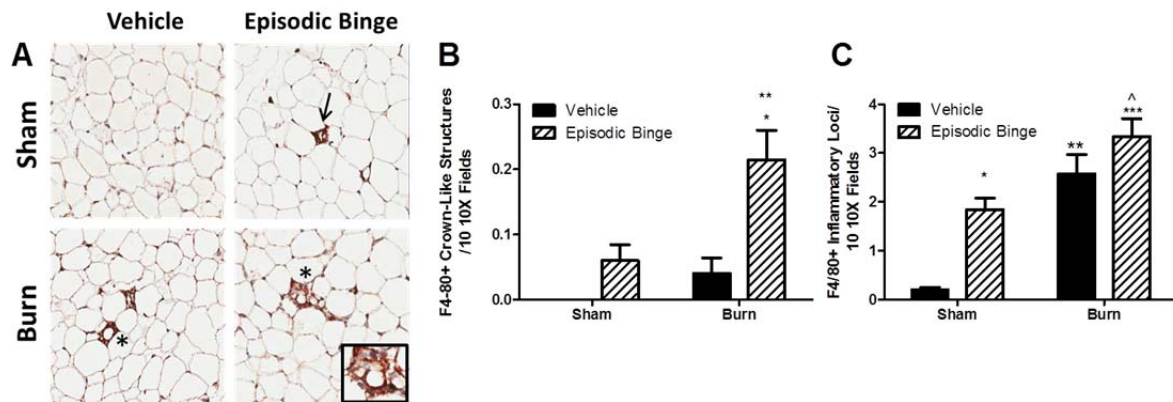


Figure 2.3. Episodic binge ethanol and burn injury drives crown like structure formation. A. Representative immunohistochemical images of macrophage marker F4/80-positive staining in adipose tissue from vehicle, episodic binge, sham or burn injured mice (10X, N= 4,5, 5 and 7 for sham vehicle, sham ethanol, burn vehicle and burn ethanol, respectively). Inflammatory loci (arrow) and crown like structure (*, and inset) are indicated. Ten randomly selected 10× fields were assessed for F4/80+ crown like structures (B, $P < 0.01$ vs. both vehicle groups, $P < 0.05$ vs. sham ethanol) and inflammatory loci (C, * $P < 0.05$, ** $P < 0.01$, *** $P < 0.001$ vs. sham vehicle mice and \wedge $P < 0.05$ vs. sham ethanol). No significant interaction was found between burn and ethanol.

Figure 2.4

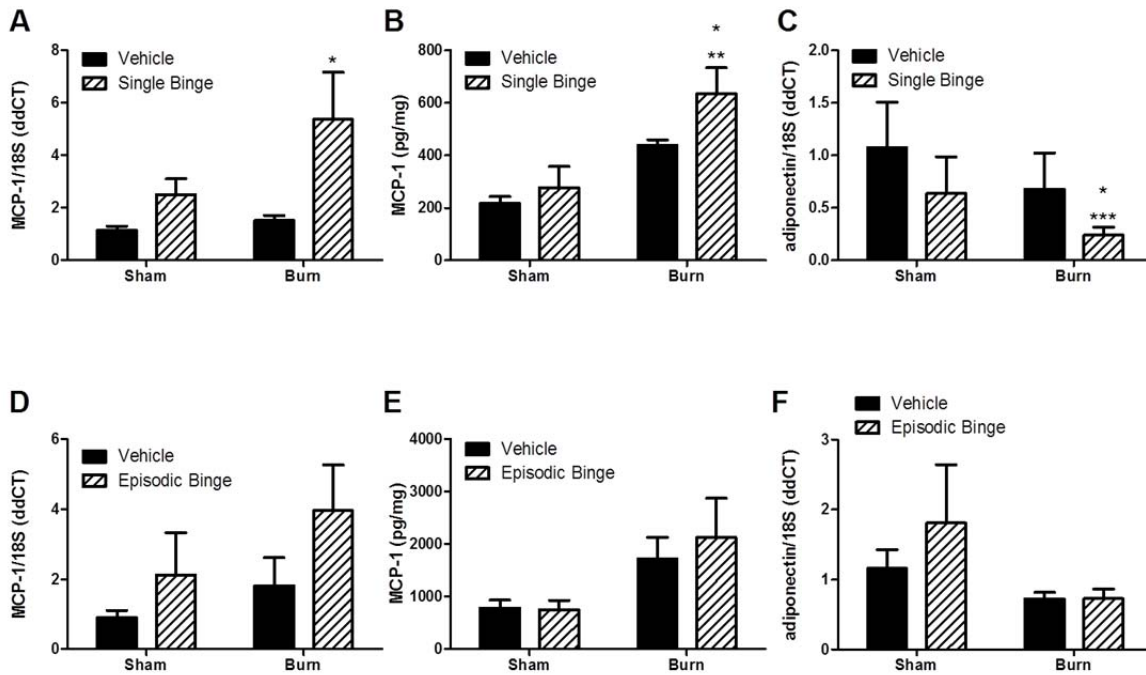


Figure 2.4. Adipose chemokine levels of monocyte chemotactic protein-1 (MCP-1) and adiponectin were inversely regulated after single and episodic binge ethanol and burn injury. Mice received single (A-C) or episodic binge ethanol (D-F), or vehicle control and burn. A. Adipose tissue MCP-1 and 18S mRNA levels were measured. N=16, 16, 20 and 19 for sham vehicle, sham ethanol, burn vehicle and burn ethanol, respectively. * P<0.05 vs. vehicle. B. MCP-1 protein levels were examined and normalized to total protein. N=4, 3, 3 and 4 for sham vehicle, sham ethanol, burn vehicle and burn ethanol, respectively. *P<0.05 vs. sham ethanol, **P<0.01 vs. sham vehicle. C. Adipose tissue adiponectin and 18S mRNA levels were measured. N=8, 8, 9 and 8 for sham vehicle, sham ethanol, burn vehicle and burn ethanol, respectively. *P<0.05 vs. burn vehicle, ***P<0.001 vs. sham vehicle. D. In adipose tissue from mice exposed to episodic binge or burn, MCP-1 and 18S mRNA levels were measured. N=6, 4, 6 and 13 for sham vehicle, sham ethanol, burn vehicle and burn ethanol, respectively. E. MCP-1 protein was normalized to the total amount of protein lysate. N=7, 4, 12 and 11 for sham vehicle, sham ethanol, burn vehicle and burn ethanol, respectively. F. After episodic binge, adipose tissue adiponectin and 18S mRNA levels were measured. N=7, 4, 7 and 14 for sham vehicle, sham ethanol, burn vehicle and burn ethanol, respectively. No significant interactions between burn and ethanol were found with single or episodic binge treatment for MCP-1 and adiponectin levels.

Figure 2.5

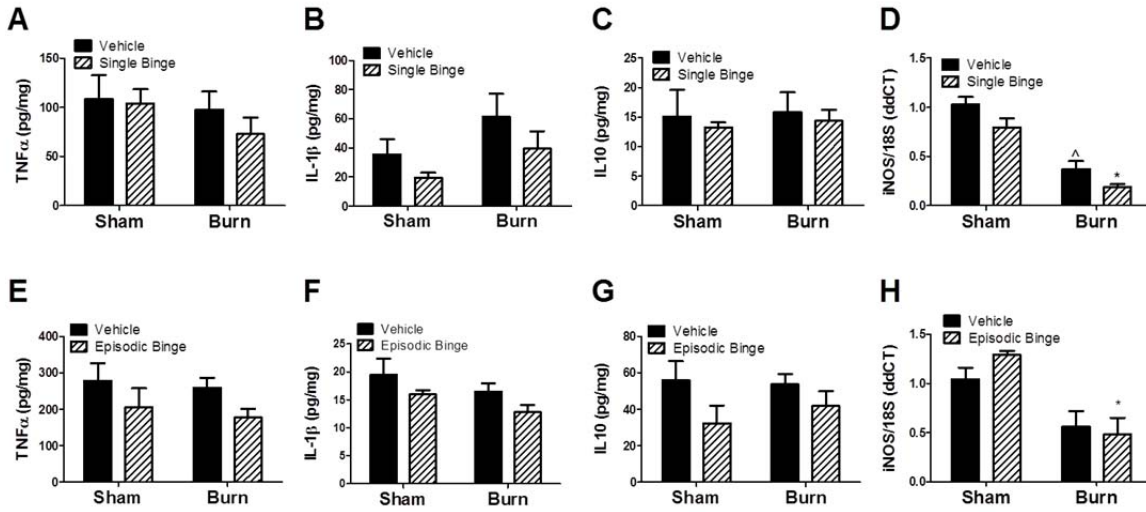


Figure 2.5. Single and episodic binge followed by burn injury failed to upregulate pro-inflammatory mediators. Mice received single (A-D) or episodic binge (E-H), or vehicle control and burn. A-C. Adipose tissue TNF α , IL-1 β , or IL-10 was measured and normalized to total protein. N=4, 3, 5 and 5 for sham vehicle, sham ethanol, burn vehicle and burn ethanol, respectively. D. Adipose tissue iNOS mRNA level was measured by qPCR. N=12, 12, 15 and 15 for sham vehicle, sham ethanol, burn vehicle and burn ethanol, respectively. ***P<0.001 vs. sham groups. ^^^P<0.001 vs. sham groups. E-G. After episodic binge and burn, adipose tissue levels of TNF α , IL-1 β , or IL-10 were measured and normalized to total protein. N=6, 5, 12 and 11 for sham vehicle, sham ethanol, burn vehicle and burn ethanol, respectively. H. Adipose tissue iNOS mRNA level was measured after episodic binge by qPCR as above. N=7, 4, 7 and 13 for sham vehicle, sham ethanol, burn vehicle and burn ethanol, respectively. *P<0.05 vs. sham ethanol. There were no significant interactions between burn and ethanol detected.

CHAPTER III: MACROPHAGE FATTY ACID TRANSPORTER 1 (FATP1) DRIVES ALTERNATIVE MACROPHAGE POLARIZATION AND LIMITS OBESITY-INDUCED INFLAMMATION

Amy R. Johnson, Yuanyuan Qin, Alex J. Freerman, Megan J. Huang, Alyssa J. Cozzo, Liyang Zhao, Brante P. Sampey, J. Justin Milner, Melinda A. Beck, Blossom A. Damania, Joseph A. Galanko, Matthew L. Edin, Darryl C. Zeldin, Patrick T. Fueger, Brittney Bivins, Andreas Stahl, Ying Wu, Karen L. Mohlke, Liza Makowski

Submitted to the Journal of Clinical Investigation (JCI)

Overview

Obese adipose recruits monocytes that become classically-activated macrophages (MΦs) associated with insulin resistance. In contrast, alternatively-activated MΦs safeguard insulin sensitivity. How the adipose microenvironment directs MΦ polarization remains unclear. MΦ subtypes display specific metabolic signatures; the process of alternative activation requires lipid metabolism. We discovered an unprecedented role for fatty acid transport and acyl-CoA synthetase function through activity of fatty acid transporter 1 (FATP1) which was necessary to establish the alternatively-activated MΦ phenotype and maintain glucose tolerance in diet-induced obesity. C57BL/6J mice transplanted with *Fatp1*^{-/-} bone marrow and fed a high fat diet gained more weight, were hyperglycemic, and glucose intolerant. Lack of MΦ FATP1 increased white adipose mass, inflammation, lipid peroxidation, and NLRP3 inflammasome activation. Using *Fatp1*^{-/-} bone marrow derived MΦs (BMDM) and a FATP1 over-expressing (FATP1-OE) MΦ cell line, we demonstrated that FATP1 profoundly regulated alternative MΦ polarization through controlling substrate metabolism. *Fatp1*^{-/-} BMDMs exhibited an exaggerated classically-

activated phenotype while FATP1-OE cells failed to mount a classic LPS response. Importantly, specific genetic variations were identified that significantly associated with FATP1 expression levels in humans. FATP1 expression level was inversely proportional to waist circumference, a strong risk factor for metabolic disease, suggesting FATP1 activity as a novel therapeutic target.

Introduction

Chronically inflamed white adipose tissue is a hallmark of obesity and this perpetual, low-grade inflammation contributes to systemic metabolic dysregulation such as insulin resistance, type 2 diabetes, cardiovascular disease, and cancer^{13,18}. The adipose microenvironment is shaped by local and systemic conditions. Within the adipose milieu, alternatively activated MΦs (AAM) safeguard insulin sensitivity and maintain tissue homeostasis via remodeling, wound healing, and secretion of anti-inflammatory cytokines like IL-10¹⁸. With the onset and progression of obesity, dramatic changes within the adipose microenvironment occur, including an influx of monocytes that are directed by the conditions within the microenvironment to differentiate into classically activated, pro-inflammatory MΦs (CAM). Persistent CAM activation sustains adipose inflammation, eventually leading to impaired function of this tissue.

An array of MΦ subtypes exists which lie along a polarization continuum with CAM and AAM at either extreme. Upon activation, CAM and AAM populations can be distinguished by characteristic differences in metabolic reprogramming events. CAM exhibit a significant up-regulation of glucose metabolism, particularly flux through the pentose phosphate pathway to generate reactive oxygen species (ROS) that are used to destroy invading pathogens. As second messengers, ROS enhance production of inflammatory enzymes, cytokines, and chemokines such as iNOS, TNF- α , MCP-1 and IL-6^{18,21}. Indeed, in a demonstration of the tight link between

MΦ metabolic reprogramming and polarization state, we reported that CAM polarization is achievable by enhancing glucose metabolism via glucose transporter 1 (GLUT1) over-expression in an *in vitro* model²²². We showed that the GLUT1-mediated enhancement of glucose metabolism through the glycolytic and pentose phosphate pathways was necessary and sufficient to polarize MΦs to the CAM phenotype in the absence of other activating stimuli²²². Other activated immune cells, including T effector cells, exhibit a similar Warburg-like metabolic shift similar to that of CAM⁶⁴. In contrast to CAM, fatty acid metabolism, particularly fatty acid oxidative metabolism in the mitochondria, is required to achieve the AAM polarization phenotype²⁰.

Exactly how MΦ phenotypes are regulated within tissue microenvironments remains unclear; however, investigation into these processes will reveal unique therapeutic targets aimed at controlling obesity-associated inflammation -- an early event in Metabolic Syndrome. It's likely that MΦ inflammatory tone can be modulated by the relative availability of fuel substrates to adipose tissue infiltrating monocytes and MΦs^{18,222}. Herein, we aimed to identify novel mediators of MΦ metabolism that would control CAM/AMM activation. We hypothesized that maintaining persistent AAM activation could be achieved by modulating transport and metabolism of specific fatty acids which would ultimately suppress MΦ-mediated inflammation and, thus, preserve metabolic health. Fatty acid transport protein 1 (FATP1, SLC27A1) is an ideal candidate for controlling AAM polarization: FATP1 is an acyl-CoA synthetase with affinity for long and very long chain fatty acids (LCFA and VLCFA, respectively), which lends specificity to its function. To date, there are no reports detailing the role of FATP1 in MΦ function and inflammatory diseases. We demonstrate for the first time that FATP1 provides a unique mechanism by which AAM/CAM ratio may be regulated. FATP1 expression is highest in

AAM compared to CAM and plays a critical role in suppressing adipose tissue inflammation and maintaining systemic glucose tolerance. C57BL/6J mice lacking MΦ FATP1 after bone (“B”) marrow transplant (*Fatp1^{B-/-}*) gained more weight when fed a high fat diet (HFD), which resulted in exacerbated glucose intolerance compared to mice that were transplanted with wild-type littermate marrow (*Fatp1^{B+/+}*) fed the same diet. Systemic glucose dysregulation resulted from larger adipose mass in obese *Fatp1^{B-/-}* mice as well as enhanced inflammation characterized by increased MΦ infiltration, crown-like structure formation, greater pro-inflammatory cytokine expression, and elevated lipid oxidative damage compared to HFD-fed *Fatp1^{B+/+}*. The absence of MΦ FATP1 increased inflammation was due, in part, to elevated priming and activation of the NLRP3 inflammasome in HFD-fed *Fatp1^{B-/-}* adipose compared to controls.

To determine the internal MΦ metabolic and inflammatory consequences of loss or gain of FATP1 function, we turned to *in vitro* models. *Fatp1^{-/-}* bone marrow derived MΦs (BMDM) underwent a primary substrate switch from fatty acid to glucose as determined by reduced acyl-CoA synthetase (ACSL) activity, fatty acid uptake and oxidation, with concomitant enhanced *Glut1* expression, glycolytic rate and shunting of glucose to the pentose phosphate pathway. Deletion of *Fatp1* primed BMDM for an enhanced pro-inflammatory phenotype and an inability to polarize to AAM. In contrast, FATP1-over-expressing RAW246.7 MΦs (FATP1-OE) induced the reverse metabolic substrate switch away from glucose and toward fatty acid metabolism: FATP1-OE displayed elevated ACSL enzymatic activity and fatty acid uptake, along with decreased *Glut1* expression, diminished glycolytic rate and glucose oxidation. LPS-stimulated expression and secretion of inflammatory cytokines were dramatically blunted in FATP1-OE MΦs. Together these data indicate that FATP1 directs MΦ metabolic reprogramming and promotes AAM polarization.

Finally, we identified variants located in and near *FATP1* associated with *FATP1* expression in human adipose tissue. *FATP1* transcript levels were inversely correlated with waist circumference in population studies. Because central adiposity is a risk factor for metabolic disease, our observations suggest that *FATP1* expression may influence metabolic health in humans. In summary, MΦ *FATP1* protects against obesity-induced inflammation and safeguards systemic glucose metabolism through maintenance of AAMs and adipose tissue homeostasis.

RESULTS

***Fatp1* is expressed at greater levels in AAM compared to CAM-polarized BMDM.** To compare the levels of *Fatp1* expression in the CAM and AAM polarization states, BMDMs were isolated from C57BL/6J mice and polarized to either the CAM phenotype (5ng/mL LPS, 10ng/mL IFN γ) or to the AAM phenotype (10ng/mL IL-4) for 24 hours^{20,222}. *Fatp1* mRNA was expressed at a level 60% higher in AAM-polarized BMDM compared to CAM-polarized BMDM (**Figure 3.1A**). *In silico* interrogation of existing mouse expression data suggested that *Fatp1* was down-regulated when BMDM or thioglycollate-elicited peritoneal MΦs isolated from mice were stimulated with LPS for 24 or 7 hours, respectively, whereas *Fatp1* expression was not detected in other immune cells²²³.

A lack of *FATP1* in MΦs exacerbates HFD-induced weight gain, hyperglycemia, and glucose intolerance. Based on the observed differential expression pattern of *Fatp1* in CAM and AAM, we investigated the extent to which MΦ *FATP1* contributed to inflammation and HFD-induced obesity. Male C57BL/6J recipient mice were randomized onto either LFD or HFD at 3 weeks of age. After 3 weeks on the diets (i.e., at 6 weeks of age), fasting glucose and MRI-determined body composition were identical for all mice regardless of diet group (data not shown). At this time point, recipient mice were lethally irradiated and transplanted with bone

marrow from *Fatp1*^{+/+} and *Fatp1*^{-/-} donor mice to generate chimeric mice harboring either *Fatp1*^{bonemarrow+/+} (*FATP1*^{B+/+}) or *Fatp1*^{bonemarrow-/-} (*Fatp1*^{B-/-}) (**Figure 3.1B**). Control mice that were irradiated but did not receive marrow died within 10 days of irradiation. Hematologic and flow cytometric analysis of *Fatp1*^{+/+} and *Fatp1*^{-/-} donor mice demonstrated no significant differences in any measure including white blood cells, lymphocytes, granulocytes, monocytes, by either total numbers of cells or percentage of cells within the total blood cell population (**Tables 3.1 and 3.2**).

To confirm successful ablation and reconstitution of *Fatp1*-deficient marrow, BMDM were isolated from a cohort of LFD-fed and HFD-fed *Fatp1*^{B+/+} and *Fatp1*^{B-/-} mice; there were no significant differences in number or appearance of BMDM isolated from the transplanted and diet-exposed mice (**Figure 3.1C**). **Figure 3.1D** illustrates that the irradiation and reconstitution with *Fatp1*^{+/+} or *Fatp1*^{-/-} marrow was successful as only the mutated *Fatp1* allele was detectable in the BMDM isolated from mice transplanted with *Fatp1*^{-/-} bone marrow. Gene expression (not shown) and immunoblot analysis of these BMDM demonstrated that FATP1 was successfully ablated from MΦs in this model (**Figure 3.1E**).

As expected, C57BL/6J recipient mice fed HFD gained more weight compared to LFD-fed mice, regardless of *Fatp1* bone marrow genotype until the time of BMT (**Figure 3.2A**). After irradiation and reconstitution, *Fatp1*^{B-/-} mice gained significantly more weight compared to *Fatp1*^{B+/+} on HFD (P<0.0001 from 15 weeks through to sacrifice at 23 weeks on diet). After 23 weeks on diet, random-fed blood glucose concentrations were significantly elevated in *Fatp1*^{B-/-} mice compared to *Fatp1*^{B+/+} on HFD (P< 0.05, **Figure 3.2B**). At termination, however, 6-hour-fasted blood glucose concentrations did not differ significantly by genotype (data not shown). LFD-fed *Fatp1*^{B+/+} and *Fatp1*^{B-/-} fasted blood glucose concentrations were an average of 133

mg/dL for both genotypes, whereas HFD-fed concentrations were 131.5 and 147 mg/dL, respectively. Six-hour-fasted plasma insulin concentrations at termination revealed no significant differences among the groups (**Figure 3.2C**). Likewise, there were no differences in homeostasis model assessment of insulin resistance (HOMA_{IR}) or homeostasis model % β cell function ($\text{HOMA}_{\% \beta}$) (data not shown).

Glucose tolerance test (GTT) and insulin tolerance tests (ITT) were performed to evaluate systemic metabolic responses in *Fatp1*^{B+/+} and *Fatp1*^{B-/-} LFD- and HFD-fed mice. Overall, HFD in this BMT model did not induce dramatic defects in glucose disposal, similar to other BMT models (**Figure 3.2D**). However, circulating glucose concentration at 15 minutes post glucose injection was significantly higher in *Fatp1*^{B-/-} mice on HFD ($P < 0.001$), which correlated to delayed and inefficient disposal of glucose compared to *Fatp1*^{B+/+} for the remainder of the time course (30 minutes: $P = 0.004$; 60 minutes: $P = 0.03$, 120 minutes: $P = 0.04$). Area under the curve (AUC) calculations of the GTT results corroborated the HFD-fed *Fatp1*^{B-/-} glucose intolerance (**Figure 3.2E**). Interestingly, ITT and AUC calculations indicated that neither diet nor genotype affected the glucose response to an injection of insulin (**Figures 3.2F and G**). Furthermore, histologic and immunohistologic analysis of insulin staining and morphology of islets in pancreata did not demonstrate significant alterations in number or size of islets between diet and genotypes (data not shown).

***Fatp1*^{B-/-} mice have greater fat mass and larger eWAT fat pads when fed HFD.** Body composition was next investigated to determine if M Φ FATP1 contributed to alterations in adipose tissue. Mice fed a HFD displayed significantly increased percent body fat as measured by MRI as well as elevated plasma leptin concentrations, yet no genotype differences were evident in either measure ($P < 0.001$, **Figures 3.2H and I**, respectively). However, eWAT depots

in HFD-fed *Fatp1*^{B^{-/-}} mice were 40% heavier compared to HFD-fed *Fatp1*^{B^{+/+}} mice (P<0.01, **Figure 3.2J**). Lean mass, liver and brown adipose weights were not altered by genotype (**Figures 3.8A-C**).

Deletion of MΦ *Fatp1* led to augmented eWAT MΦ influx, CAM-associated inflammation, activation of the NLRP3 inflammasome, and oxidative damage. Infiltration of MΦs from transplanted marrow into eWAT was confirmed by PCR-based genotyping of eWAT genomic DNA to detect the mutated *Fatp1* allele (**Figure 3.3A**). Histological examination of eWAT sections (**Figure 3.3B-E**) revealed slightly increased adipocyte size with HFD feeding in *Fatp1*^{B^{+/+}} and *Fatp1*^{B^{-/-}} mice, but no genotype-mediated differences were evident (data not shown). However, there was a 60% increase in the number of F4/80+ crown-like structures (CLS) observed in eWAT from HFD-fed *Fatp1*^{B^{-/-}} mice compared to HFD-fed wild type controls (**Figures 3.3F-I** and quantified in **3.3J**, P<0.01). Furthermore, qPCR gene expression analysis for monocyte/MΦ markers *emr1* (F4/80), *Cd11b*, and *Cd11c* indicated dramatic increases in obesity-associated MΦ influx in HFD-fed *Fatp1*^{B^{-/-}} eWAT compared to *Fatp1*^{B^{+/+}} (P<0.01, P<0.05, and P<0.001, respectively, **Figure 3.3K**). Expression of the pro-inflammatory cytokine *Il-6* was 5-fold higher in eWAT from *Fatp1*^{B^{-/-}} mice compared to *Fatp1*^{B^{+/+}} on HFD (P<0.01, **Figure 3.3L**). Likewise, expression of the pro-inflammatory cytokine *Il-1β*, was doubled in eWAT from *Fatp1*^{B^{-/-}} mice compared to *Fatp1*^{B^{+/+}} on HFD (P<0.05, **Figure 3.3M**). IL-1β production results from activation of the inflammasome²²⁴. We observed significantly elevated expression of NLRP3 inflammasome subunits including *Nlrp3* and *Pycard* in eWAT from *Fatp1*^{B^{-/-}} mice compared to *Fatp1*^{B^{+/+}} on HFD (P<0.01, **Figure 3.3N**). Furthermore, significantly increased concentrations of 8-iso-PGF_{2α}, an indicator of non-enzymatic oxidative damage, in conjunction with elevated positive staining for 4-hydroxynonenal (4-HNE), a marker of lipid

peroxidation, indicated increased oxidative damage in eWAT from HFD-fed *Fatp1*^{B-/-} mice compared to HFD-fed *Fatp1*^{B+/+} mice (**Figures 3.3O (P<0.05) and 3.3P**).

Lack of FATP1 induces a metabolic substrate switch from fatty acid toward glucose metabolism. We hypothesized that MΦ FATP1 plays a role in supporting the AAM phenotype by directing lipid metabolism in MΦs. To test this hypothesis, BMDM were isolated and differentiated from age-matched, chow-fed male *Fatp1*^{+/+} and *Fatp1*^{-/-} total body knockout mice. There were no differences in the number or gross morphology of BMDM generated from *Fatp1*^{-/-} mice compared to *Fatp1*^{+/+} mice (**data not shown and Figure 3.4A**), similar to the results from the BMT study (**Figure 3.1C**). The lack of FATP1 protein (**Figure 3.4B**) and a 40% reduction in total ACSL enzymatic activity (P<0.01, **Figure 3.4C**) had no effect on the size or viability of the generated BMDM (**Figure 3.9A-B**).

To determine if deletion of *Fatp1* led to compensatory up-regulation of other *Fatp* family members, *Fatp* gene expression was profiled in unpolarized (Un), CAM and AAM-polarized *Fatp1*^{+/+} and *Fatp1*^{-/-} BMDM by qPCR. Only expression of *Fatp1* and *Fatp4* were detected at meaningful concentrations, with *Fatp6* being minimally detectable (**Figure 3.4D**). In *Fatp1*^{+/+} BMDM, *Fatp1* expression was 2-fold higher in AAM compared to CAM BMDM, replicating our previous observation (**Figure 3.1A**). *Fatp1* expression was reduced in *Fatp1*^{-/-} BMDM, as expected. Relative to *Fatp1*, BMDMs express *Fatp4* at higher concentrations in all polarization states. In contrast to *Fatp1*, *Fatp4* expression is increased 3-fold in CAM-polarized MΦs compared to unstimulated and AAM. We did not detect compensation for *Fatp1* deficiency by *Fatp4* or *Fatp6*; in fact, in CAM-polarized BMDM, *Fatp4* was detected at lower levels in *Fatp1*^{-/-} compared to *Fatp1*^{+/+} BMDM (P<0.0001, **Figure 3.4D**).

To examine effects of lack of FATP1 on MΦ metabolism, we next examined cellular bioenergetics, fatty acid uptake, and substrate metabolism. Mitochondrial metabolism, as measured by oxygen consumption rate (OCR), was elevated in AAM compared to unstimulated or CAM. OCR was significantly elevated in *Fatp1*^{-/-} compared to *Fatp1*^{+/+} in both unstimulated (P<0.01) and AAM-polarized (P<0.05) BMDM (**Figure 3.4E**). In *Fatp1*^{+/+} BMDM, AAM-polarization induced a 57% and 97% increase in palmitate internalization, respectively, when compared to unstimulated (P<0.0001) or CAM (P<0.001; **Figure 3.4F**). Fatty acid uptake was reduced by 21% and 24% in unstimulated (P<0.05) and AAM-polarized *Fatp1*^{-/-} BMDM (P<0.0001), respectively. The diminished fatty acid uptake in AAM-polarized *Fatp1*^{-/-} BMDM correlated to a 17% reduction in complete oleate oxidation (P<0.0001, **Figure 3.4G**). There were no significant differences in incomplete fatty acid oxidation as measured by ¹⁴C incorporation into acid soluble metabolites (**Figure 3.4H**).

Because MΦs markedly enhance glucose metabolism when CAM polarized^{20,21,222}, we determined if inhibition of lipid metabolism via deletion of FATP1 would reprogram BMDM metabolism toward increased glucose usage, similar to the CAM phenotype. We found that expression of *glucose transporter 1* (*Glut1*) was significantly increased in CAM-polarized *Fatp1*^{-/-} compared to *Fatp1*^{+/+} BMDM (P<0.0001, **Figure 3.4I**), yet there was no significant increase in acute glucose uptake (**Figure 3.4J**). Thus, extracellular acidification rate (ECAR) was used to measure glycolytic rate. *Fatp1*^{-/-} BMDM displayed significantly increased glycolytic rates, as measured by ECAR in unpolarized (P<0.05), CAM- (P<0.001) and AAM-polarized (P<0.05) states compared to *Fatp1*^{+/+} BMDM (**Figure 3.4K**). Glycolytic capacity was similarly elevated in the absence of FATP1 (**Figure 3.4L**). Neither glucose oxidation or glycogen synthesis were affected by *Fatp1* genotype (**Figures 3.4M-N**).

Lack of FATP1 primes MΦs for exaggerated pro-inflammatory activation upon CAM polarization and hinders polarization to the AAM phenotype. Expanding on our observations that *Fatp1*^{-/-} BMDM internalized and oxidized less fatty acid compared to *Fatp1*^{+/+}, together with existing evidence linking MΦ substrate metabolism and inflammatory phenotype, we next measured the basal expression and inflammatory response of CAM or AAM-polarized *Fatp1*^{+/+} and *Fatp1*^{-/-} BMDM. Expression of the classic CAM marker *inducible nitric oxide synthase* (*Nos2*) was 2-fold higher in *Fatp1*^{-/-} compared to *Fatp1*^{+/+} CAM-polarized BMDM (P<0.0001, **Figure 3.4O**). In addition, CAM-polarization resulted in increased *Tnfα* gene transcription in *Fatp1*^{-/-} BMDM compared to *Fatp1*^{+/+} control (P<0.05, **Figure 3.4P**). A commonly used AAM MΦ marker is expression of *Arginase-1*²⁰. We observed that *Arginase-1* transcription was up-regulated in AAM BMDM, but this up-regulation was significantly blunted in *Fatp1*^{-/-} compared to *Fatp1*^{+/+} BMDM (P<0.05, **Figure 3.4Q**).

Metabolomic analysis of *Fatp1*^{-/-} BMDM indicates enhanced glucose metabolism, particularly through the pentose phosphate pathway. The intracellular metabolic signature of *Fatp1*^{-/-} BMDM was significantly different than that of the *Fatp1*^{+/+} BMDM when comparing CAM-polarized cells relative to unstimulated (**Figure 3.5**). Intermediates of the first half of the glycolytic pathway were significantly increased in *Fatp1*^{-/-} BMDM, while glycolytic end products phosphoenolpyruvate and lactate were reduced, corroborating our bioenergetics results. CAM-polarized *Fatp1*^{-/-} BMDM exhibited enhanced pentose phosphate pathway activity as evidenced by increased 6-phosphogluconate, ribose, and arabinol. Purine metabolism, drawing on intermediates from the pentose phosphate pathway and increased biopterin, was significantly up-regulated, while thymidine concentration was decreased. Deletion of *Fatp1* also resulted in increased concentrations of glycerolipid metabolites glycerol 3-phosphate,

glycerophosphorylcholine, and ethanolamine. Cytidine 5'-diphosphocholine concentrations were significantly decreased possibly indicating a block in the CDP-choline pathway. A significant down-regulation in *Fatp1*^{B-/-} BMDM of amino acid metabolism was evident, particularly in branch-chain amino acids. B-vitamin metabolism was altered with significant decreases observed in concentrations of pyridoxal (vitamin B₆), niacin-containing electron carriers including NAD⁺ and NADH, and riboflavin (vitamin B₂). Interestingly, there were significant increases in both phosphopantetheine (vitamin B₅) which is required for the formation of coenzyme A (CoA), and CoA itself a necessary cofactor for FATP1's ACSL activity. Lastly, increased concentrations of the polyamines spermidine and spermine indicate enhanced polyamine synthesis in BMDM lacking *Fatp1*.

FATP1 over-expression increased ACSL activity and fatty acid uptake into RAW264.7

MΦs. We next determined if the CAM-like RAW mouse MΦ cell line could be metabolically reprogrammed toward an AAM phenotype via FATP1 over-expression (FATP1-OE). First, we profiled expression levels of the 6 members of the *Fatp* family. RAW MΦs expressed only *Fatp1* and *Fatp4*, both of which were induced 2-fold by 24 hour LPS activation (**Figure 3.6A**). We successfully achieved over-expression of both *Fatp1* mRNA (P<0.001, **Figure 3.6A**) and FATP1 protein in FATP1-OE compared to empty vector controls (FATP1-EV, **Figure 3.6B**). FATP1 protein is essentially undetected in unstimulated RAW MΦs, thus FATP1 over-expression created a gain of function model. A significant decrease in *Fatp4* expression in FATP1-OE MΦs upon LPS activation was evident compared to FATP1-EV (P<0.05). FATP1 over expression had no effect on cell size, viability, or growth (**Figure 3.9C-D**).

ACSL activity assays were performed on FATP1-EV and FATP1-OE MΦs to ensure that the over-expressed FATP1 was functional. Total ACSL activity was increased by 20% in

FATP1-OE compared to FATP1-EV ($P < 0.05$, **Figure 3.6C**). We also observed a 17% increase in fatty acid uptake in FATP1-OE compared to FATP1-EV in the unstimulated state ($P < 0.01$, **Figure 3.6D**). LPS activation increased fatty acid uptake by 2.3-fold in FATP1-EV, while FATP1-OE showed a 2.7-fold increase. Thus, after LPS stimulation, fatty acid uptake into FATP1-OE was 36% greater than FATP1-EV controls with ($P < 0.0001$).

FATP1 over-expression reprograms RAW MΦs toward an AAM metabolic phenotype.

LPS-activation of RAW MΦ led to dramatically reduced complete fatty acid oxidation regardless of FATP1 genotype, demonstrating a disconnect between fatty acid uptake and oxidation. There were no FATP1-mediated differences in either complete or incomplete oleate oxidation (**Figures 3.6E-F**). At baseline, there were no differences in *Glut1* expression, however with LPS stimulation *Glut1* expression was 39% lower in FATP1-OE compared to FATP1-EV ($P < 0.01$, **Figure 3.6G**). Acute glucose uptake was reduced in FATP1-OE MΦs, though this result did not reach statistical significance (**Figure 3.6H**). However, bioenergetics measurements taken over 2 hours demonstrated a 60% reduction in glycolytic rate in FATP1-OE MΦs compared to FATP1-EV controls in both unstimulated and LPS-stimulated conditions ($P < 0.01$, **Figure 3.6I**). Glycolytic capacity was also significantly reduced with FATP1 over-expression to levels 60% of those in FATP1-EV ($P < 0.05$, **Figure 3.6J**). In addition, FATP1-OE MΦs demonstrated a 23% reduction in glucose oxidation upon LPS-activation ($P < 0.05$, **Figure 3.6K**). Finally, glycogen synthesis was unaffected by FATP1 expression in either unstimulated or LPS-activated MΦs (**Figure 3.6L**).

FATP1 gain of function inhibits MΦ pro-inflammatory response. To examine the consequence of FATP1-mediated alterations in metabolism on the inflammatory response in RAW MΦ, we performed mRNA and cytokine production analyses of pro- and anti-

inflammatory markers in unstimulated and LPS-stimulated cells. FATP1 over-expression significantly suppressed the expression of LPS-induced pro-inflammatory enzyme *Nos2* ($P < 0.01$, **Figure 3.6M**) and pro-inflammatory cytokine *Tnfa* ($P < 0.01$, **Figure 3.6N**). Secretion of IL-6 and MCP-1 protein was inhibited in response to LPS stimulation in FATP1-OE compared to FATP1-EV ($P < 0.01$ and $P < 0.05$, **Figures 3.6O and P**, respectively). IL-1 β protein secretion was also reduced in FATP1-OE compared to FATP1-EV ($P < 0.01$, **Figures 3.6Q**). AAM-markers *Mrc-1* and *Arginase-1* were not detectable in FATP1-EV and FATP1-OE cells in either the unstimulated or LPS-stimulated state (data not shown).

FATP1 over-expression down-regulated glucose metabolic pathways. Concentrations of glycolytic, pentose phosphate pathway, and TCA cycle intermediates, including succinate, malate, and fumarate, were all decreased in CAM-polarized FATP1-OE compared to CAM-polarized FATP1-EV (**Figure 3.7A**). FATP1 over-expression led to decreased intracellular concentrations of specific amino acids including alanine, aspartate and branched-chain amino acids in CAM-polarized FATP1-OE versus FATP1-EV RAW M Φ s. N-acetyl-beta-alanine, a metabolite significantly reduced in *Fatp1*^{-/-} BMDM, was increased, as were glutamate and glutamine in FATP1-OE. Purine and pyrimidine metabolism was diminished in the FATP1 over-expressing cells. FATP1 over-expression modulated one-carbon metabolism as demonstrated by reduced 5-methyltetrahydrofolate and biopterin, along with associated metabolites cysteine, glycine, serine, and methionine compared to controls. Elevated concentrations of S-adenosylmethionine (SAM) were measured in CAM-polarized FATP1-OE cells which correlated with significantly higher concentrations of putrescine, spermine, and spermidine whose synthetic enzymes require SAM. LCFA and eicosanoid metabolism was reduced with the exception of 9-HODE, which was significantly increased by FATP1 over-expression compared to empty vector

controls. Finally, FATP1 over-expression blunted induction of iNOS in response to CAM polarization as evidenced by a significant decrease in citrulline concentration and a concomitant increase in polyamine-associated metabolites, all indications of redirection of arginine from being a substrate for iNOS toward use by ARGINASE-1 (**Figure 3.7B**).

***FATP1* SNPs are associated with *FATP1* expression levels in human adipose.** We searched public databases for genetic variants located within 1 Mb of *FATP1* that were associated with *FATP1* expression (eQTLs) in human adipose tissue. The Multiple Tissue Human Expression Resource (MuTHER) study of 856 female twins showed the strongest eQTL for *FATP1* with rs9137 ($P=1.3 \times 10^{-13}$), which is located in the 3'UTR of *FATP1*. In the METabolic Syndromes In Men (METSIM) study of 1,381 men, the strongest association with adipose *FATP1* expression was observed for rs3212793 ($P=1.8 \times 10^{-4}$), located ~300 kb downstream of the *FATP1* gene. These results demonstrate that *FATP1* levels vary between individuals and that these and/or other nearby variants may be involved in the regulation of *FATP1* expression.

We next examined the relationship between *FATP1* expression and eight metabolic traits in the METSIM study. Increased *FATP1* expression showed a trend toward an association with decreased waist circumference (beta = -0.33; $P = 0.056$).

DISCUSSION

Understanding the link between metabolism and inflammation is of particular interest, especially within the context of understanding diabetes risk. In lean white adipose tissue, AAM maintain tissue homeostasis by mediating tissue remodeling and secreting cytokines that promote insulin sensitivity. With obesity, the heightened demand for lipid storage promotes rapid expansion of adipose tissue and increased adipocyte stress and death. Recruited in response to stress signals and to phagocytize the dead and dying adipocytes, monocytes entering the obese

adipose microenvironment are differentiated and polarized to the CAM phenotype. Thus, the dominant MΦ phenotype shifts toward CAM and the adipose becomes inflamed. Due to the distinct metabolic characteristics of CAM versus AAM, the availability of fuel substrates within the adipose microenvironment can be an important modifier of MΦ polarization. Obese adipose exposes local MΦs to high levels of free fatty acids and triacylglycerides resulting from enhanced lipolysis and engulfment of dying adipocytes; subsequently, MΦs become engorged with lipid¹⁸. In uncontrolled diabetes, MΦs are also exposed to high blood glucose concentrations, thus, setting the stage for the sustained expansion of the CAM population within adipose. MΦs are especially sensitive to toxicity induced by high concentrations of glucose, cholesterol, as well as fatty acids²²⁵⁻²²⁷. Yet, generation of the AAM phenotype is a fatty acid oxidation-dependent process²⁰. Due to this seemingly contradictory response to fatty acids, we hypothesized that metabolism of *specific* fatty acids plays a critical role in suppressing inflammation and maintaining insulin sensitivity. Integrating the use of loss- and gain-of-function models, we report for the first time that FATP1 is necessary to maintain the AAM phenotype, plays an important role in systemic glucose metabolism, and that SNPs exist in human *FATP1* that regulate expression relevant to body composition.

Herein, we demonstrate the reliance of AAM on FATP1 function. FATP1 expression levels are highest in tissues characterized by active fatty acid uptake and lipid metabolism, such as adipose, heart, and skeletal muscle^{71,73}. Functional characterization of FATP1 and activation of fatty acids through its ACSL activity have been conducted in these tissue and cell types^{80,88,92,228}. FATP1 has an affinity for L/VLCFA⁷⁴, which is unique compared to other MΦ fatty acid transporters such as CD36, which is highly promiscuous as a fatty acid transporter and scavenger receptor. Studies of total-body *Fatp1* knockout mice demonstrated that loss of FATP1

protected mice from HFD-induced obesity, insulin resistance and intramuscular accumulation of fatty acyl-CoAs. Lipids were redistributed from adipose and muscle to the liver, accounting for the observed protection from diet-induced obesity and insulin resistance⁸⁸. Because of its complex pattern of expression among different tissue types, the contribution of FATP1 to the development of insulin resistance is likely to be tissue- and cell-type specific. Our focus on preferential metabolic substrate usage by MΦ has demonstrated that FATP1 is a novel metabolic reprogramming regulator and, as such, directly controls MΦ polarization and adipose inflammation.

MΦs have a high capacity for lipid metabolism²⁶. We demonstrated that FATP1 is expressed at highest levels in AAM, the MΦ subtype especially reliant upon lipid metabolism²⁰. In striking contrast to the total-body *Fatp1*^{-/-} mice, we now present data indicating that chimeric mice harboring MΦ that are deficient in FATP1 were more susceptible to diet-induced obesity in terms of weight gain and adiposity, hyperglycemia, and glucose intolerance compared to diet-matched *Fatp1*^{B+/+} mice, indicating that MΦ FATP1 plays a specific role in limiting obesity.

How can MΦ FATP1, specifically, have such an effect on systemic metabolism? *Fatp1*^{B-/-} mice fed a HFD had a dramatic shift in body composition with massive fat pads that were characterized by excessive crown-like structures (CLS), MΦ infiltration and inflammatory cytokine production. CLS are classic histologic markers of inflammation in adipose, the presence of which are hallmarks of obesity associated with Metabolic Syndrome¹⁸. Oxidative stress is another hallmark of obesity; ROS are signaling cascade second messengers associated with enhanced expression of pro-inflammatory mediators. We and others have shown that persistent activation the ROS-generating pathways results in increased oxidative stress^{222,229}. Evidence of oxidative stress was detected through targeted analysis of 8-iso-PGF_{2α}, as well as histological

detection of 4-HNE, suggesting that FATP1 normally suppresses MΦ ROS production, further demonstrating the regulatory role of FATP1 in AAM. Finally, priming and activation of the NLRP3 inflammasome, an intracellular stress sensor for nutrients and other stimuli, as well as its potent pro-inflammatory product, *Il-1β*, was highest in HFD-fed *Fatp1^{B-/-}* adipose tissue. It is well-established that the NLRP3 inflammasome contributes to insulin resistance²³⁰ and can be regulated by metabolism of glucose and fatty acids^{224,230,231}. Therefore, our data support that FATP1 functions as a MΦ regulatory protein maintaining the AAM phenotype since deletion of MΦ FATP1 primes and activates the inflammasome, potentially through a metabolic shift in metabolism and ROS production.

By using etomoxir to block CPT1-mediated fatty acid β-oxidation, Vats *et al.* demonstrated that oxidative metabolism was essential for generate of the AAM phenotype. This seminal article was among the first publications to document a role for metabolism in regulating MΦ function. To characterize the metabolic alterations resulting from modulation of *Fatp1* expression, our approach entailed using an *ex vivo* BMDM loss-of-function model as well as a gain-of-function *in vitro* RAW MΦ cell line. BMDM and RAW MΦs express only *Fatp1* and *Fatp4*. We did not detect compensatory *Fatp* expression in response to loss of FATP1. Additionally, total ACSL activity was significantly reduced in *Fatp1^{-/-}* BMDM, demonstrating that while other acyl-CoA synthetases were present to activate fatty acids, such as ACSL1²²⁷, there was a lack of enzymatic compensation overall. ACSL-mediated addition of CoA targets fatty acids to certain metabolic fates, which participate in the regulation of inflammation. For example, ACSL1 is active in MΦs²²⁷. However, in direct contrast to our findings, deletion of ACSL1 protects MΦs from the inflammatory effects of diabetes and atherogenesis²²⁷, thus highlighting the existence of non-redundant roles for ACSLs within MΦs. Metabolic analysis of

Fatp1^{-/-} BMDM demonstrated that, along with reduced ACSL activity, deletion of FATP1 resulted in blunted fatty acid uptake and reduced oxidation of fatty acids, particularly in AAM-polarized BMDMs, even in the context of elevated mitochondrial respiration. These data suggest that deletion of FATP1 fundamentally altered an aspect of mitochondrial function or the electron transport chain – perhaps uncoupling-- which is under further investigation. As deletion of FATP1 served to blunt lipid metabolism, it reprogrammed MΦ metabolism toward activated carbohydrate pathways. Specifically, we observed transcriptional up-regulation of the MΦ glucose transporter *Glut1* and glycolytic rates in *Fatp1*^{-/-} BMDM. While deletion of FATP1 enhanced glucose metabolism, we observed the opposite shift in substrate metabolism in RAW MΦs over-expressing FATP1: FATP1 over-expression suppressed *Glut1* expression, which subsequently reduced glucose oxidation, glucose uptake, glycolytic rate and capacity. Along with reduced glycolysis, CAM-like RAW MΦs expressing more FATP1 failed to be activated by LPS as illustrated by reduced *Nos2*, *Tnfα*, IL-6, MCP-1, and IL-1β. RAW MΦs are originally derived from viral-induced mouse leukemia and display a Warburg-like metabolism reminiscent of the CAM phenotype, thus the inhibition of activation by the metabolic switch due to FATP1 is striking.

In accordance with the higher expression of pro-inflammatory cytokines in eWAT from HFD-fed *Fatp1*^{B/-} mice, BMDM from *Fatp1*^{-/-} mice displayed an exaggerated inflammatory response, as well as more CAM-like and less AAM-like polarization upon activation to the different MΦ subtypes. CAM and AAM polarization results in distinct shifts in arginine metabolism (**Figure 3.7B**). CAM-polarized MΦs shunt arginine to iNOS, which catalyzes the conversion of arginine to the ROS species nitric oxide. In contrast, AAM-polarized MΦs divert arginine instead to ARGINASE-1, which converts arginine to ornithine. Ornithine, a precursor to

collagen synthesis, is necessary for AAM's regulator function in tissue remodeling and wound repair. Importantly, with greater ARGINASE-1 expression, less arginine is directed towards iNOS and, therefore, production of ROS and collateral tissue oxidative damage is reduced. Expression and metabolomic analysis of BMDM from *Fatp1*^{-/-} revealed increased *iNos* (*Nos2*) and metabolites supportive of a shift in arginine metabolism. Oxidative damage due to lack of MΦ *Fatp1* was evident in obese adipose in *Fatp1*^{B-/-} mice, further supporting metabolic shifts linked to increased ROS production.

In complementary gain-of-function studies, over-expression of FATP1 in RAW MΦs enhanced total ACSL activity and fatty acid uptake. Despite the increased fatty acid uptake, FATP1 over-expression did not enhance fatty acid oxidation, indicating that fatty acids were being directed to compartments other than the mitochondrial matrix for β -oxidation. Metabolomics data indicated that FATP1 modulated glycerolipid metabolism with significant changes observed in ethanolamine, glycerophosphocholine and CDP-choline. Phospholipids serve as a pool of bioactive lipids including arachidonic acid and palmitate, both substrates of FATP1, which could modulate MΦ-mediated inflammation. Therefore, future studies will determine if FATP1 regulates polarization via regulation of ratios of phospholipid classes, fatty acid composition within those classes, as well as eicosanoid production.

One regulatory complex of the innate immune system that is at the nexus between metabolism and inflammation is the NLRP3 inflammasome. The NLRP3 inflammasome is activated in obesity, leading to insulin resistance and diabetes²³¹. Transcription of NLRP3 inflammasome components and its product *Il-1 β* was significantly increased in adipose from HFD-fed *Fatp1*^{B-/-} compared to controls. The NLRP3 inflammasome is a nutrient sensitive sensor that is activated by a "two-hit" process typically initiated by signal 1 (e.g. excessive

glucose, palmitate, uric acid, or LPS, among other TLR4 ligands), which serves to prime the inflammasome by driving increased expression of inflammasome components. Subsequent activation by the second signal, which could be palmitate, ceramide, ROS, glucose, uric acid, or amyloid, fully activates the inflammasome, inducing CASPASE 1-mediated cleavage of pro-IL-1 β to active IL-1 β (reviewed in²³¹). Once secreted, IL-1 β induces production of cytokines and chemokines including IL-6, IL-8, TNF α and monocyte chemoattractant protein 1 (MCP-1, or CCL2), which collectively promote further M Φ activation and migration. Our data indicated that FATP1 plays a central role in both priming and activation of the NLRP3 inflammasome both *in vivo* and *in vitro*.

Finally, we identified variants located in and near *FATP1* associated with *FATP1* expression in human adipose tissue. Furthermore, *FATP1* transcript levels were inversely correlated with waist circumference, a strong risk factor for Metabolic Syndrome. As these findings were detected in total subcutaneous adipose tissue, we were unable to take into account the complexity of the cellular composition of the adipose microenvironment and its effect specifically on adipose M Φ s. Indeed, few large population genetic studies focus solely on monocyte/ M Φ s. However, the existence of *FATP1* variants that regulate expression suggests that animal M Φ FATP1 findings presented here may translate to human metabolic disease. Future studies are aimed at investigating the relationship between *FATP1* variants and M Φ function *in vitro*.

In summary, we present mechanistic insight into the relationship between a novel regulator of M Φ substrate metabolism and the inflammatory response. M Φ s are an extremely heterogeneous population of cells whose capacity for metabolic flexibility has important implications for local and systemic responses. We have demonstrated the ability to manipulate or

“metabolically reprogram” the inflammatory potential of MΦs via novel FATP1-mediated pathways. Over the past 30 years, the prevalence of obesity has increased in both Western nations and developing countries¹². Current treatment approaches for Type 2 diabetes are focused on increasing pancreatic insulin release while also reversing hyperglycemia by inhibiting gluconeogenesis or increasing insulin sensitivity and glucose excretion. Additionally, immune-based therapies offer promising interventions^{232,233} including several approaches aimed at increasing insulin sensitivity by blocking the action of inflammatory mediators, specifically previous reports implicate IL-1 α , IL-1 β , TNF α , MCP-1 (CCL2) and IL-6 as important mediators²³²⁻²³⁵. Studies suggest that targeting the inflammatory response is beneficial; patients with chronic auto-immune diseases who are taking anti-inflammatory medicines as part of their treatment regimen have reduced risk of diabetes^{236,237}. Our previous work demonstrated that modulating lipid mediator generation and trafficking in MΦs is an effective tool against obesity, insulin resistance, and diabetes^{25,26,238}. We now propose that controlling MΦ metabolic phenotype through FATP1 activity could be a significant advance in the treatment of altered body composition and glucose intolerance. Identifying novel regulators of FATP1 ACSL activity could open the door to macrophage-specific therapeutics such as nanoparticles targeted to the mononuclear/ MΦ phagocytic system (MPS). Controlling the “immune-metabolic” milieu could break the pro-inflammatory cycle by restoring tissue homeostasis and a healthy AAM/CAM ratio within adipose tissue.

Methods

Reagents

All reagents were obtained from Sigma-Aldrich (St. Louis, MO) unless otherwise noted. IFN γ and IL-4 were obtained from R&D Systems (Minneapolis, MN). Lipopolysaccharide (LPS,

Sigma E. coli L4391) was diluted in sterile PBS at a final concentration of 1mg/mL. Novolin® human insulin was purchased from Novo Nordisk (Plainsboro, NJ). Antibodies were purchased from the following sources: F4/80 (AbD Serotec/BioRad, Hercules, CA); 4-hydroxynonenal (4-HNE) (Abcam, Cambridge, MA); CD16/32 (Fc Block, BioLegend, San Diego, CA), CD45-FITC, F4/80-PE, Ly6G/C-PE-Cy7, CD11b-APC, CD11c-APC-eFluor 780 (Ebioscience, San Diego, CA), and insulin (H-86; Santa Cruz Biotechnology, Inc., Santa Cruz, CA).

Animals and diets

Mice were housed in a climate controlled Department of Laboratory Animal Medicine facility with a 12 hour light:dark cycle and *ad libitum* access to food and water. *Fatp1*^{-/-} mice²²⁸ were backcrossed >12 generations to the C57BL/6J genetic background. *Fatp1* total body knockout (*Fatp1*^{-/-}) and *Fatp1* wild type (*Fatp1*^{+/+}) bone marrow donor mice were generated using *Fatp1*^{-/+} breeding pairs to generate littermate controls. MΦ *Fatp1*^{+/+} (*Fatp1*^{bonemarrow+/+}, *Fatp1*^{B+/+}) and deficient (*Fatp1*^{B-/-}) chimeric mice were generated using bone marrow transplant (BMT) strategy as outlined in **Figure 3.1B**. Briefly, 3-week-old male C57BL/6J recipient mice were purchased from Jackson Laboratories (Bar Harbor, ME). Upon arrival, C57BL/6J mice were randomized to either a purified low fat diet (10% kcal from fat, LFD; D07010502, Research Diets, New Brunswick, NJ) or an obesogenic high fat diet (HFD, 45% kcal from fat, HFD; D06011802, Research Diets, New Brunswick, NJ). At 6 weeks of age, recipient mice were administered 2 doses of X-ray radiation (500cGy x 2, spaced 4 hours apart; X-RAD, North Branford, CT). Simultaneously, bone marrow was harvested from 6 week old male *Fatp1*^{-/-} and *Fatp1*^{+/+} donor mice maintained on standard chow and transplanted as in Makowski et al.²⁴. Control irradiated animals that were not reconstituted with bone marrow died within 10 days of irradiation.

Fatp1^{B+/+} and *Fatp1*^{B-/-} chimeric animals were maintained on LFD or HFD for a total of 23 weeks. N=16-17 mice per diet group and genotype.

Metabolic phenotyping

Body composition was measured immediately prior to BMT and prior to sacrifice (at 23 weeks on diet) using magnetic resonance imaging (MRI, EchoMRI, Houston, TX). Blood glucose was measured at 3 weeks on the diets and again at termination, both following a 6 hour fatty acidst. Randomly fed blood glucose was measured at 9:00 AM after 23 weeks on diet. Intraperitoneal glucose tolerance tests (GTT) and insulin tolerance tests (ITT) were performed at weeks 19 and 20 on diet, following 6 or 4 hour fatty acidsts, respectively²³⁹. Briefly, 2.0gm/kg body weight of glucose or 0.75U of insulin was injected intraperitoneally, and blood glucose was measured over 120 minutes. All blood glucose measurements were performed using a FreeStyle Freedom Lite glucometer (Abbot Diabetes Care, Inc., Alameda, CA). Plasma insulin was measured by ELISA (EMD Millipore, Billerica, MA). Fatty acidsting glucose (mg/dL) and insulin (pmol/L) concentrations measured just prior to euthanasia were used to calculate HOMA_{IR} and HOMA_{%B}.

Tissue and blood collection

Animals were euthanized with tribromoethanol/amylene hydrate (1.25%, Sigma Aldrich, St. Louis, MO). Blood was collected via cardiac puncture and plasma was separated from other blood components by centrifugation at 200xg for 5 minutes at 4°C. Epididymal white adipose (eWAT) and pancreata were collected and fixed in 10% formalin for histological analyses. A portion of eWAT tissue was flash frozen and pulverized in liquid nitrogen.

Hematologic analysis

Hematologic analysis was conducted on fed 10-week-old *Fatp1*^{+/+} and *Fatp1*^{-/-} age-matched male and female mice maintained on *ad libitum* chow. Blood was collected by submandibular

bleed into EDTA-coated tubes. Hematologic analysis occurred in the UNC Mouse Clinical Chemistry Core using an automated hematology analyzer. In addition, flow cytometry was used to enumerate circulating leukocyte populations. Blood was collected from samples for hematologic analysis, and red blood cells were lysed in ACK lysis buffer. Cells were washed twice in HBSS, resuspended in PBS, counted, and then 1×10^5 cells were stained with CD45-FITC, F4/80-PE, Ly6G/C-PE-Cy7, CD11b-APC, CD11c-APC-eFluor 780 in the presence of anti-CD16/32 (Fc block) in FACS buffer (1% FBS in PBS) as described in Murphy et al.²⁴⁰. Samples were analyzed on the Dako CyAN ADP flow cytometer (Beckman Coulter, Inc., Fullerton, CA) and FlowJo Software (TreeStar, Ashland, OR).

Quantitation of secreted cytokines and chemokines

Concentrations of plasma leptin, IL-6, TNF α , and MCP-1 or conditioned media IL-1 β , IL-6, IL-10, and MCP-1 were measured using a MAGPIX Luminex kit (EMD Millipore, Billerica, MA).

***Fatp1* genotyping**

Genomic DNA was isolated from tail biopsies, eWAT, and BMDM using a DNeasy Blood and Tissue kit (Qiagen, Valencia, CA). Genotyping was performed using the following primers:

Fatp1 forward: GGCGGTCAATGTAAAGTAAACTGG, *Fatp1*^{+/+} reverse:

CTCACACCACCCTGCAAGACTCT, *Fatp1*^{-/-} neomycin cassette reverse:

GTAATGGGATAGGTCACGTTGGTG²²⁸. iProof High-Fidelity PCR super mix (Bio-Rad, Hercules, CA)-based genotyping was performed on a C1000 thermocycler (Bio-Rad, Hercules, CA).

Gene expression analysis

Total mRNA was isolated from eWAT and cultured cells using a RNeasy kit (Qiagen, Valencia, CA). RNA quantity and quality was determined using Nanodrop (ThermoScientific, Wilmington,

DE) and reverse transcribed using the iScript cDNA synthesis kit (Bio-Rad, Hercules, CA). Gene expression was quantitated by qPCR using Assay-On-Demand chemistries on an ABI 7900HT machine (Life Technologies, Grand Island, NY)⁵². Expression levels of genes of interest were normalized to expression of *18S*. Animals whose body weight was at or above the mean body weight for the experimental group were selected for analysis; therefore, unless indicated, N= 8-9/group for mouse data and N=3-6 experiments for cell culture studies.

Morphological and immunohistochemical analyses of eWAT and pancreata

Adipocyte size was determined by measuring the longest diameter of 100 adipocytes from each sample on H&E-stained 5 μ M sections. Anti-F4/80 and 4-HNE immunohistochemistry staining was conducted as previously described²³. Pancreatic islets of Langerhans were visualized by positive insulin staining as previously described^{23,241}. All histological sections were scanned on an Aperio ScanScope CS Ultra-Resolution Digital Scanner and analyzed using ScanScope Image Analysis Toolbox software (Buffalo Grove, IL)²⁴².

Bone marrow derived M Φ (BMDM) isolation, differentiation, and activation

Bone marrow was collected from gender- and age-matched male *Fatp1*^{+/+} and *Fatp1*^{-/-} mice. Marrow was cultured in RPMI-1640 containing 30% L929 conditioned media supplemented with 10% FBS, 2mM glutamine, 100 IU/mL penicillin and 100 μ g/mL streptomycin (Sigma-Aldrich, St. Louis, MO). For bioenergetics assays, BMDM were differentiated using M-CSF (20ng/ml). BMDM were left as naïve unstimulated M Φ s (Un), or polarized using 5ng/mL LPS and 10ng/mL IFN γ (CAM) or 10ng/mL IL-4 (AAM) for 24 hours²⁰. Cell densities and viability were determined by hemacytometer and trypan blue exclusion, respectively. Cell size, volume, and viability were determined using a Sceptor™ handheld automated cell counter (Millipore, Billerica, MA).

FATP1-OE stable MΦ cell line generation and characterization

The DNA sequence for *Fatp1* was obtained from the National Institutes of Health Mammalian Gene Collection. *Fatp1* cDNA containing a 5' *EcoRI* site followed by a Kozak sequence and Flag tag and a 3' *NotI* site was cloned into the pCI-neo Mammalian Expression vector (Promega, Madison, WI). The upstream primer: 5'-

GATCGAATTCGCCACCATGGATTACAAGGATGACGACGATAAGCGGGCTCC

TGGAGCAGGAACAGCC-3'. The downstream primer: 5'-

GATCGCGGCCGCTCAGAGTGAGAAGTCGCCTGC-3'. Sequencing confirmed the fidelity

of the sequence. Mouse RAW264.7 MΦ cells (ATCC, Manassas, VA; ATCC# TIB-71) were

transfected with either the empty vector (FATP1-EV) or FATP1 expression construct (FATP1-

OE) using the AMAXA Nucleofector V kit (Lonza, Cologne, Germany). Stable cell lines were

established and diluted serially to obtain clonal isolates under selection using 400 µg/ml G418

Sulfate (Cellgro, Manassas, VA) for 2 weeks. All transfected MΦs were subsequently

maintained in 200 µg/mL G418 Sulfate. RAW264.7 FATP1-EV and FATP1-OE cells were

grown in Dulbecco's minimal essential media (DMEM) 4.5g/L glucose supplemented with 10%

FBS, 100 IU/mL penicillin and 100µg/mL streptomycin (Sigma-Aldrich, St. Louis, MO). Studies

reported herein were repeated in a second set of clones and the parent heterologous population of

FATP-EV and FATP1-OE from which the clones were isolated (data not shown). Cell viability,

size and volume were determined as above. Cell proliferation was determined by 3-(4, 5-

dimethylthiazolyl-2)-2,5-diphenyltetrazolium bromide (MTT) assay (ATCC) over 24-96 hours of

culture²²².

Immunoblot

FATP1 protein expression was measured by immunoblotting as described⁷⁶. Polyclonal anti-sera raised against the C-terminus of FATP1 or antibody against β -tubulin diluted 1:1000 in PBS with 0.1% Tween-20, overnight was used. Primary antibodies were detected with LI-COR secondary antibodies and imaged on the LI-COR Odyssey Imaging System (Lincoln, NE).

ACSL activity assay

Total long chain acyl-CoA synthetase (ACSL) activity was measured as described²⁴³. ¹⁴C-Oleate acid (PerkinElmer Life Sciences, Akron, OH) was incubated with cell homogenate and reactions were terminated after 10 minutes. Heptane-washed aqueous phase (0.6mL) was counted on a Wallac 1409 Liquid scintillation counter (PerkinElmer Life Science, Waltham, MA). Total ACSL activity was expressed as nanomoles of oleate-CoA ester formed/minute/mg protein.

Substrate uptake and metabolism

FATP1-EV and FATP1-OE RAW264.7, or *Fatp1*^{+/+} and *Fatp1*^{-/-} BMDM were plated at 1.5×10^5 or 7.5×10^5 cells/well, respectively, into 24 well plates, allowed to attach overnight and stimulated as above. Cells were washed with PBS and then incubated untreated or with 2 μ M BODIPY[®] C₁₆ fluorescent palmitic acid (Molecular Probe, Grand Island, NY) in DMEM for 30 minutes at 37°C²⁴⁴. Fluorescence was measured using a CyAn ADP Analyzer flow cytometer (Beckman Coulter, Fullerton, CA) and FlowJo software (TreeStar, Ashland, OR)²⁴⁵. To measure fatty acid oxidation, 1.0 μ Ci/mL BSA-conjugated 1-[¹⁴C]-oleic acid (PerkinElmer Life Sciences, Waltham, MA) was added to DMEM containing 12.5mM HEPES, 1mM L-carnitine to a final concentration of 0.5%, 100 μ M sodium oleate. ¹⁴C-CO₂ was captured and counted using EcoScint H. Glucose uptake, oxidation and glycogen synthesis were measured as previously described²²². Results were normalized to protein concentration.

Cellular bioenergetics

FATP1-EV or FATP1-OE RAW MΦs (6×10^4 /well) were seeded into a Seahorse Bioscience (Billerica, MA) tissue culture plate, allowed to attach for 3 hours and activated with 100ng/mL LPS (RAW264.7) or PBS vehicle control. *Fatp1*^{+/+} or *Fatp1*^{-/-} BMDMs (2×10^5 /well) were seeded and allowed to attach for 3 hours and then either left as naïve unstimulated MΦs (Un), CAM, or AAM polarized for 24 hrs as above. Prior to analysis, cells were washed twice with DMEM (RAW) or RPMI (BMDM) assay media (sodium bicarbonate- and glucose-free DMEM or RPMI supplemented with 2mM glutamine, 100 IU/mL penicillin and 100μg/mL streptomycin (Sigma-Aldrich, St. Louis, MO) and equilibrated for 1 hour at 37°C without CO₂. Measures of glycolytic rate and glycolytic capacity were determined by recording extracellular acidification rates (ECAR, mpH/min) and oxygen consumption rates (OCR, pmol/min) on a Seahorse Bioscience XF24 Extracellular Flux Analyzer (Billerica, MA). The injection of glucose was used to measure glycolytic rate (final concentration 25 mM (RAW) or 11mM (BMDM); Sigma, St. Louis, MO). Oligomycin was injected to measure glycolytic capacity (final concentration 2.5 μM; Sigma, St. Louis, MO). 2-deoxyglucose was used to blunt glycolysis (final concentration 20 mM). N=6 replicates per genotype/treatment. Equal plating density was confirmed by protein assay. Experiments were repeated three times.

Metabolomics

FATP1-EV and FATP1-OE RAW264.7, or *Fatp1*^{+/+} and *Fatp1*^{-/-} BMDM were plated on low binding, non-tissue culture treated plates. 24 hours after plating, both RAW MΦs and BMDM were left untreated (Un) or polarized to CAM as above. PBS-washed cells were detached by scraping, flash frozen in liquid nitrogen, and metabolomics analysis was completed by Metabolon, Inc. (Research Triangle Park, NC)²⁴⁶. N = 4 replicates per group. Missing values

were imputed with the minimum. Data are presented as relative measures of “scaled intensity” after normalization to protein and median scaling to 1. For measurement of eWAT 8-iso-PGF_{2α}, lipids were extracted from 25mg of pulverized tissue and 8-iso-PGF_{2α} was quantified by liquid chromatography with an Agilent 1200 Series capillary HPLC (Agilent Technologies, Santa Clara, CA, USA) as described²⁴⁷. Negative ion electrospray ionization tandem mass spectrometry was used for detection. N = 8 per group.

Human gene expression, variants, and trait association

To determine whether human genetic variants may act as *cis*-regulators of *FATP1* expression, we searched for expression quantitative trait loci (eQTLs) for *FATP1* (*SLC27A1*) located within 1 Mb of the coding sequence. We searched the Multiple Tissue Human Expression Resource (MuTHER) study of HapMap-imputed variants associated with gene expression in subcutaneous adipose tissue from 856 female twins available in the Genvar database. We used the same criteria to look up *cis*-eQTLs in subcutaneous adipose expression data from the METabolic Syndrome In Men (METSIM) study of 1000 Genomes-imputed variants in 1,381 men. Expression levels were analyzed after adjustment for 40 inferred determinants from factor analysis. We further tested for association between adipose *FATP1* expression residuals and eight obesity, lipid and adiponectin traits (body mass index, waist circumference, waist-hip ratio, triglycerides, HDL-C, LDL-C, total cholesterol and adiponectin) in 1,184-1,380 METSIM individuals using models adjusted for age and body mass index, except association with body mass index was only adjusted for age.

Statistics

For body weight data analyses, a regression model was run with genotype/diet group and week (0 thru 23) as predictors. To account for the repeated measures over time within animals an

autoregressive within-subject correlation matrix was fit. F-tests using the resulting parameter and standard error estimates were constructed to make comparisons of interest. All analyses were performed using SAS Version 9.3 (SAS Institute, Cary NC). For all other *in vivo*, *ex vivo* or *in vitro* data, statistical differences between experimental groups were determined by two-way ANOVA followed by multiple comparisons tests using statistical software within GraphPad Prism (GraphPad Software, Inc., La Jolla, CA). For *ex vivo* and *in vitro* experiments, representative results are reported; at least N=3 experiments were conducted with N=3-6 replicates per assay. All data are shown as mean \pm standard error of the mean (SEM). P values less than 0.05 were considered statistically significant.

Approval for animal studies

All animal procedures were approved by the University of North Carolina at Chapel Hill Institutional Animal Care and Use Committee.

Acknowledgements

We thank E. Klett for assessment of pancreata morphology, L.O.Li for technical assistance on ACSL assays, and H. Wen for advice regarding the inflammasome. This work was supported by NIH grants F32HL75970 (A.R.J), P30DK056350 (J.J.M., J.A.G., L.M.), Z01ES025034 (M.L.E., D.C.Z.), DK034987 (J.A.G.), DK099311 (P.T.F.), R01CA096500 (B.D.), DK089202 and DK101293 (A.S.), AA017376 (L.M.), UNC undergraduate research fellowship (M.J.H.), Sanofi Global Scholar pre-doctoral fellowship (Y.Q.), UNC Chancellor's Fellowship (A.J.C.), American Heart Association 1-14-BS-191 (A.S.), American Heart Association (L.M.) and UNC University Cancer Research Fund (L.M.). The METSIM adipose study was supported by the Academy of Finland (contract 124243), the Finnish Heart Foundation, the Finnish Diabetes Foundation, Tekes contract 1510/31/06, the Commission of the European Community

(HEALTH-F2-2007-201681) and US NIH grants DK093757, DK072193, DK062370 and 1Z01 HG000024 (KM).

Figures and Tables

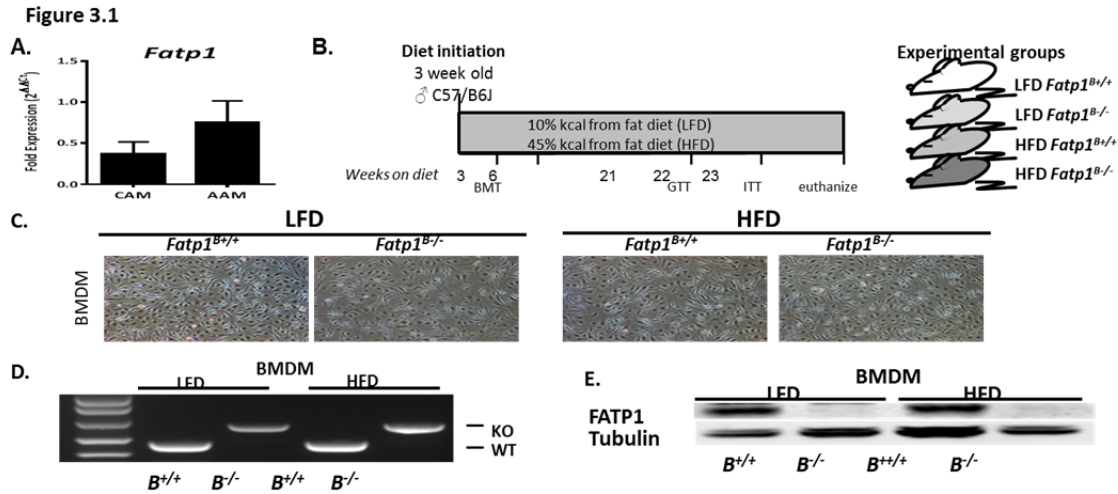


Figure 3.1: FATP1 is predominantly expressed in AAMs and transplant of *fatp1^{-/-}* marrow results in FATP1 deficient macrophages A. *Fatp1* mRNA expression by qPCR in CAM or AAM polarized BMDM. B. Male C57BL/6J weanling mice were randomized to a 10% fat diet (LFD) or 45% fat diet (HFD). Mice were lethally irradiated and transplanted with bone marrow from either *Fatp1^{+/+}* or *Fatp1^{-/-}* mice as described in Methods. Diet exposure was continued for a total of 23 weeks, during which time body weight and body composition data were collected along with analyses of systemic metabolism. C. Representative transplant-derived BMDM from a subset of diet-exposed mice (20X). D. *Fatp1* genotype of BMDM derived from chimeric mice. E. FATP1 protein expression is detected by immunoblot in *Fatp1^{+/+}* and *Fatp1^{-/-}* BMDM from chimeric mice. Tubulin is used for loading control.

Figure 3.2

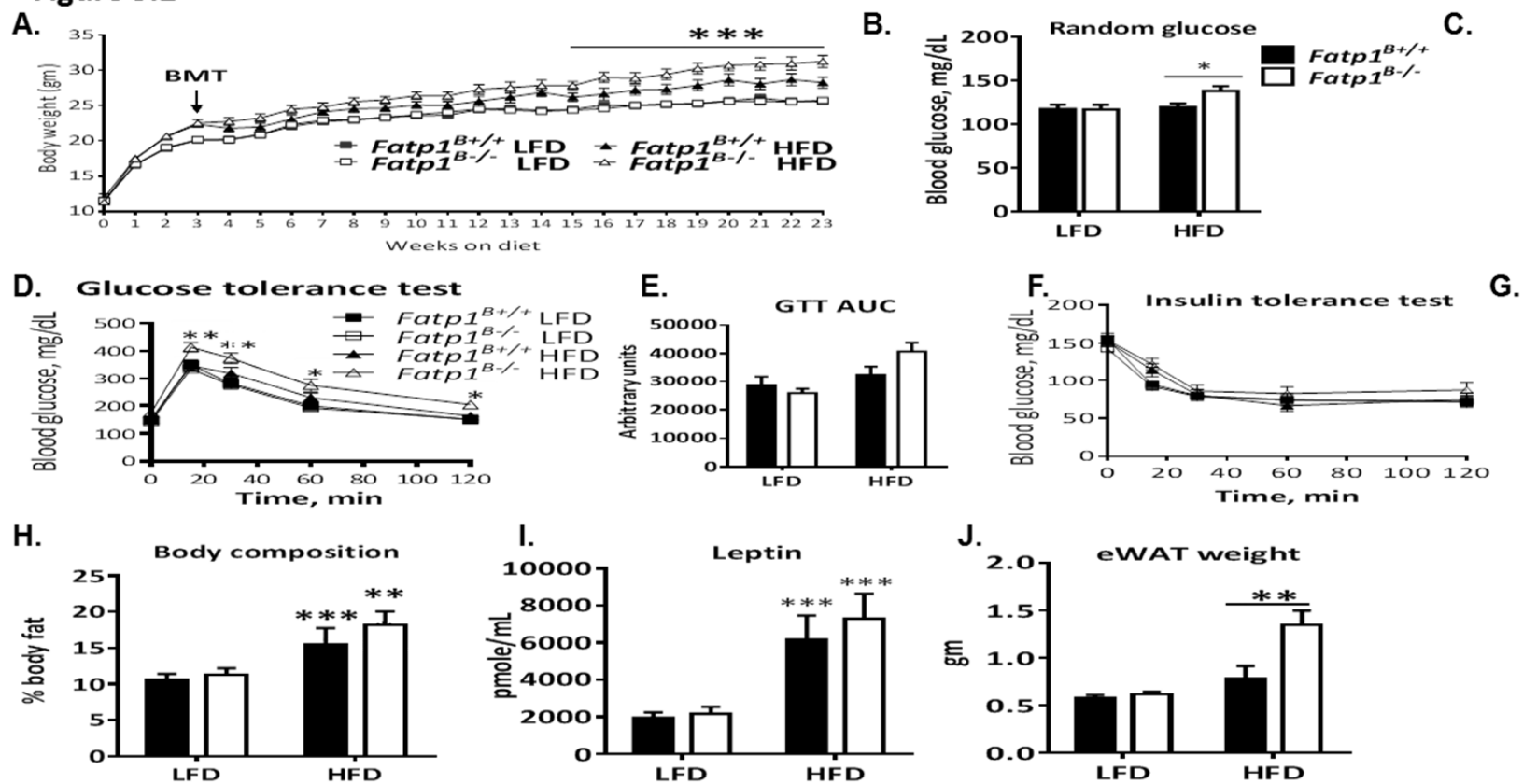


Figure 3.2: Deletion of MΦ *Fatp1* increased susceptibility to weight gain, glucose intolerance, and increased white fat mass. A. Body weights were measured weekly ($P < 0.0001$ *Fatp1*^{B-/-} vs. *Fatp1*^{B+/+} mice on HFD; *** $P < 0.001$ by mixed regression modeling; N=16-17 mice per group). B. Randomly fed blood glucose was measured at 23 weeks on diet (* $P < 0.05$). C. Insulin was measured by ELISA. D. Intraperitoneal glucose tolerance tests (GTT) were conducted at 19 weeks on diet after a 6hr fast. HFD-fed *Fatp1*^{B+/+} versus *Fatp1*^{B-/-} (** $P < 0.01$ and * $P < 0.05$ N=16-17). E. Area under the curve (AUC) was calculated for GTT. F. Insulin tolerance tests (ITT) were conducted at 20 weeks on diet after a 4hr fast. G. AUC was calculated for ITT. H. Body composition was measured by MRI (*** $P < 0.001$ LFD vs. HFD). I. Plasma leptin concentration was measured by Luminex (*** $P < 0.001$ LFD vs. HFD). J. Wet weight of eWAT was measured at sacrifice ($P < 0.01$, LFD vs. HFD). In HFD-fed mice, ** $P < 0.01$ in *Fatp1*^{B+/+} vs. *Fatp1*^{B-/-} mice. Data are means \pm SEM; all differences detected by Two-way ANOVA, except for panel “A”; N=16-17 mice per group.

Figure 3.3

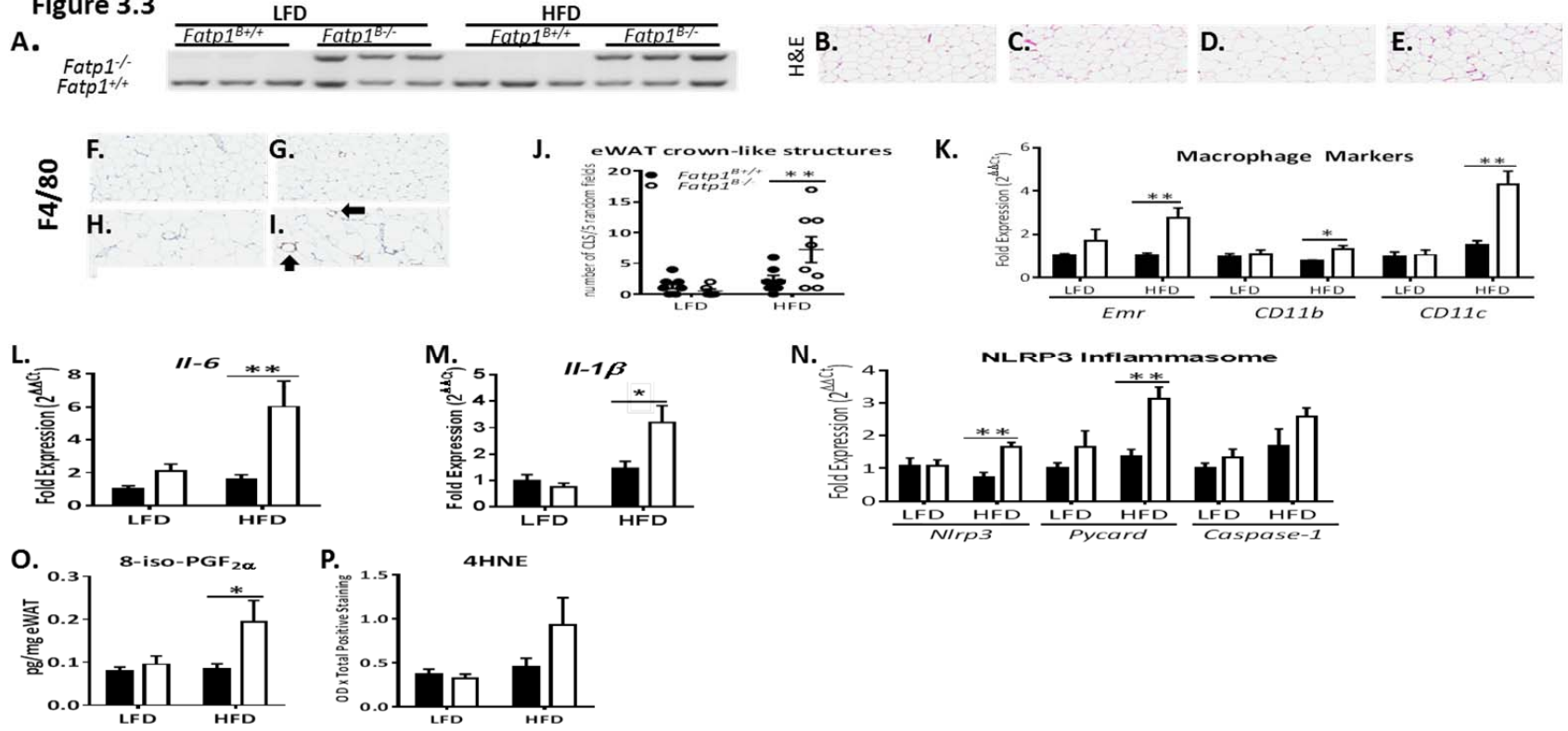


Figure 3.3: Lack of MΦ FATP1 increased adipose inflammation, inflammasome priming, and markers of oxidative stress in HFD-fed mice. A. Migration of transplanted *Fatp1*^{-/-} bone marrow cells into epididymal white adipose tissue (eWAT) was confirmed by genotyping adipose tissue for the null allele. B-E. Adipose tissue morphology was assessed by H&E staining. Representative 10X images presented. F-I. F4/80+ macrophage staining was conducted. Representative 10X images presented. J. Quantification of crown like structures (CLS, arrows) in eWAT in 5 random 20X fields (P<0.01 in *Fatp1*^{B+/+} vs. *Fatp1*^{B-/-}). K. mRNA expression of MΦ markers *emr1* (*F4/80*), *Cd11b* and *Cd11c* was measured by qPCR in eWAT (**P < 0.01 and *P < 0.05 *Fatp1*^{B+/+} vs. *Fatp1*^{B-/-} within diet. *Cd11c* expression interacts with diet, P < 0.01). *Il-6* (L) and *Il-1β* (M) mRNA expression was measured by qPCR (**P<0.01,*P<0.05). N. Inflammasome mRNA expression in eWAT was measured by qPCR (**P<0.01). Oxidative damage assessed by 8-iso-PGF_{2α} concentration (O; *P < 0.05) and 4HNE immunostaining (P). Data are means ± SEM; differences detected by two-way ANOVA; N = 7-9 mice per group.

Figure 3.4

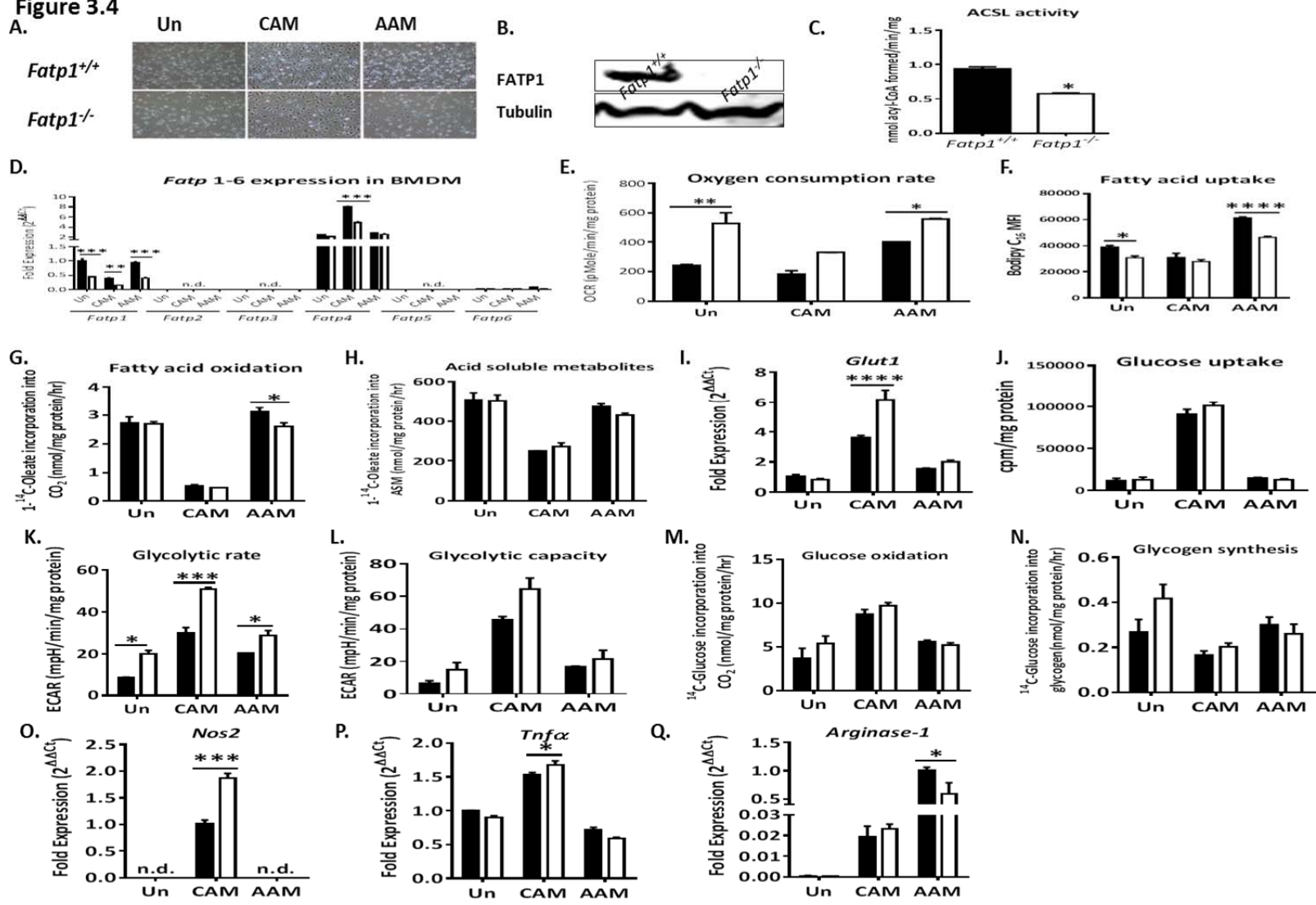


Figure 3.4: *Fatp1* deletion decreased acyl-CoA synthetase (ACSL) activity and resulted in a metabolic shift from lipid oxidation to glycolysis that resulted in exacerbated CAM and less AAM activation. A. Morphology was evaluated in representative (20X) photomicrographs in unstimulated (Un), classically activated by 5ng/ml LPS and 10ng/ml IFN γ (CAM), or alternatively activated using 10ng/ml IL-4 (AAM) BMDM. B. FATP1 protein expression was measured by immunoblot in unstimulated BMDM. Tubulin is used as a loading control. C. ACSL activity was measured using 14 C-oleate in unstimulated *Fatp1*^{+/+} and *Fatp1*^{-/-} BMDMs (*P<0.05). D. *Fatp1-Fatp6* mRNA was measured in BMDM generated from *Fatp1*^{+/+} and *Fatp1*^{-/-} mice on chow diet (**P<0.01; ****P<0.0001 *Fatp1*^{+/+} vs. *Fatp1*^{-/-}). E. Oxygen consumption rate (OCR) was measured using the Seahorse Bioanalyzer in Un, CAM, and AAM-polarized BMDM from *Fatp1*^{+/+} and *Fatp1*^{-/-} mice. (**P<0.01 and *P<0.05). F. Fatty acid uptake was measured using BODIPY®-palmitate (*P<0.05 and ****P<0.0001, *Fatp1*^{+/+} vs. *Fatp1*^{-/-}). Complete (G) and incomplete oxidation (H), as measured by acid-soluble metabolites (ASMs), was measured using 14 C-oleate (*P<0.05). I. *Glucose transporter 1 (Glut1)* mRNA was quantified by qPCR (****P<0.0001). J. Glucose uptake was measured by 3 H-2-deoxyglucose uptake. K. Glycolytic rate, as measured by extracellular acidification rate (ECAR), was measured using the Seahorse Bioanalyzer (*P<0.05, ***P<0.001, N=3). L. Glycolytic capacity was determined using the Seahorse. 14 C-glucose oxidation (M) and incorporation into glycogen (N) was measured. O. *Inducible nitric oxide synthase (Nos2)*, (P) *Tnfa* and (Q) *Arginase-1* mRNA expression concentrations were measured by qPCR (*P<0.05, ***P<0.001); polarization has an effect in all figures (P<0.0001). * denote differences between *Fatp1*^{+/+} vs. *Fatp1*^{-/-} within a polarization group. Data are mean \pm SEM; differences were detected by two-way ANOVA. Representative of at least N=3 experiments with n=4 replicates per experiment.

Figure 3.5

PATHWAY	BIOCHEMICAL NAME	BMDM <i>Fatp1</i> ^{-/-} / <i>Fatp1</i> ^{+/+}
		CAM/M0:CAM/M0
Alanine and aspartate metabolism	N-acetyl-beta-alanine	2+
Valine, leucine and isoleucine metabolism	2-methylbutyrylcarnitine	2-
	isovalerylcarnitine	2-
Polyamine metabolism	putrescine	2-
	spermidine	2+
	spermine	2+
Glycolysis, gluconeogenesis, pyruvate metabolism	glucose-6-phosphate (G6P)	2+
	glucose 1-phosphate	2+
	fructose-6-phosphate	2+
	3-phosphoglycerate	2+
	phosphoenolpyruvate (PEP)	2-
	lactate	2-
Purine metabolism	xanthosine	2+
	xanthosine 5'-monophosphate (xmp)	2+
	inosine 5'-monophosphate (IMP)	2+
	N1-methyladenosine	2-
	adenylosuccinate	2+
	guanosine 5'-diphosphofucose	2-
Pyrimidine metabolism, thymine	thymidine	2-
Nucleotide sugars, pentose metabolism	6-phosphogluconate	2+
	arabitol	2+
	ribose	2+
Essential fatty acid	docosapentaenoate (n6 DPA; 22:5n6)	2-
Fatty acid, dicarboxylate	azelate (nonanedioate)	2+
Glycerolipid metabolism	ethanolamine	2+
	glycerol 3-phosphate (G3P)	2+
	glycerophosphorylcholine (GPC)	2+
	cytidine 5'-diphosphocholine	2-
Sterol/Steroid	lanosterol	2-
Folate metabolism	biopterin	2+
Nicotinate and nicotinamide metabolism	nicotinamide adenine dinucleotide (NAD+)	2-
	nicotinamide adenine dinucleotide reduced	2-
	adenosine 5'diphosphoribose	2-
	phosphopantetheine	2+
Pantothenate and CoA metabolism	coenzyme A	2+
	pyridoxal	2-
Riboflavin metabolism	riboflavin (Vitamin B2)	2-

Figure 3.5: Lack of FATP1 in CAM-polarized BMDM enhanced Pentose Phosphate Pathway activity. Key indicates -2 to +2 fold relative concentration of CAM-polarized *Fatp1*^{-/-} BMDM normalized to unstimulated *Fatp1*^{-/-} BMDM macrophages over CAM-polarized *Fatp1*^{+/+} BMDM normalized to unstimulated *Fatp1*^{+/+} BMDM macrophages. Metabolomic profiling demonstrated that deletion of *Fatp1* primed BMDM for an enhanced shunting of glucose to the pentose phosphate pathway rather than glycolysis (red boxes). N = 4 per group.

Figure 3.6

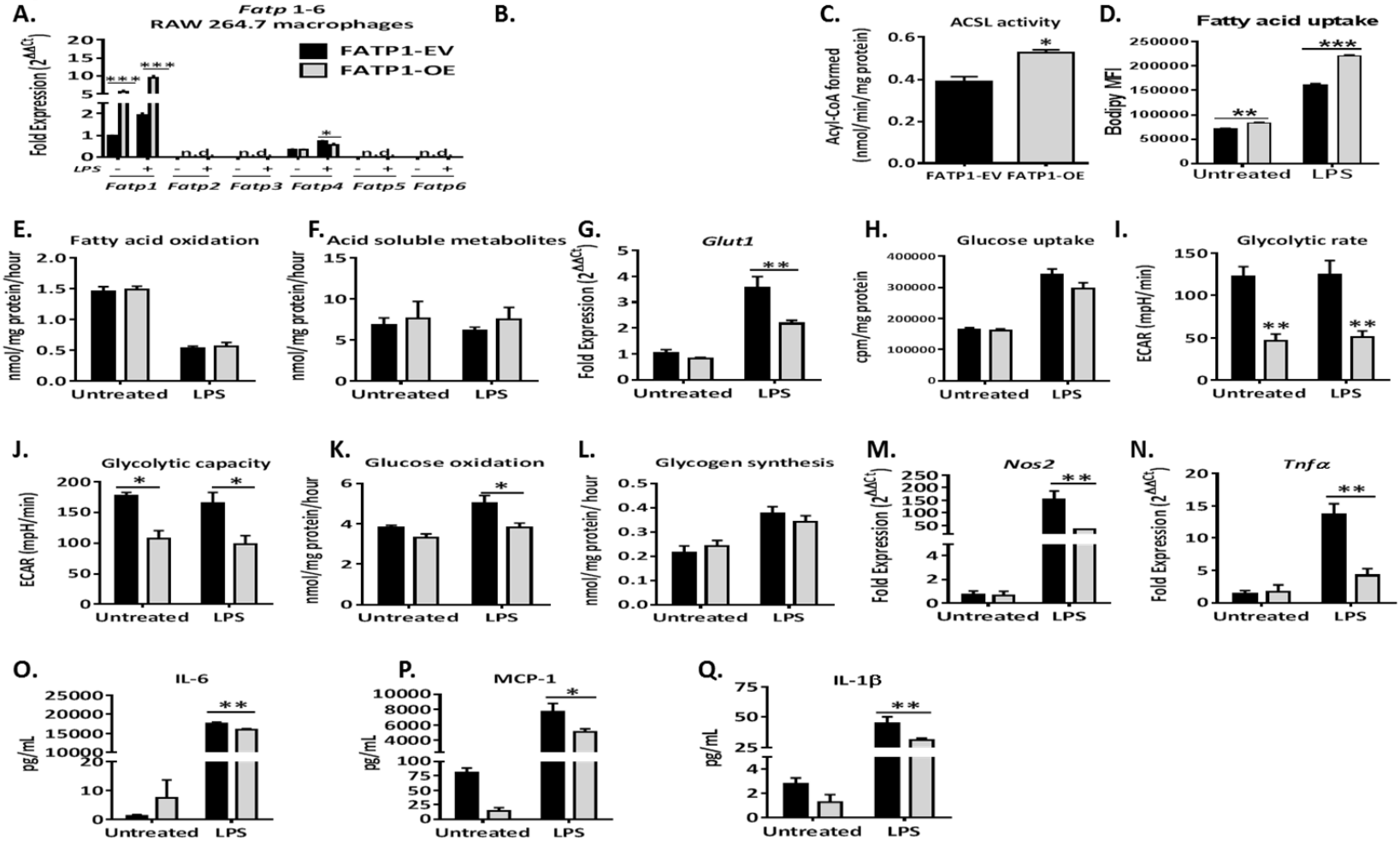
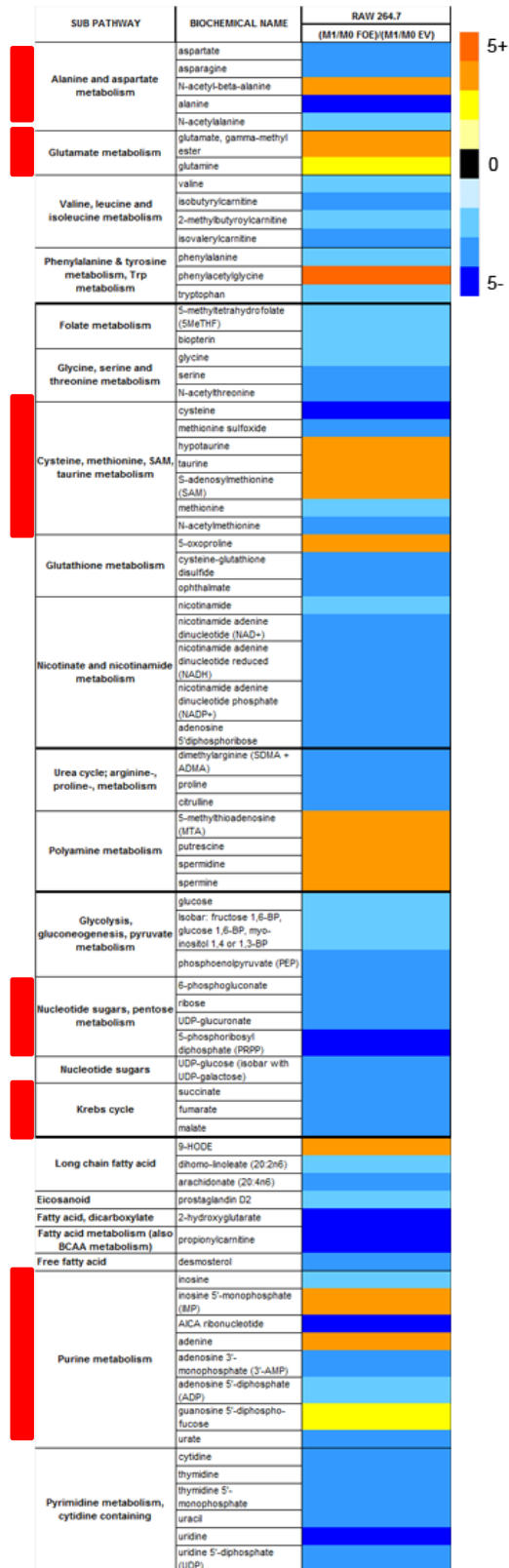


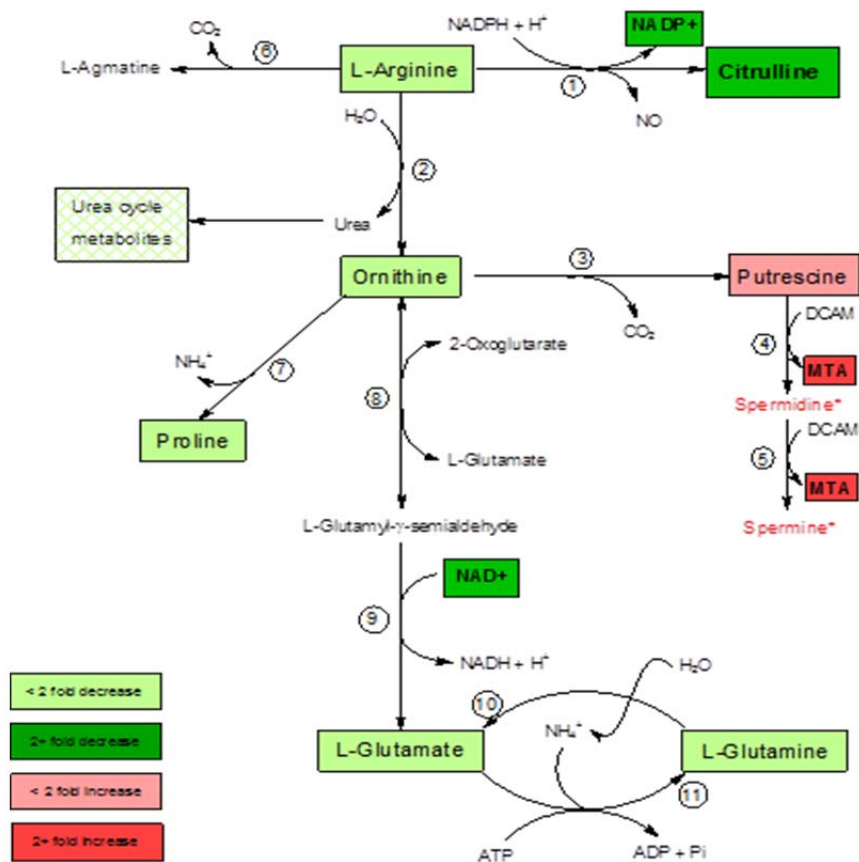
Figure 3.6. Over-expression of FATP1 in RAW264.7 MΦs induced a substrate switch with enhanced lipid metabolism and reduced glucose metabolism resulting in blunted CAM-activation. *Fatp1* was stably over-expressed in RAW264.7 MΦs (FATP1-OE). FATP1-OE were left untreated or stimulated for 24 hrs with 100ng/ml LPS and were compared to empty vector controls (FATP1-EV). A. *Fatp1-6* were measured by qPCR. (n.d., not determined; ***P<0.001, *P<0.05). B. FATP1 immunoblot in unstimulated RAW264.7 (RAW) MΦs, FATP1-EV, and FATP1-OE. Tubulin was used as a loading control. C. FATP1-mediated long chain ACSL activity was measured using ¹⁴C-oleate (P<0.05). D. Fatty acid uptake was measured using BODIPY®-palmitate (**P<0.01, ***P<0.001). Complete (E) and incomplete oxidation (F) of ¹⁴C-oleate were measured. G. *Glut1* expression was measured by qPCR (**P<0.01). H. ³H-2-deoxyglucose uptake was measured. Glycolytic rate (I) and glycolytic capacity (J) were measured using a Seahorse Bioanalyzer (**P<0.01, *P<0.05). ¹⁴C-glucose oxidation (K) and glycogen synthesis (L) was measured (*P<0.05). Data are mean ± SEM. Representative of at least N=3 experiments with n=4 replicates per experiment. *Nos2* (M) and *Tnfα* (N) expression was measured by qPCR (**P<0.01, ***P<0.001). Secreted IL-6 (O) and MCP-1 (P) were measured by Luminex (**P<0.01, *P<0.05). The inflammasome product IL-1β was measured by Luminex (Q, ***P<0.001, **P<0.01). Data are mean ± SEM; differences were detected by two-way ANOVA. Representative of at least N=3 experiments with n=4 replicates per experiment.

Figure 3.7

A.



B.



C.

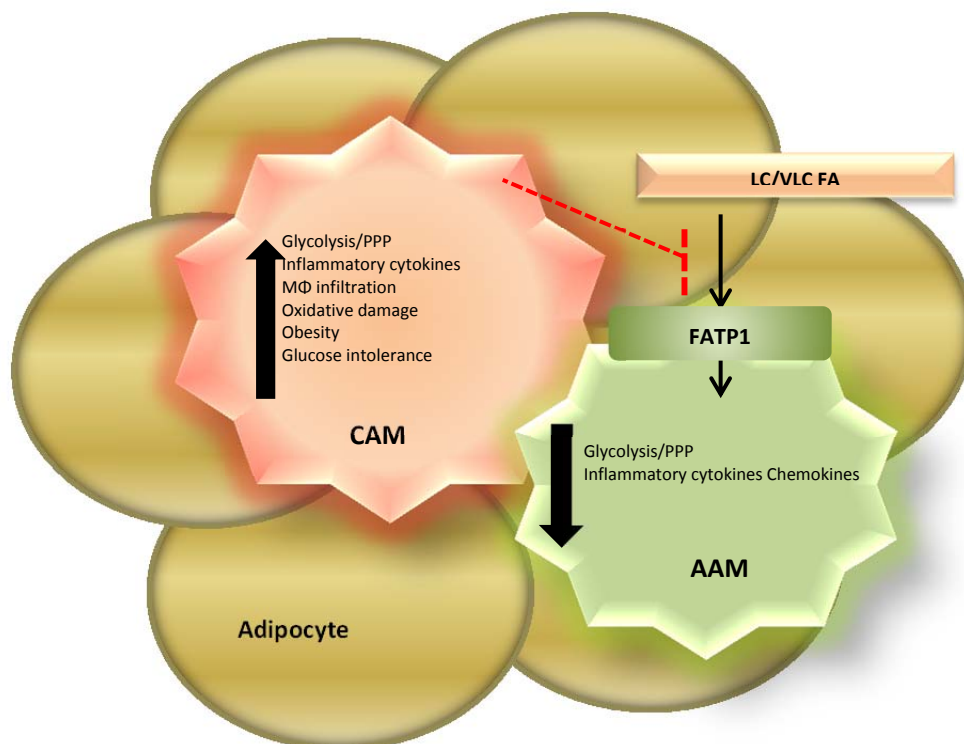


Figure 3.7. Over-expression of FATP1 reduced inflammatory response in RAW264.7 macrophages. A. FATP1 over-expression resulted in significant changes in concentrations of metabolites involved in amino acid, nucleotide, one-carbon, polyamine, carbohydrate and lipid metabolic pathways upon CAM polarization. Key indicates -5 to +5 fold relative expression of CAM- polarized normalized to unstimulated FATP1-OE macrophages over CAM-polarized normalized to unstimulated FATP1-EV macrophages. FATP1 over-expression blunted activation of iNOS in response to CAM (B, modified from (51). C. Model: FATP1 is necessary to maintain the AAM phenotype and to reduce HFD-induced adipose tissue inflammation and systemic glucose intolerance.

Table 3.1

Table 3.1. Hematologic analysis of *Fatp1^{+/+}* and *Fatp1^{-/-}* blood. Blood was collected by submandibular bleed into EDTA-coated tubes and analyzed by the UNC Animal Clinical Chemistry Core to measure differentials of blood cells including cells defined in Key. N=5.

Hematological Tests	<i>Fatp1^{+/+}</i>	<i>Fatp1^{-/-}</i>	<i>P value</i>
WBC (x10 ³ /uL)	3.76	4.30	0.72
LYMF (x10 ³ /uL)	2.72	3.10	0.76
GRAN (x10 ³ /uL)	0.64	0.76	0.59
MONO (x10 ³ /uL)	0.40	0.44	0.73
LYMF%	62.50	69.12	0.57
GRAN%	24.20	20.50	0.62
MON%	13.30	10.38	0.51
HCT %	41.60	39.52	0.67
MCV (fL)	46.50	45.70	0.48
RBC (x10 ⁶)	8.91	8.67	0.81
HGB (g/dl)	13.88	13.16	0.65
MCH (pg)	15.50	15.26	0.49
MCHC (g/dL)	33.40	33.40	1.00
RDW%	15.38	15.46	0.90
MPV (fL)	6.00	6.14	0.10
PLT (10 ³ /uL)	764.80	473.68	0.15

KEY: white blood cell number (WBC#), lymphocytes percentage (Lym%), concentration of lymphocytes (Lym#), percentage of monocytes (Mon%), concentration of monocytes (Mon#), percentage of granulocytes (Gra%), concentration of granulocytes (Gra#), RBC# (red blood cells), HGB (hemoglobin), HCT (hematocrit), MCV (mean corpuscular volume), mean corpuscular hemoglobin (MCH), mean corpuscular hemoglobin concentration MCHC (MCHC), red blood cell distribution width (RDW %), platelets (PLT), mean platelet volume (MPV). P values determined by student's *t*-test.

Table 3.2

Table 3.2. Flow cytometric analysis of circulating *Fatp1*^{+/+} and *Fatp1*^{-/-} lymphocytes. Blood was collected by submandibular bleed into EDTA-coated tubes, lymphocytes washed and stained as outlined in "Methods". N=5. P values determined by student's *t*-test.

Flow Cytometric Measures	<i>Fatp1</i> ^{+/+}	<i>Fatp1</i> ^{-/-}	<i>P</i> value
Cell/uL of Blood	3100.86	2839.14	0.63
MFI CD11c	74.58	75.88	0.76
MFI CD11b	3643.00	4319.20	0.40
General Lymphocyte	83.74	83.30	0.89
CD45+	98.32	99.10	0.12
CD45hi cells	86.84	87.90	0.58
CD45hi/CD115hi	12.86	13.19	0.91
CD45hi/CD115hi/Ly6Gclo	25.26	24.04	0.77
CD45hi/CD115hi/Ly6GChi	74.58	75.88	0.76
CD45hi/CD115lo	58.48	57.84	0.73
CD45hi/CD115lo/Ly6GChi	9.62	10.58	0.38
General Granulocyte	2.76	3.16	0.60
General Monocyte	13.35	13.29	0.99
General Lymphocyte	2548.28	2329.56	0.61
CD45+	3047.67	2814.55	0.67
CD45hi cells	2694.93	2492.34	0.67
CD45hi/CD115hi	352.01	339.78	0.91
CD45hi/CD115hi/Ly6Gclo	92.96	73.34	0.47
CD45hi/CD115hi/Ly6GChi	258.62	266.27	0.94
CD45hi/CD115lo	1577.64	1434.75	0.61
CD45hi/CD115lo/Ly6GChi	152.89	153.02	1.00
General Granulocyte	86.91	88.23	0.96
General Monocyte	408.29	389.75	0.89

Figure 3.8

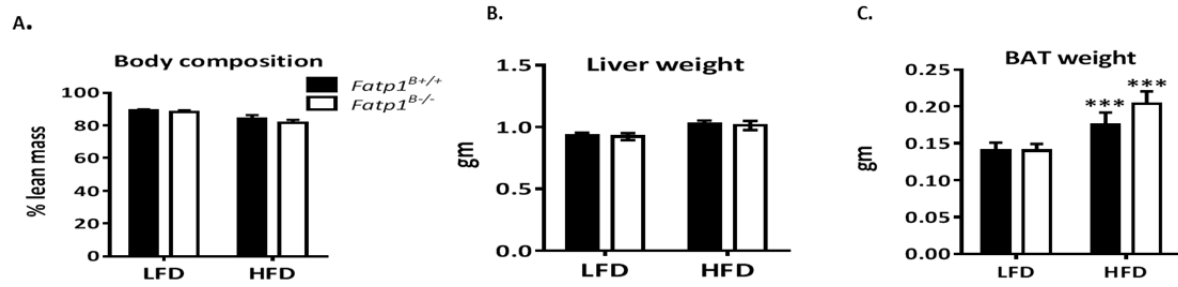


Figure 3.8. FATP1 expression level had no effect on lean body mass, liver weight or brown adipose (BAT) weight. A. Body composition is measured by MRI. Liver (B) and BAT (C) weights were measured at euthanasia. Data are mean \pm SEM; differences were detected by two-way ANOVA. ***P<0.001, LFD vs HFD. N=17-19 animals per group.

Figure 3.9

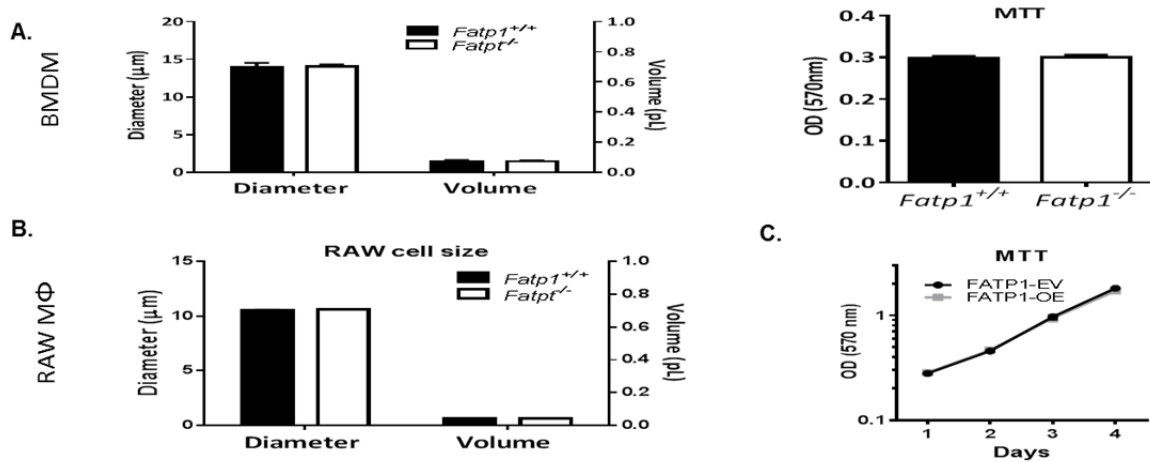


Figure 3.9. Deletion or over-expression of FATP1 had no effect on cell size or viability.

Fatp1^{+/+} and *Fatp1*^{-/-} BMDM (A) and FATP1-EV and FATP1-OE RAW (C) cell diameter and volume were measured by Millipore Sceptor. B. BMDM viability was measured by MTT assay. Only one MTT measurement was taken for BMDM since these are non-proliferating cells. D. RAW cell viability was also measured by MTT assay over three days. For BMDM, data were collected from an average of 35,000 cells per genotype. For RAW, data was collected from 373000 (FATP1-EV) and 348000 (FATP1-OE) cells.

CHAPTER IV: REMODELING THE MICROENVIRONMENT IN EARLY ADULTHOOD BY WEIGHT LOSS RESTRAINED DIET-INDUCED BASAL-LIKE BREAST CANCER PROGRESSION

Yuanyuan Qin, Sneha Sundaram, Luma Essaid, Xin Chen, Samantha M. Miller, David B. Darr, Joseph Galanko, Stephanie A. Montgomery, Ben Major, Gary L. Johnson, Melissa A. Troester, Liza Makowski

Submitted to Breast Cancer Research and Treatment

Overview

Obesity is associated with an aggressive subtype of breast cancer called basal-like breast cancer (BBC). BBC is fast proliferating and aggressive, with no targeted therapies, making the need for mechanistic insight urgent. Using the C3(1)-Tag murine model of BBC, we previously reported that obesity decreased tumor latency. Weight gain in adulthood is a common period of risk and is an important period to understand contributors to BBC oncogenesis. Reducing adiposity is predicted to lower incidence of BBC in human populations. Thus, the objective of this study was to test the hypothesis that a dietary intervention to reduce adiposity prior to tumor onset would reverse HFD-induced BBC latency and early progression. Adult C3(1)-Tag mice were fed a low fat diet (LFD, 10% calories from fat) or high-fat diet (HFD, 60% calories from fat) to induce changes in body composition akin to obesity, and a group initially exposed to HFD was then switched to LFD to induce weight loss. Two weeks after weight loss, mice in the diet-switch group displayed body weight and adiposity similar to the lean mice on LFD. Importantly, mice that lost weight after diet switch displayed significantly delayed median tumor latency (17.1 weeks) compared to mice fed HFD (15.9 weeks). No difference was found in latency between mice in the LFD group (17.6 weeks) and in the diet-switch group. Spearman correlation analysis

demonstrated that adiposity and bodyweight predicted tumor latency. There was no change in tumor burden amongst any of the diet groups. While there were no changes in plasma insulin or blood glucose concentrations associated with body composition, plasma leptin concentrations significantly increased with weight gain and were reduced to control levels with weight loss. Plasma leptin concentration negatively correlated with tumor latency. A second group of mice were fed the same diets and were sacrificed prior to average tumor latency to examine changes in the unaffected mammary gland microenvironment at 15 weeks of age. Diet switch-induced weight loss decreased atypical ductal hyperplasia and ductal carcinoma in situ in mammary glands of mice at 15 weeks of age. Therefore the HFD-exposed microenvironment that promoted early tumor onset was reprogrammed by weight loss and the restoration of a lean phenotype. To determine mechanisms underlying the protection associated with weight loss, we performed comprehensive activated kinase analysis in unaffected mammary glands isolated from mice at 15 weeks of age. Importantly, weight loss reversed HFD-induced activation of PKC- α , PKD1, PKA, and MEK3 in unaffected mammary glands, which all likely led to inactivation of the mitogen-activated protein kinase MAPK pathway and proliferation, resulting in delayed tumor latency in mice on the 60-10% diet switch compared to mice fed the 60% HFD.. In sum, HFD-induced tumor aggressiveness could be reversed by a diet switch that reduced adiposity and leptin levels to those of lean controls. In addition, several kinases were demonstrated to be inversely regulated by HFD and weight loss indicating novel regulators of BBC progression which can be translated to human studies using conserved biological approaches.

Introduction

Breast cancer is the most common cancer for women worldwide, and the second most important contributor to cancer mortality in the US. Of all the breast cancers, basal-like breast cancer (BBC) remains the greatest challenge because it is highly aggressive and lacks the molecular targets for current targeted drug treatments¹³. Epidemiologic studies indicate that obesity is strongly associated with BBC in both pre- and post-menopausal women^{30,31}. Understanding the reversibility and molecular underpinnings of obesity-induced risk is necessary to design prevention and treatment strategies.

Our previous studies have recapitulated epidemiologic findings by showing that HFD-induced obesity led to an early onset of BBC tumors in a genetically engineered mouse model (GEMM)²⁴². Despite correlative findings in humans and mice, the mechanism of how obesity increases BBC risk remains unknown¹³. Obesity alters whole-organism physiology, resulting in dysfunctional inflammatory and insulin signaling, among others¹⁸. In addition to these complex changes, it is also possible that alterations to the microenvironment surrounding a pre-cancerous lesion or tumor account for additional obesity-driven contributors to cancer risk. Indeed, it has been recognized that the microenvironment plays an important role in tumor formation and progression³². The cellular composition, metabolites, growth factors including adipokines such as leptin, and modifications to the extracellular matrix in the microenvironment have critical effects on tumor biology^{13,32}. Reports from our lab have demonstrated that BBC is characterized by unique epithelia-stroma interactions, which likely play a role in the tumor etiology¹⁶⁴. Thus, a convergence of hyperinsulinemia and hyperleptinemia with alterations to the microenvironment may contribute to the conversion of normal epithelial cells to hyperplastic cells and/or drive the progression from atypical hyperplasia to carcinoma.

The WHO suggested that body weight and physical inactivity account for approximately 1/5 to 1/3 of several of the most common cancers including breast cancer, and posit that more than 1/3 of cancers could be avoided by maintaining a healthy life style. Millikan et al. indicated that up to 68% of BBC could be prevented by promoting breastfeeding and reducing abdominal adiposity³¹. Therefore, weight loss may have a protective effect on tumorigenesis or tumor progression-possibly through alterations to the microenvironment. The window of dietary exposures, including weight gain and weight loss, is another important variable to consider in breast cancer risk. Epidemiological studies have shown that weight gain in adult life specifically is associated with increased breast cancer risk.

Based on these findings, we hypothesized that early adulthood HFD-induced carcinogenic effects on BBC can be reversed through weight loss and are dependent upon the changes in the microenvironment of mammary glands before tumor onset. To test our hypotheses, we used C3(1)-Tag GEMMs, which have been previously shown to be a faithful preclinical model of human BBC¹³⁵. Herein, we demonstrate that HFD-accelerated BBC can be delayed by weight loss induced by switching from HFD to LFD. HFD-induced changes to the mammary gland microenvironment included significantly increased atypical ductal hyperplasia and ductal carcinoma in situ in mammary glands before tumor onset. Most importantly, in HFD exposed mice, subsequent weight loss and reduction of adiposity successfully reversed atypical ductal hyperplasia and ductal carcinoma in situ to the levels detected in lean mice, i.e. the earliest markers of disease are affected by body composition. To determine if specific pathways regulated by weight loss could explain the reductions in atypical ductal hyperplasia and ductal carcinoma in situ, unaffected mammary glands isolated prior to average latency were subjected to activated kinome profiling. HFD exposure increased 6 and reduced activity of 4 kinases

relative to lean mice. Weight loss induced by diet switch increased activity of 14 and reduced activity of 5 kinases relative to lean controls. Importantly, compared to HFD-induced kinase changes, weight loss induced regulation included significantly reduced activity of PKC- α , PKD1, PKA, and MAPK kinase MEK3 in unaffected mammary glands, which together may result in inactivation of the mitogen-activated protein kinase MAPK/ERK pathway associated with proliferation. Weight loss after weight gain also decreased the activity of autophagy kinase unc-51 like kinase 3 (ULK3), and increased the activity of metabolically sensitive kinases such as 5'-AMP-activated protein kinase AMPK which may alter the metabolic milieu in the microenvironment. Our findings suggest that HFD alters the mammary gland prior to frank tumor onset, which contributes to atypical ductal hyperplasia, ductal carcinoma in situ and tumor latency, and these changes can be controlled by weight loss and reduction in adiposity.

Results

Tumor latency reduced by HFD exposure could be delayed by weight loss prior to tumor onset. To determine if weight loss in mice fed HFD prior to tumor onset would alter the course of tumorigenesis and/or progression, mice were subjected to various diet exposures (**Figure 4.1A**). At 8 weeks of age, C3(1)-Tag mice were fed control 10% (n =28) or 60% diets (n=59). There were no significant differences in body weight before starting the diet study (8 weeks of age, **Figure 4.1B**). Mice on 60% diet gained more weight than those on control 10% diet, and were significantly different after 1 week on diet ($P < 0.01$) and remained significantly different until the end of the study (**Figure 4.1B**). At 11 weeks of age, n=28 mice on the 60% diet were switched to 10% diet to induce weight loss (60-10% group, **Figure 4.1A**). At week 13 (1week post diet switch), mice on 60%-10% diet lost weight to the level of 10%-fed mice, and remained lean like 10%-fed mice for the remainder of the study. Mice from 60-10% diet group weighed

significantly less compared to mice on 60% diet from week 13 to the end of study ($P < 0.0001$, **Figure 4.1B**).

Time to first tumor was detected as tumor latency in the three C3(1)-Tag diet exposure groups. A log-rank Test was performed and chi square was equal to 6.73, with 2 degrees of freedom. The hazard ratios comparing either 60% or 60-10% to 10 % were 0.51 and 1.96, respectively. Hazard ratios comparing 60% to 10% was 0.51, $P < 0.01$, 60% to 60-10% was 1.961, 10% to 60-10% was 0.87, $p = \text{not significant}$. (**Figure 4.1C**). Mice exposed to 60% HFD diet exhibited a significant decrease in median tumor latency compared with lean controls (10%), from a median of 17.6 weeks in 60%-fed mice to 15.9 in 10%-fed mice ($P < 0.01$, **Figure 4.1C**). Mean latencies were 16.1 and 17.2 weeks for mice in 60% and 10% diet groups, respectively ($P < 0.05$, data not shown). Mice that first gained weight and then lost weight after diet switch had significantly delayed tumor latency of 17.1 weeks compared to 60%-fed mice (15.9 weeks, $P < 0.01$, **Figure 4.1C**). No difference in median or mean tumor latency was found between mice on 10% diet and on 60-10% diet. There was no change in total tumor burden with a mean of 4.9, 4.9, 5.0 tumors per mouse in groups fed 10, 60% and 60-10% diet, respectively (**Figure 4.7A**). Interestingly, tumors from mice on 60% diet grew at a significantly slower rate compared to tumors from mice on 10% ($P < 0.05$, **Figure 4.1D**). No significant difference in tumor growth was found between 60% and 60-10% groups. Furthermore, no difference was found in the tumor volumes among 3 groups at different time points (**Figure 4.7B**).

Early adulthood high fat diet-induced changes in body composition are rapidly reversed by weight loss. Although the mice only gained a few grams on the 60% HFD, which is typical for FVB/N and C3(1)-Tag mice²⁴², there was a significant effect of diet exposure and diet switch on body composition. Mice fed the 60% diet gained body fat in the first three weeks (from 8 to 11

weeks of age) as determined by MRI (**Figure 4.2A**). Mice fed 60% diet had significantly greater body fat mass compared to the mice on 10% diet at 11 weeks of age ($P < 0.0001$, **Figure 4.2A**). At 13 weeks of age (2 weeks after diet switch), body fat content of mice on the 60-10% diet decreased significantly, and remained similar to 10%-fed mice until sacrifice. Mice on 60% diet exhibited greater body fat content compared to 10% and 60-10% fed mice from 13 weeks of age until sacrifice ($P < 0.0001$ at weeks 13 and 15, and at sacrifice; **Figure 4.2A**). There were no significant differences in absolute lean mass in grams in any of the diet groups tested (data not shown). In line with changes in adiposity, plasma concentrations of the adipokine leptin increased significantly in mice fed the 60% diet compared to mice fed 10% diet after 3 weeks on diet ($P < 0.0001$, **Figure 4.2B**). After diet switch from 60% to 10% diet, leptin concentrations of mice in the 60-10% group were significantly reduced to the concentrations of leptin in lean mice, consistent with the adiposity and body weights ($P < 0.0001$, 60-10% vs. 60%; **Figure 4.2B**). No significant difference in leptin was found between 10% and 60-10% groups. The 60%-fed group had significantly greater leptin concentrations than the other 2 groups as soon as 2 weeks after the diet switch and at sacrifice ($P < 0.0001$, 60-10% vs. 60%; 10% vs. 60%, **Figure 4.2B**). No correlation of plasma leptin concentration and tumor latency was found before diet start at 8 weeks of age (data not shown). However, at 11 and 13 weeks of age, and at sacrifice, plasma leptin concentration negatively and significantly correlated with tumor latency ($P = 0.017$, 0.0043 , and 0.0029 , respectively) (**Figure 4.2C-E**). There were no diet-induced changes in 6-hour fasting plasma insulin (**Figure 4.8A**) or blood glucose levels (**Figure 4.8B**) over the course of the study. Likewise, $HOMA_{IR}$, a proxy measure of insulin resistance, did not reveal significant diet effects (**Figure 4.8C**).

Adiposity or body weight predicted BBC latency in C3(1)-Tag mice. To further explore the association between adiposity, body weight, and tumor latency, we stratified adiposity and body weight of all the mice from the 3 diet groups by quartiles. Quartile 1, defined as the bottom 25%, includes the mice with the lowest adiposity or bodyweight, while quartile 4 (top 25%) has the mice with the highest adiposity or body weight. Adiposity at diet start did not predict latency (**Table 4.1**). However, at 11, 13 and 15 weeks of age (i.e. 3, 5, and 7 weeks on diet) and at sacrifice, quartile 4 had significantly shorter latency compared to quartile 1 ($P=0.028$, 0.046 , 0.035 , 0.012 respectively, **Table 4.1**). Similar results were observed for body weight (**Table 4.2**). Before diet started (8 weeks of age) no difference was found in latency between quartiles 1 and 4 for body weight. At 13 and 15 weeks of age (i.e. 5, and 7 weeks on diet), quartile 4 had significantly shorter latency compared to quartile 1 ($P=0.033$, 0.0074 , respectively, **Table 4.2**).

Tumor progression is regulated by the microenvironment of mammary glands. Since HFD exposure and weight loss significantly altered tumor latency in this GEMM that is already induced, we next sought to examine alterations to the microenvironment that influence growth prior to palpation of tumor or latency. Mice were placed on diets as above at 8 weeks of age, and diet switch occurred at 11 weeks of age, however all mice were sacrificed at 15 weeks of age to examine “unaffected” mammary glands (**Figure 4.3A**). First, we examined if initiation of diet at 8 weeks of age altered the number of cells expressing the SV40 Tag transgene. Tag immunohistochemistry analysis exhibited no significant changes in unaffected mammary glands of mice (quantification in **Figure 4.3B** and representative images in **4.3C**). Second, we determined if HFD exposure and diet-induced weight loss altered pre-cancerous lesion formation. Histopathologic analysis of unaffected mammary glands was examined for regions of normal gland architecture including atypical ductal hyperplasia, ductal carcinoma in situ, and

invasive ductal carcinoma (**Figures 4.4A-D**). C3(1)-Tag mice fed the 60% diet had significantly increased atypical ductal hyperplasia in unaffected mammary glands at 15 weeks of age ($P < 0.05$, **Figure 4.4E**). Dietary intervention-induced weight loss significantly decreased atypical ductal hyperplasia to the levels detected in mammary glands from lean mice on 10% diet ($P < 0.05$, 60% vs. 60-10%, **Figure 4.4E**). HFD exposure increased ductal carcinoma in situ by about 3-fold; interestingly, weight loss significantly decreased ductal carcinoma in situ ($P < 0.05$, 60% vs. 60-10%, **Figure 4.4F**). Although mammary glands from mice fed 60% diet had increased numbers of invasive ductal carcinoma in unaffected mammary glands, no statistical differences were found between diet exposures (**Figure 4.4G**).

Kinome analysis revealed dramatic regulation of kinases by HFD, and diet-induced weight loss with important implications for BBC. Global analysis of kinase activity in unaffected mammary glands was carried out using MIBs, which consist of mixtures of sepharose beads with covalently immobilized, linker adapted, broad pan-kinase inhibitors for different kinases, which captures kinases in the active state in a reproducible and reliable assay (**Figure 4.5A**). Using MIB and subsequent mass spectrometry (MIB/MS) analysis, we identified a total of 155 kinases from unaffected mammary glands of C3(1)-Tag mice at 15 weeks of age (**Figure 4.9**). Individual runs of 2-4 pooled samples are displayed by kinase family normalized to 10%-fed controls for 60%-fed mice (**Figure 4.9A**) and 60-10%-fed mice (**Figure 4.9B**). Means of the runs for the 60% and 60-10%-fed mice are displayed (**Figure 4.9C**). **Figure 4.5B** shows a kinase signature defining a reprogrammed kinome in response to HFD-induced changes to the mammary gland microenvironment prior to average tumor latency. Six kinases displayed increased activity by > 1.5 fold when normalized to control mice on 10% diet, while the activity of 4 kinases were decreased to < 0.5 fold of mammary glands from mice fed 10% diet. The six kinases elevated by

HFD included protein kinase C alpha type (KPCA, *Prkca*), bone morphogenetic protein-2-inducible protein kinase (BMP2K, *Bmp2K*), phosphatidylinositol 3-kinase catalytic subunit type 3 (PK3C3, *Pik3c3*), serine/threonine-protein kinase D1 (KPCD1, *Prkd1*), serine/threonine-protein kinase MARK1(MARK1, *mark1*), and mast/stem cell growth factor receptor Kit (KIT, *Kit*). The 4 kinases decreased by HFD included 5'-AMP-activated protein kinase catalytic subunit alpha-2 (AAPK2, *Prkaa2*), interleukin-1 receptor-associated kinase 1 (IRAK1, *Irak1*), ketosamine-3-kinase (FN3K, *Fn3k*), and epithelial discoidin domain-containing receptor 1 (DDR1, *Ddr1*) in unaffected mammary glands (**Figure 4.5B**).

Weight loss resulted in decreased expression of all kinases that were elevated in HFD-fed mice, since no kinases in the diet switch group increased more than 1.5 fold when normalized to mice on 10% diet (**Figure 4.9B**). Fourteen kinases from the diet switch group showed more than a 1.25-fold increase in activity when normalized to mice on 10% diet. In the diet-switch group, five kinases decreased to more than 0.5 fold of the 10% diet mice(**Figure 4.5C**).

When directly comparing activity of kinases from unaffected mammary glands isolated from mice on HFD versus diet switch groups, several important kinases were discovered to be regulated by HFD and inversely regulated by weight loss (**Figure 4.5D**). Five kinases that were elevated by HFD feeding and decreased by weight loss included KPCA (*Prkca*), serine/threonine-protein kinase D1 KPCD1 (*Prkd1*), dual specificity mitogen-activated protein kinase kinase 3 (MP2K3) MEK3 (*Map2k3*, P=0.0044), PKA (*Prkacb*, P=0.0035), and unc-51 like kinase 3 ULK3 (*Ulk3*, P=0.034). In contrast, two kinases were unchanged or reduced by obesity and significantly increased by weight loss, respectively, including adenosine kinase ADK (*Adk*, P=0.045) and 5'-AMP-activated protein kinase catalytic subunit alpha-2 (AAPK2/AMPK (*Prkaa2*, P=0.037).

Discussion

One third of US population is obese and another 1/3 is overweight. Considering the high prevalence, obesity could be a target for breast cancer prevention with effective intervention strategy including weight loss or dietary modification. Indeed, weight loss after bariatric surgery is associated with a reduced incidence of cancer and a decreased incidence of metastasis. Weight loss induced by decreased dietary fat intake in early-stage breast cancer patients has been shown to improve the rate of relapse-free survival. However, the mechanisms mediating protection remain unknown. In murine studies, weight loss induced through caloric restriction protected against the development of breast cancer^{148,157,160,161}. For example, intermittent caloric restriction provided a moderate protective effect against mammary tumor development in MMTV-neu mice¹⁶¹. A meta-analysis of experimental murine models also suggested that weight loss induced by energy restriction decreased tumorigenesis in mammary glands¹⁶⁰. Our lab was the first to use a GEMM to study the effect of weight loss induced by dietary intervention on BBC risk. We previously reported that in mice fed HFD from weaning and then switched to a LFD in adulthood, HFD-induced tumor progression was reversed. Likewise, caloric restriction using a murine xenograft model of BBC demonstrated reduced tumor growth¹⁴⁸. Furthermore, exercise has been reported to reduce body weight and tumor progression in C3(1)-Tag mice¹⁶². Thus, BBC in humans and varied murine models is responsive to energetics and body composition status, but the exact timing and mechanisms remain unclear.

Herein, we aimed to focus solely on the adult window of susceptibility. Epidemiologic observations have demonstrated increase BBC risk in premenopausal women with high BMI^{30,31}. Thus, we aimed to induce changes in adiposity akin to weight gain in early adulthood. This is important because BBC is detected at a high prevalence in African Americans, a group more

susceptible to both obesity and weight retention after pregnancy, a period most likely in early adulthood³¹. In this study, C3(1)-Tag mice were fed HFD to induce obesity-like changes or left lean on LFD control diets starting at 8 weeks of age. Eight weeks of age is after pubertal development and is considered early adulthood in the murine life cycle. C3(1)-Tag mice develop tumors due to transgenic the simian virus (SV) 40 large T antigen (Tag) under the control of the rat prostatic steroid binding protein C3(1) gene¹³². Tag can bind to and inactivate p53 and Rb, two tumor suppressors critical for maintaining homeostasis of cell growth¹³³. It is well-established that at 8 weeks old, C(3)1-Tag mice develop atypical hyperplasia of ductal epithelium as reported previously¹³³. At 12 weeks of age, ductal carcinoma in situ appears, and at 16-18 weeks of age on average, 100% of female mice develop tumors when ductal carcinoma in situ becomes invasive ductal carcinoma^{132,133}. Using this unique BBC GEMM, we demonstrated that HFD-feeding in adulthood drove aggressive tumor formation, which resulted in a significant reduction in tumor latency, similar to our previous report²⁴². Importantly, weight loss prior to average tumor onset significantly delayed tumor latency, reversing the effects of HFD. There were no early effects on tumor initiation in C(3)1-Tag mice as there were no diet-induced differences in initiating cells expressing Tag. Therefore, it is likely that HFD doesn't play a dramatic role in the very early regulation of tumor initiation in C3(1)-Tag mice, but rather the progression through hyperplasia to ductal carcinoma in situ to detectable malignancy.

Bissell et al. stated that a normal microenvironment can suppress tumor progression, but when the homeostasis is interrupted (e.g. by obesity, certain exposures such as high fat diet, etc.), the microenvironment would promote tumor growth. BBC has been reported to have unique and significant epithelial-stroma interactions that contribute to oncogenesis^{164,165}. In addition, BBCs are more likely to recur locally than non-BBC cancers¹⁶⁶, even after mastectomy with clean

margins, suggesting a field defect¹⁶⁷ that may arise from epithelial or stromal alterations in the microenvironment. As defined by morphological features, breast cancer lesions progress through atypical ductal hyperplasia, ductal carcinoma in situ, and invasive ductal carcinoma. Importantly, the C(3)1-Tag mouse model has intact stroma of mammary glands which allows us to study how the microenvironment affects the development of breast cancer. Therefore, histopathologic analysis was undertaken on mammary glands isolated from C(3)1-Tag mice at 15 weeks of age to detect changes to the microenvironment at a time before frank tumors could be detected by palpation. Analysis revealed significantly increased atypical ductal hyperplasia and ductal carcinoma in situ after just 7 weeks of HFD exposure. Mice that lost weight and adiposity secondary to diet switch were significantly protected from HFD-induced atypical ductal hyperplasia and ductal carcinoma in situ development. The number of invasive carcinomas was also decreased by diet switch-induced weight loss compared to HFD-fed, but this reduction was not statistically significant. The fact that atypical ductal hyperplasia and ductal carcinoma in situ were increased by HFD and reversed to the level of lean mice by weight loss indicated that adiposity - or other changes to the mammary gland - could affect already initiated proliferating cell through modulating tumor progression during a unique window of susceptibility (e.g. from initiated cancer stem cells to atypical ductal hyperplasia, or from atypical ductal hyperplasia to ductal carcinoma in situ, and from ductal carcinoma in situ to invasive ductal carcinoma)¹³³. Thus, the pathological changes in the mammary gland at this critical period of tumorigenesis indicated that the early progression of basal-like tumors can be delayed or reversed by HFD and weight loss.

Adipokines associated with adiposity include growth factors and metabolic regulators such as leptin. Leptin is a hormone produced by adipocytes in proportion to adiposity as reflected

by concentrations detected in HFD- and diet switch-fed C3(1)-Tag mice. Weight gain in early adulthood increased circulating leptin concentrations and weight loss reversed the leptin levels to those detected in LFD-fed controls. Spearman correlation analysis revealed significant correlations between leptin and latency as early as 3 weeks on diet, with greatest significance at sacrifice which suggests a potential role for leptin signaling in BBC. A meta-analysis reported that women with breast cancer have elevated plasma leptin levels. High leptin receptor mRNA expression in breast cancer tissue was also established to predict poor prognosis in patients with high serum leptin levels. Therefore leptin plays a central role at the interface of obesity and breast cancer and may act through several pathways¹³. One way in that leptin may drive BBC is that leptin signaling maintains cancer stem-like properties in triple negative breast cancer cells, which was shown to mediate tumor recurrence and metastasis in orthotopically transplanted mice. Leptin signaling also induces breast tumor cell growth through activation of the JAK-STAK and PI3K signaling pathway in both human and mouse cell lines. Leptin receptor deficiency in MMTV-PyMT mice was shown to attenuate tumor growth and metastasis through increasing mitochondrial respiration capacity in tumor cells and deactivating the downstream ERK and STAT3 pathways. Considering the crucial role of leptin signaling in breast cancer development, weight loss-associated changes in leptin concentrations could have an important contribution to BBC prevention. Other contributors often associated with obesity-induced carcinogenesis including glucose and insulin were not altered by diet exposures. The role of leptin receptor and stem cells in diet-induced effects on BBC are currently under investigation.

Obesity can also disturb the microenvironment by reprogramming the kinome, or activating and interrupting growth factor/receptor signaling, such as leptin and other mediators^{13,18}. Weight loss may help restore these changes in the mammary gland and rebuild

homeostasis of the microenvironment. Thus we hypothesized that kinases in the microenvironment of mammary glands prior to latency could be regulated by diet-induced body composition changes. About one fourth of all kinases may be involved in oncogenesis. Protein kinases regulate cell proliferation, survival, and metabolism and can contribute to tumor progression. Using novel kinome profiling of activated kinases, our results from unaffected mammary glands of mice at 15 weeks of age captured 155 activated kinases from all major kinome subfamilies. HFD feeding and weight loss by diet switch up- and down-regulated several kinases (**Figure 4.6A**). Our analysis focused on 7 kinases specifically reciprocally regulated by HFD and diet-switch. The kinase that was most elevated by HFD feeding and displayed the greatest decrease in activity after weight loss was a serine/threonine protein kinase (KPCA, *Prkca*) known as PKC- α . PKC- α is activated by calcium, phospholipids, phorbol esters, and diacylglycerol. PKC- α activates diverse functions in a cell including cell proliferation through phosphorylating and activating RAF1, which activates the MAPK/ERK signaling cascade. PKC- α is a marker for breast cancer aggressiveness and BBC have high levels of MAPK activation. Recent studies have identified PKC- α as over-expressed in triple negative breast cancer cells expressing stem-like properties. PKC- α can also activate Y-box binding protein-1, an RNA and DNA-binding protein and a marker of aggressive tumors which has been reported in 73% of BBC. Inhibitors targeting PKC- α and cMet, another kinase that we have discovered to be regulated by HFD-induced exposure and weight loss²⁴², decreased triple-negative breast tumor growth in murine models. Therefore, the fact that PKC- α was positively and negatively regulated by HFD and weight loss, respectively, provides a novel mechanism of obesity-associated BBC progression with exciting potential for intervention by lifestyle changes or pharmacologic intervention in uniquely susceptible overweight or obese populations.

An important upstream regulator of PKC- α was demonstrated to be the second most potently upregulated kinase by HFD-induced weight gain and dramatically reduced by weight loss; the serine/threonine-protein kinase D1 (KPCD1, *Prkd1*). KPCD1 is also known as PKD1, not to be confused with 3-phosphoinositide-dependent protein kinase 1 (PDK1 or PDPK1), which is downstream of PI3K which phosphorylates Akt/PkB. KPCD1 or PKD1, activated by DAG and phorbol ester, is downstream of novel PKC signals and is involved in the regulation of MAPK1/3 (ERK1/2), MAPK8/JNK1 and RAS signaling, and regulates proliferation, similar to PKC- α above. PKD1 has been shown to increase cell proliferation in breast, prostate, salivary tumors and pancreatic cancers. In MCF-7 human breast cancer cells, PKD1 stimulated proliferation and enhanced tumorigenesis through MEK/ERK signaling. PKD1 also reduced serum- and anchorage-dependence for proliferation and survival *in vitro* and drove tumorigenesis in xenograft models of breast cancer. However, some studies on PKD1 and breast cancer are contradictory, and suggest that PKD1's actions may depend on control of tumor initiation and progression versus metastasis. Borges et al. demonstrated that PKD1 is expressed in cells of the unaffected mammary gland, and is necessary for preventing epithelial-to-mesenchymal transition and invasive carcinoma. Of great relevance to studies presented herein, PKD1 is one of the *few* genes identified as regulator of obesity. Through genome-wide association studies (GWAS), PKD1 was identified as a loci associated with human obesity, especially in obesity prevalent young adults, which is similar to the window of diet exposure and latency in C3(1)-Tag mice studied. Clearly, PKD1 must be further investigated, especially its role in obesity-associated breast tumorigenesis. Downstream of PKD1 and PKC- α is cAMP-dependent protein kinase catalytic subunit beta (KAPCB, *Prkacb*), also known as PKA. PKA mediates the activation of the MAPK/ERK signaling cascade through cAMP-dependent signaling triggered by receptor binding

to G-protein coupled receptors, which is involved in tumor progression. Elevated PKA activity in the mammary epithelium generated tumors in a murine model and was associated with BBC and poorer outcomes in patients.

The above kinases all act through the MAPK kinase family. Kinome analysis of C3(1)-Tag mammary glands revealed significant regulation of the MAP kinase kinase family member the dual specificity mitogen-activated protein kinase kinase 3 (MP2K3, *Map2k3*), also known as MEK3 or MKK3. MEK3 is a kinase activated by mitogenic and environmental signals and led to proliferation and cell survival through increased oncogene RAS expression, as well as activation of p38 α (MAPK14). RAS expression also led to increased MEK3, creating a feed forward loop driving oncogenic transformation of primary cells in breast epithelial cells. Inhibition of MEK3 led to reduction in cell proliferation and apoptosis. MEK3 was also increased by mutant p53 leading to increased proliferation and survival, and knockdown of MEK3 led to reduced cell viability as well as increased susceptibility to chemotherapeutic agents *in vitro* and *in vivo*. Interestingly, MEK3 is also linked to obesity and lipotoxicity in human populations, as well as diabetes in a murine model. In sum, **Figure 4.6B** demonstrates how weight loss reversed HFD-induced activation of PKC- α , PKD1, PKA, and MEK3 in unaffected mammary glands, which all likely led to inactivation of the mitogen-activated protein kinase MAPK/ERK pathway and proliferation, resulting in delayed tumor latency in mice on the 60-10% diet switch compared to mice fed the 60% HFD.

A final kinase moderately but significantly up-regulated by HFD and down-regulated by weight loss is the serine/threonine protein kinase unc-51 like kinase 3, ULK3 (*Ulk3*). ULK3 regulates the developmental and oncogenic pathway of sonic hedgehog (SHH) signaling and autophagy. Cancer cells often turn to autophagy at times of substrate need or hypoxia. ULK3 is

over-expressed in certain cancer cell lines but it's role in senescence versus tumorigenesis unclear. Since it is regulated by diet, and significantly reduced with weight loss after weight gain, ULK3 may be a promising target.

Two kinases were regulated in the inverse direction: reduced by HFD and increased with weight loss after diet switch. A kinase whose activity was reduced with HFD to more than 40% that of lean mice on LFD, and then reversed to control levels with weight loss is the alpha 2 catalytic subunit of AMP-activated protein kinase (AAKP2, *Prkaa2*). AMPK is an energy-sensing enzyme that controls nutrient metabolism. Under low energy or cellular stress, AMPK is activated to increase production of ATP through activation of catabolic pathways including fatty acid oxidation and glucose uptake along with inhibition of anabolic processes including fatty acid, protein, and cholesterol synthesis²⁷. Consistent with increased activated AMPK by weight loss in our results, activation of AMPK has been suggested to be a target for cancer prevention and treatment. For instance, a low incidence of cancer in diabetic patients on metformin is likely due to the drug's anti-proliferative effect through activation of AMPK. AMPK is also important in obesogenesis, diabetes, and exercise physiology. Significant associations were observed between AMPK and with weight change in patients on anti-depressants. Other groups have demonstrated that HFD-feeding decreased AMPK activity. However, the role of AMPK in cancer prevention may be complex since the EPIC population study did not detect any associations between SNPs in *PRKA*, breast cancer risk or body mass index. AMPK in BBC merits further study.

Overall, it is important to note that of all cancers, only about 5%-15% have a major genetic component. Most cancers are considered to be predominantly caused by environmental factors. Lifestyle components, like obesity, lack of exercise, smoking, etc., play an important role

in cancer initiation and progression through activating oncogenes and inactivating tumor suppressors. Thus, further understanding the tumor and microenvironment changes that occur on HFD and after weight loss will help identify novel strategies to prevent the progression of BBC to malignancy.

Methods

Reagents. Rat/Mouse Insulin ELISA kit was obtained from Millipore (EZRMI-13K; EMD Millipore, Billerica, MA, USA). Anti-SV40-Tag (sc-20800) was obtained from Santa Cruz (Santa Cruz, Santa Cruz, CA). Rat anti-F4-80 antibody is from a Bio-rad company (#MCA-497, AbD serotec, Raleigh, NC, USA). Biotin-SP (longer spacer) AffiniPure Goat anti-Rat IgG was from Jackson ImmunoResearch (#112-065-167, Jackson ImmunoResearch Inc. West Grove, PA, USA).

Animals and Diet. Animal studies were performed with approval and in accordance with the guidelines of the Institutional Animal Care and Use Committee at the University of North Carolina at Chapel Hill. Female C3(1)-Tag mice were obtained in collaboration with the UNC Lineberger Comprehensive Cancer Center (LCCC) Mouse Phase I Unit (MP1U). In female mice, the simian virus (SV40) large tumor antigen (Tag) is expressed in the distal mammary ductal epithelium and terminal ductal lobular unit in a hormone-independent manner leading to the development of mammary tumors¹³³. C3(1)-Tag mice were generated by crossing heterozygous male mice with FVB/N non-transgenic female mice. During breeding and after weaning at 3 weeks old, female C3(1)-Tag mice were put on Prolab Isopro RMH 3000 from LabDiet (St. Louis, MO, USA) until they were 8 weeks old when they were started on defined diets. Diets obtained from Research Diets Inc. (New Brunswick, NJ, USA) were matched for protein, vitamins, and minerals, and provided 10% kcal (“10%”); and 60% kcal (“60%”) derived from

fat. Details of the diet components are provided in Sundaram et al.²⁴² At 8 weeks of age, mice were randomly assigned to low fat diet (LFD) 10% (N=28) and high fat diet (HFD) 60% (N=59) diet groups. After 3 weeks on diet, at 11 weeks of age, N=28 mice on 60% were switched to 10% diet (See model of study design, **Figure 4.1A**). A second set of mice were initiated on 10% (N=8) and 60% (N=20) at 8 weeks of age. At 11 weeks of age, N=11 of 60%-fed were switched to 10% as above. This cohort was sacrificed at 15 weeks of age prior to average tumor latency and unaffected mammary glands were isolated. (See model of study design, **Figure 4.3A**).

Tumor latency, number, and progression. Mice were monitored for tumor development by palpating three times weekly. Tumor latency was defined as age at detection of first tumor in weeks. After detection of the first tumor, tumor volumes were measured weekly over 3 weeks using calipers to measure the width (short diameter) and length (long diameter) in millimeter for each tumor. The tumor volumes were calculated using the formula: $\text{length} \times \text{width}^2 \times 0.5$. The percent change in volume over time (tumor progression) was calculated as: $(\text{End volume} - \text{Start volume}) / \text{Start volume} \times 100$. Mean tumor progression (percent change in volume) of the first palpated tumor is presented. The total number of tumors per mouse was counted at sacrifice for total tumor burden.

Body weight and composition. Body weight was measured prior to starting mice on diet and weekly until sacrifice. Body composition including lean mass, fat mass, free water content, and total water content of non-anesthetized mice was also measured at 8 (diet start), 11 (diet switch), 13, and 15 weeks of age, as well as at sacrifice using the EchoMRI-100 quantitative magnetic resonance whole body composition analyzer (Echo Medical Systems, Houston, TX, USA). Fat mass is presented as percent fat mass over total body weight²⁴².

Tissue harvest. Three weeks after detection of the first tumor, mice were fasted for six hours and then anesthetized by an intraperitoneal (i.p.) injection of avertin (Fisher Scientific, Pittsburgh, PA, USA) prior to sacrifice. Blood was collected by cardiac puncture into a tube with EDTA to reach a final concentration of 0.05 mM. Plasma was separated by centrifuging blood at $500 \times g$ for 5 min and stored at -80°C . Tumors and/or unaffected 4th mammary glands were collected. Portions of the tissues were placed into a cassette and formalin-fixed for immunohistochemistry (IHC) and H&E analysis. A portion of the unaffected mammary gland from study 2 was snap frozen in liquid nitrogen for proteomic analysis.

Metabolic parameters and plasma. Blood glucose was measured on mice fasted for 6 hours prior to start of diet, at diet switch (3 weeks on diet), 2 weeks after diet switch, and at sacrifice using a Bayer Contour Blood Glucose Monitor (Bayer HealthCare LLC, Tarrytown, NY, USA). The metabolically relevant biomarker leptin was measured in the plasma collected at different time points using the MILLIPLEX MAP Mouse Angiogenesis/Growth Factor Magnetic Bead Panel - Cancer Multiplex Assay (EMD Millipore, Billerica, MA, USA). No significant differences were detected in other components of this panel. Plasma insulin concentrations were measured using Rat/Mouse Insulin ELISA kit (EZRMI-13K; EMD Millipore, Billerica, MA, USA) following the manufacturer's protocol. The homeostasis model assessment was used to calculate the approximate insulin resistance (HOMA_{IR}) using the formula $(\text{blood glucose (mg/dl at sacrifice)} \times \text{plasma insulin concentration (ng/ml)} / 405)$ as previously described²⁴².

Immunohistochemistry. Briefly, formalin-fixed and paraffin-embedded tissues were sectioned at 5 microns and mounted for histological staining²⁴². Tissues were blocked in a commercial protein blocking solution (Dako, X0909) and exposed to primary antibodies at 4°C overnight with gentle agitation. Anti-mouse F4/80 (1:100) and anti-SV40-Tag (1:250)

immunohistochemistry (IHC) staining was conducted as previously described^{23,163}.

Immunohistochemistry analysis was performed following the protocol previously described in Sundaram et al.²⁴² Following staining, slides were scanned into the Aperio Scanscope CS system (Aperio Technologies, Vista, CA, USA) at a magnification of 40× and staining was quantified using the Aperio Imagescope software. The scanned slides were analyzed using the appropriate algorithms as described previously¹⁶³. The Aperio Imagescope software positive pixel counts for diaminobenzidine (DAB) staining in the color deconvolution algorithm was completed for F4-80 and SV40-Tag^{23,242}. Aperio digital analysis of DAB prevents subjective bias in quantification. Random areas from sections ($n = 6$) were quantified and averaged per animal. $N = 8-11$ mice per diet exposure group for IHC of F4-80, SV40-Tag and H&E of unaffected mammary glands, as indicated in legends. Representative 40× images are presented.

Microenvironment pathological analysis. Histopathologic analysis was completed by a certified veterinary pathologist (S.M.). Sections from unaffected mammary isolated at 15 weeks of age in study 2 were analyzed for the presence of normal ducts, atypical ductal hyperplasia, ductal carcinoma in situ, and invasive ductal carcinoma. Histological composition in $n=6$ random areas from each section were quantified and averaged. Representative 40× images are presented.

Kinome Analysis. Multiplexed Inhibitor Bead (MIB) Affinity Chromatography: Isolation of activated kinases from tissue lysates was performed as described previously. Briefly, unaffected mammary glands from study 2 were collected at 15 weeks of age. Tissues were pulverized in liquid nitrogen and lysed on ice in MIB lysis buffer [50 mM HEPES (pH 7.5), 0.5% Triton X-100, 150 mM NaCl, 1 mM EDTA, 1 mM EGTA, 10 mM sodium fluoride, 2.5 mM sodium orthovanadate, 1X protease inhibitor cocktail (Roche), and 1% of phosphatase inhibitor cocktail 3 (Sigma-Aldrich)]. Two to four samples were pooled together for a total protein content of

2.5mg. Details of the MIB kinase analysis have been published previously. Briefly, tissue lysates were passed through a column of layered inhibitor-conjugated beads consisting of Sepharose-conjugated Shokat, AGCbead (UNC-21474), Purvalanol B, PP58, VI-16832 and CTx-0294885 (**Figure 4.5A**). Kinase-bound inhibitor beads were washed several times before elution in 1 mL of 0.5% SDS (100°C, 5 min). Eluted kinases were reduced, alkylated, and concentrated before chloroform/methanol extraction. Protein pellets were resuspended in 50 mM HEPES (pH 8.0) and were digested for 24 hours with sequencing grade modified trypsin (Promega). Digested peptides were labeled with iTRAQ reagent (AB SCIEX, Framingham, MA) for 2 hours at room temperature in the dark, according to the manufacturer's instructions. Labeled peptides were cleaned with PepClean C18 spin columns (Thermo Scientific) before fractionation on a Tempo™ LC MALDI Spotting System (AB SCIEX) using a Chromolith® CapRod® RP-18e HR analytical column (Merck KGaA, Darmstadt, Germany).

Mass spectrometry (MS) Analysis: As described previously, MS data were acquired with a MALDI TOF/TOF 5800 (AB SCIEX) and analyzed by ProteinPilot Software Version 3.0 (AB SCIEX) with a UniProtKB/Swiss-Prot database. Proteins were accepted when ≥ 1 unique peptide was identified at 99% confidence. Peptide quantitation by ProteinPilot was performed using the Pro Group Algorithm and quant ratios are bias and background-corrected.

Statistical analysis: Data are expressed as mean and standard error of the mean (SEM).

Percentage of tumor-free mice amongst the 3 diet exposure groups was compared with Kaplan-Meier analyses. Log rank and chi-square test were used to investigate differences among groups for tumor latency. Continuous variables for two groups were compared using t-tests. Continuous variables for more than two groups were compared using one way Analysis of Variance (ANOVA) with Tukey's post hoc test. The correlation of latency with body weight, adiposity or

leptin level at different time points was computed via Spearman Rank correlation. Analyses were performed using SAS Version 9.3 (SAS Institute, Cary NC USA) or GraphPad Prism 5 software (GraphPad Software, Inc. La Jolla, CA, USA). P-values <0.05 were considered statistically significant.

Figures and Tables

Figure 4.1

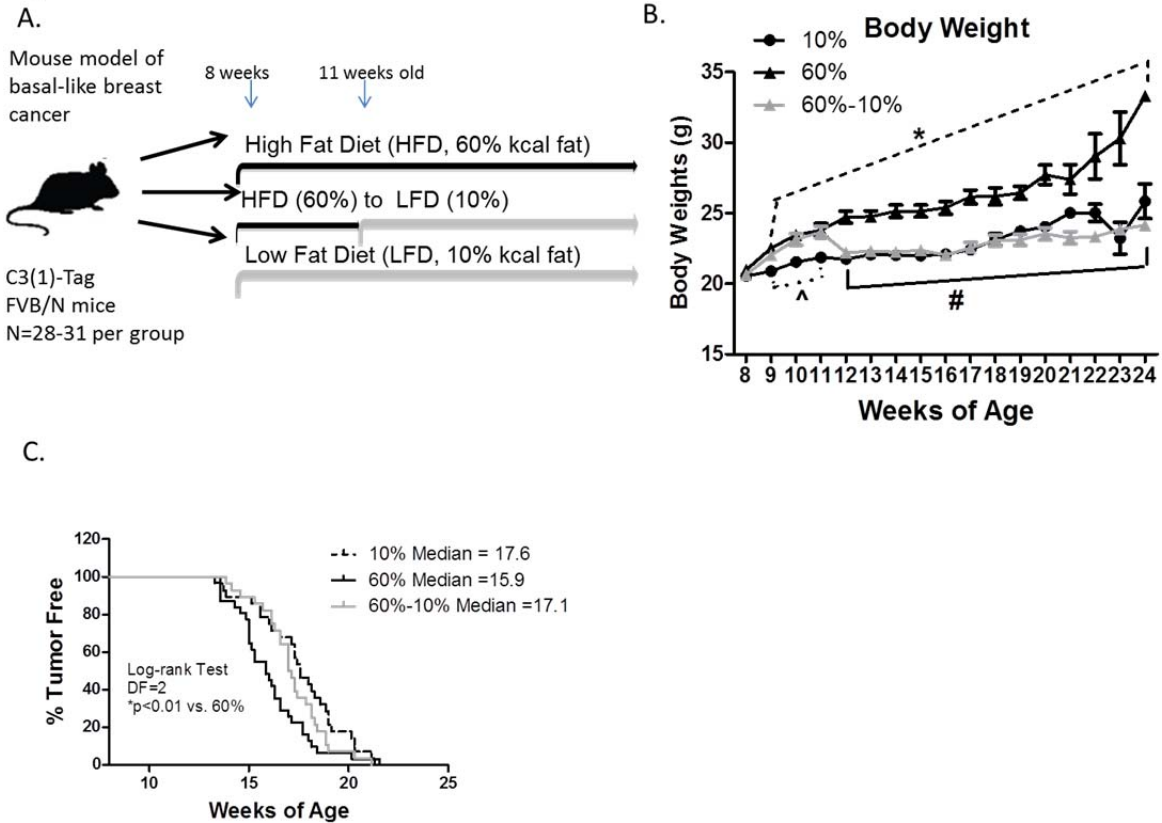


Figure 4.1. Weight loss protected against HFD-mediated early BBC onset. A. Model of study design 1. At 8 weeks of age, C3(1)-Tag mice were randomly assigned to 10% (N=28) and 60% (N=59) diet groups. After 3 weeks on diet, at 11 weeks of age, N=28 mice on 60% were switched to 10% diet. Mice were monitored for tumor onset by palpation 3 times a week. Three weeks after tumor onset, mice were sacrificed. B. Body weight was measured weekly. 10% vs. 60-10% ($\hat{P}<0.05$); 10% vs. 60% ($*P<0.01$); and 60% vs. 60-10% ($\#P<0.0001$). C. Mice were tumor free until first tumor palpated ($P<0.01$, 10% vs. 60%; 60-10% vs. 60%).

Figure 4.2

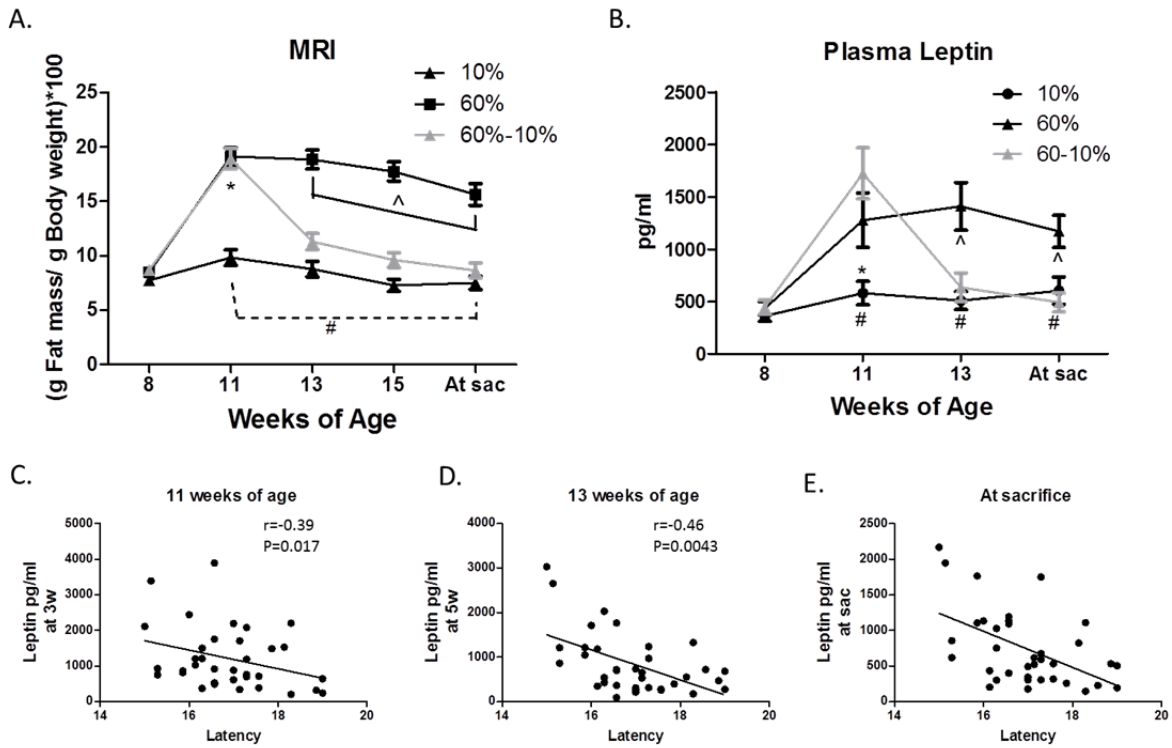


Figure 4.2. Body composition predicts latency. A. MRI was used to evaluate body composition. 10% vs. 60% (# $P < 0.0001$); 60% vs. 60-10% (^ $P < 0.0001$); and 10% vs. 60-10% (* $P < 0.0001$). N=28 10%, N=31 60%; N=28 60-10%). B. Plasma leptin was detected by Multiplex Assay. 10% vs. 60% (# $P < 0.0001$); 60% vs. 60-10% (^ $P < 0.0001$); 10% vs. 60-10%(* $P < 0.0001$). N=12 10%, N=12 60%; N=13 60-10%. C-E. Spearman correlations of plasma leptin with latency at 11 and 13 weeks of age and sacrifice ($P = 0.017, 0.043, \text{ and } 0.0029$, respectively).

Figure 4.3

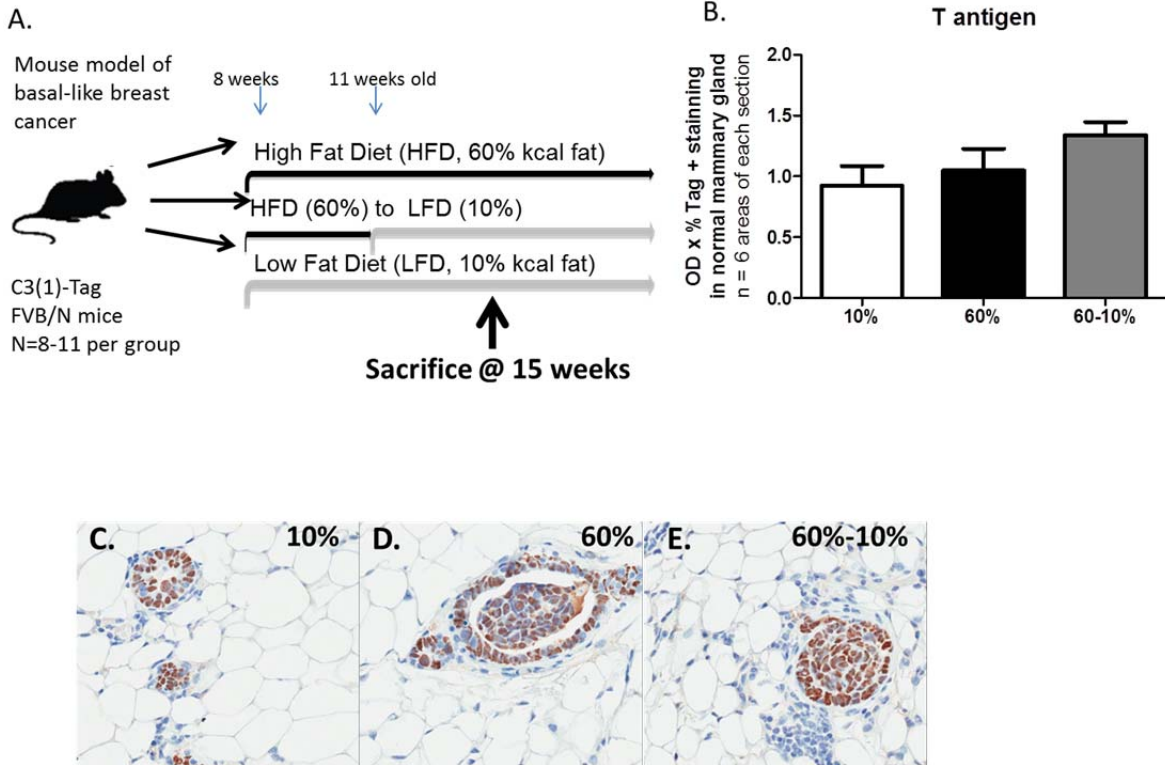


Figure 4.3. Diet did not affect tumor initiation. A. Model of study 2. A second set of mice were started on 10% (N=8) and 60% (N=20) at 8 weeks of age. At 11 weeks of age, N=11 of 60%-fed were switched to 10% as in study design 1. Mice were sacrificed at 15 weeks of age prior to average tumor latency and unaffected mammary glands were isolated. B. T antigen (Tag) expression was measured in unaffected mammary glands by immunohistochemistry staining. C-E. Representative 40X images are shown of Tag IHC staining from (C) 10% diet group, (D) 60% diet group, and (E) 60-10% diet group.

Figure 4.4

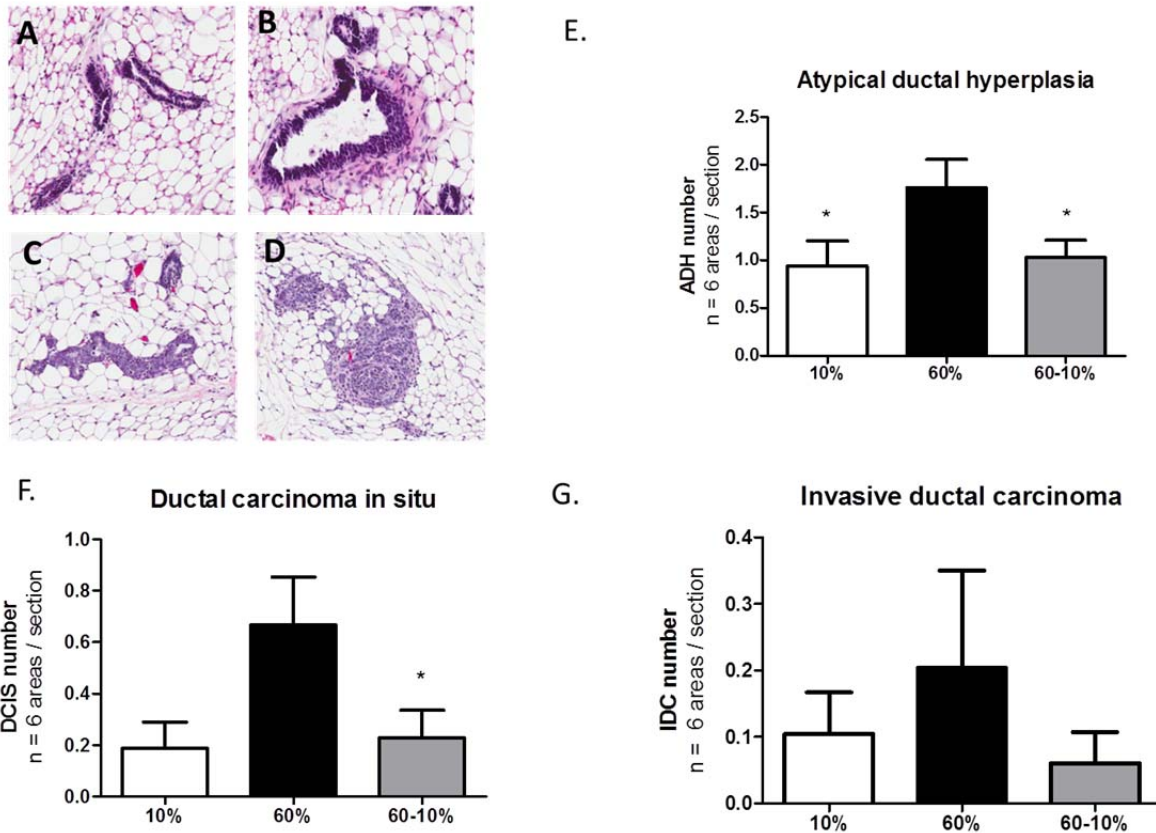


Figure 4.4. Pathological changes in the unaffected mammary gland induced by high fat diet were reversed by weight loss. Unaffected mammary glands were collected from 15-week old C3(1)-Tag mice in study 2. (A-D) Representative 40X images are shown of (A) normal duct, (B) atypical ductal hyperplasia, (C) ductal carcinoma in situ, and (D) invasive ductal carcinoma. E. Areas of atypical ductal hyperplasia were quantified in N=6 40X regions per section per mouse. *P<0.05, 10% vs. 60%; 60-10% vs. 60%. F. Areas of ductal carcinoma in situ were quantified as in E. *P<0.05, 60-10% vs. 60%. G. Areas of invasive ductal carcinoma were quantified as in E. N = 8 10%; N = 9 60%; N = 11 60-10%. Representative 40× images are presented.

Figure 4.5

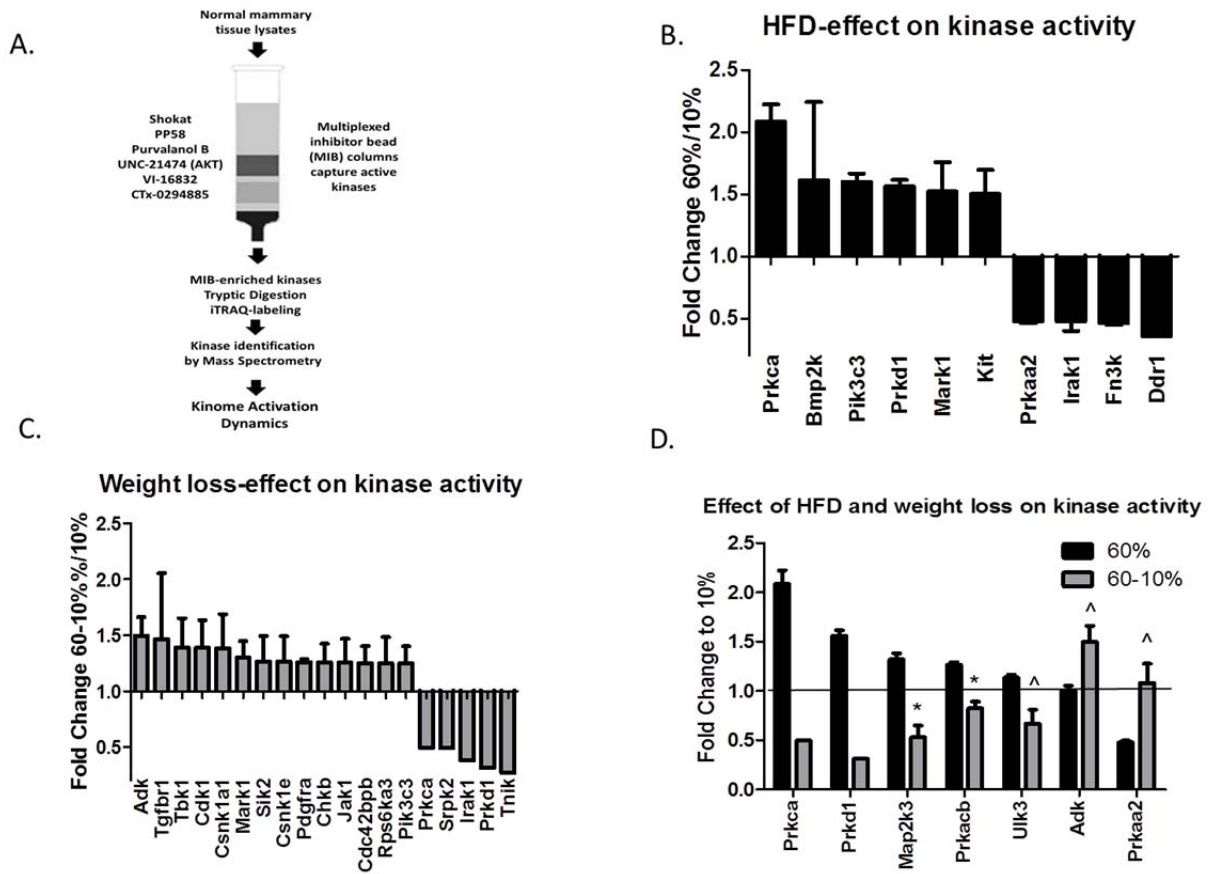
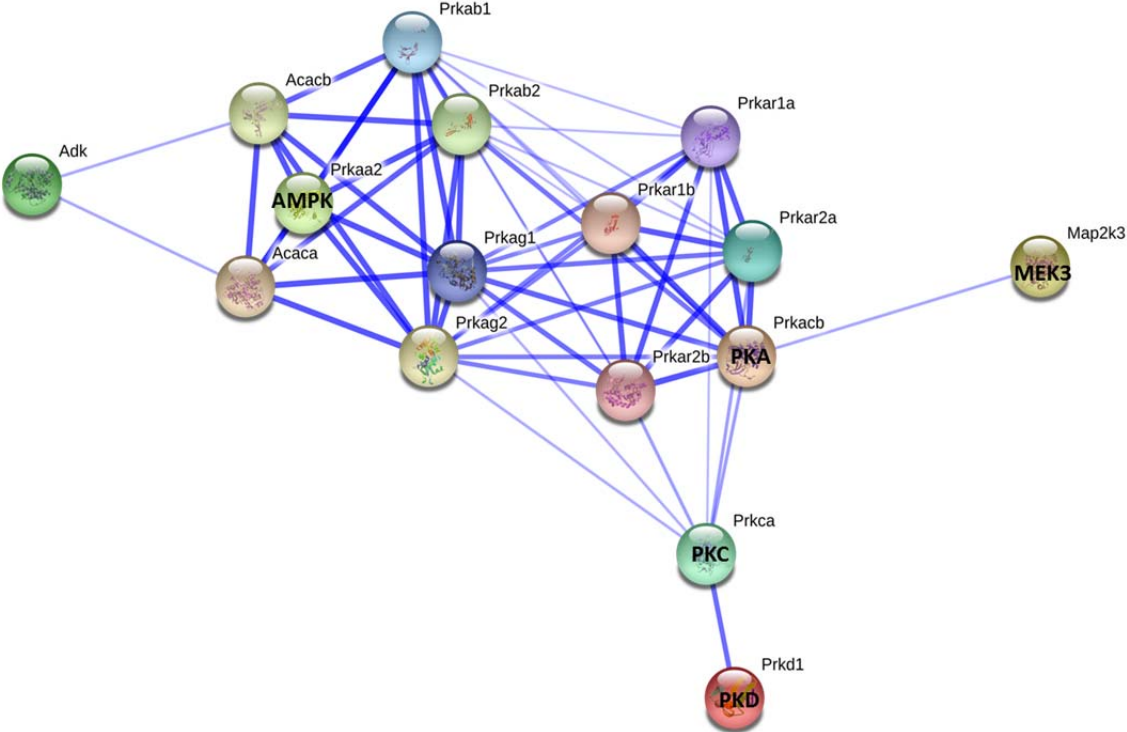


Figure 4.5. Kinome profiling of unaffected mammary glands revealed dramatic regulation of PKD1-PKC- α -PKA-MEK3 by diet exposure. To profile kinome, unaffected mammary glands from mice at 15 weeks of age were collected for Multiplexed Inhibitor Bead (MIB) Affinity Chromatography and Mass spectrometry analysis. A. MIBs consist of mixtures of sepharose beads with covalently immobilized, linker-adapted, broad pan-kinase inhibitors (listed on left of column) are designed to capture kinases in the active state in a reproducible and reliable assay. Two to 4 samples were pooled into a total of 3 runs per diet group. All kinase activity is normalized to 10%-fed controls B. HFD (60%-fed) mammary gland kinase activity of greater than 1.5 or less than 0.5 fold compared to 10%-fed is presented. C. Weight loss (60-10%-fed) mammary gland kinase activity of greater than 1.25 or less than 0.5 fold compared to 10%-fed is presented. D. Mean kinase activity is presented to compare kinases in the unaffected mammary glands that were significantly different between mice in the 60% group and 60-10% group. * $P < 0.005$, $\wedge P < 0.05$, 60% vs. 60-10%) In C and D, no error bar is present in pooled samples when kinases were down-regulated below level of detection and only 1 run detected activity.

Figure 4.6
A.



B.

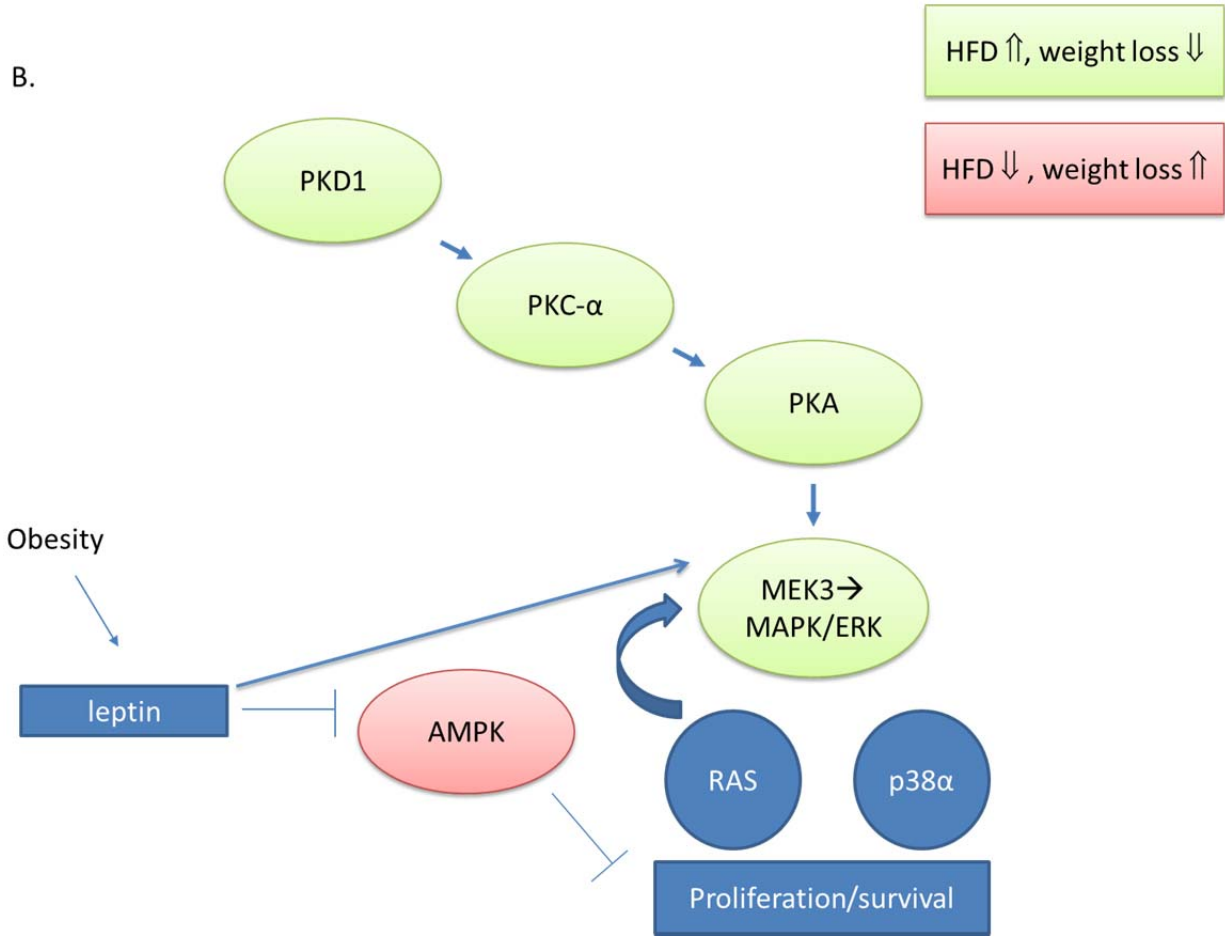


Figure 4.6. Protein-Protein interactions of significantly altered kinases in unaffected mammary gland of mice on 60-10% diet compared to mice on 60% diet. A. Search Tool for the Retrieval of Interacting Genes/Proteins (STRING version 10) was used to visualize known protein-protein interactions between significantly regulated kinases. Confidence view was shown. Stronger associations are represented by thicker lines. B. Cartoon of a subset of kinases regulated by HFD and reversed by weight loss and the contribution of obesity-induced leptin signaling.

Figure 4.7

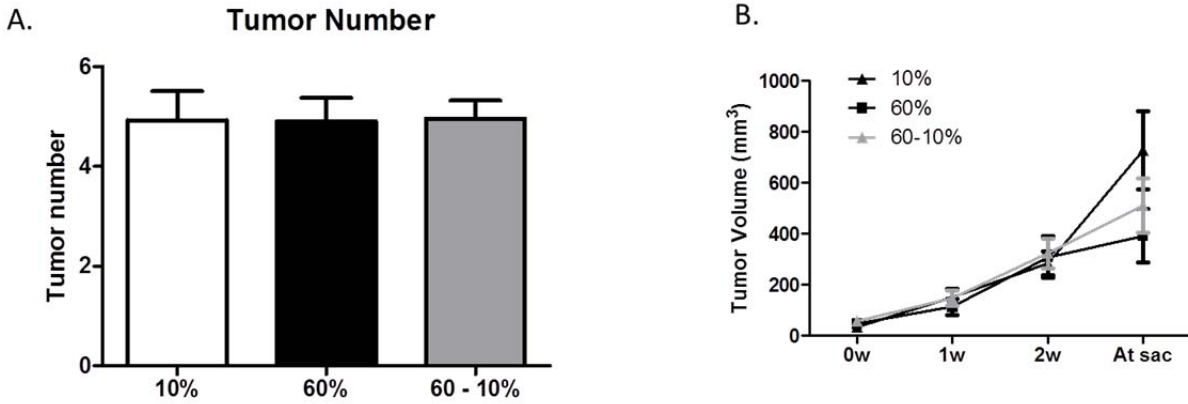


Figure 4.7. Tumor burden and size are not affected by diets. A. Tumor burden was quantified at sacrifice. B&C. Tumor volume was measured by calipers at detection and sacrifice. B. Volume of the primary tumor was detected over 3 weeks. (N=28 10%; N=31 60%; N=29 60-10%).

Figure 4.8

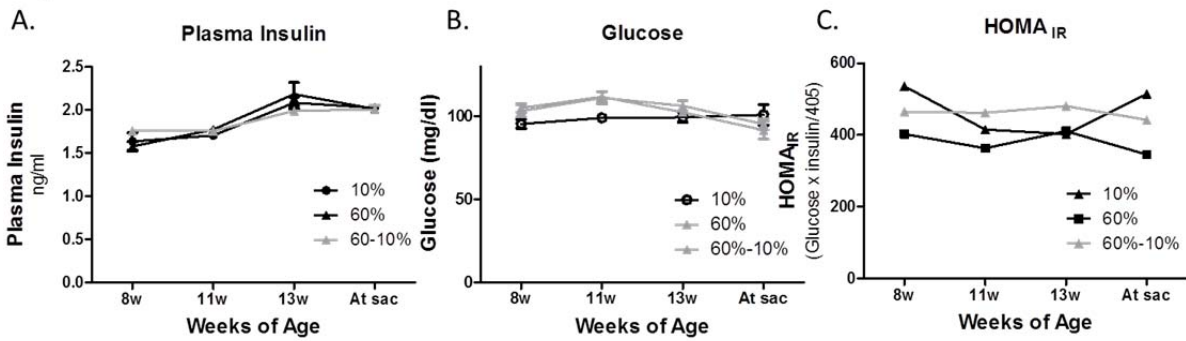
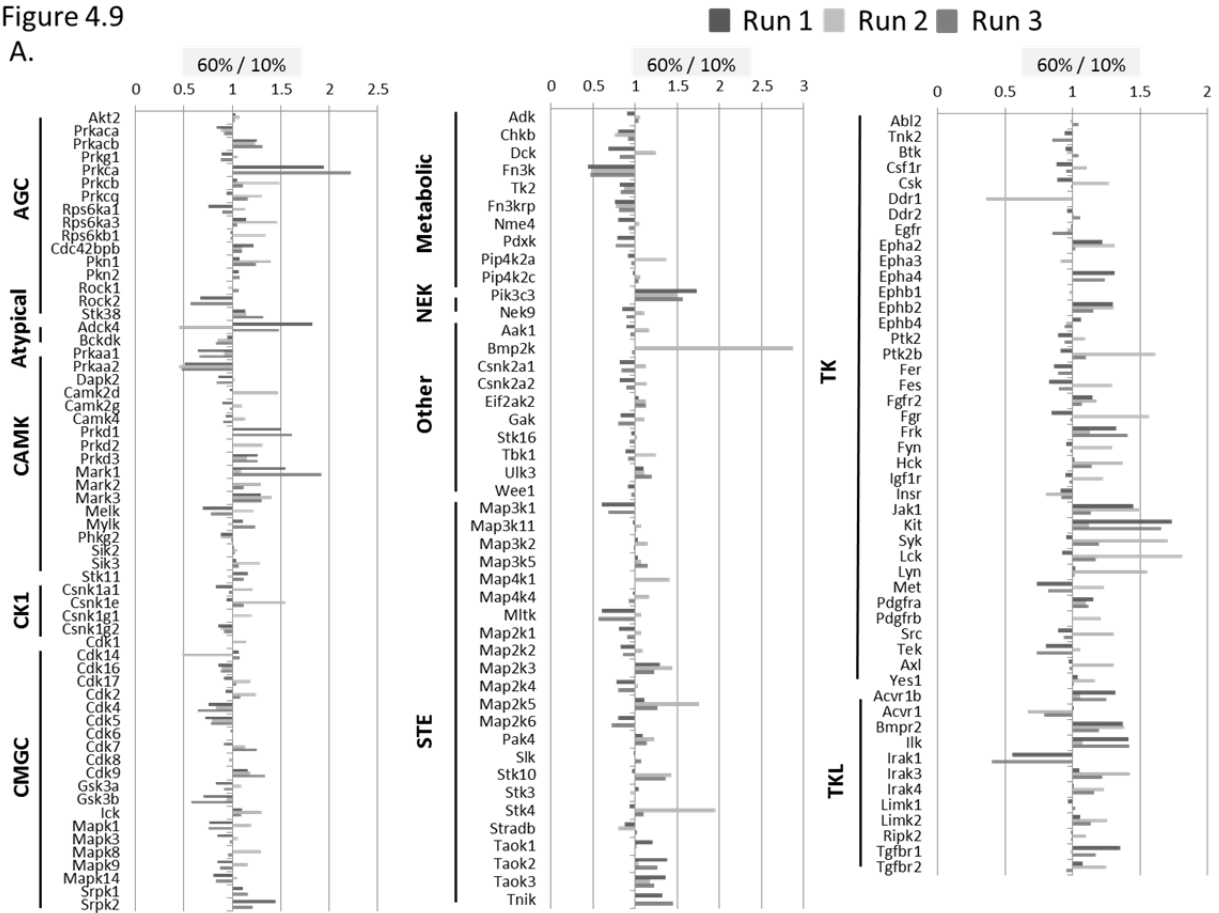
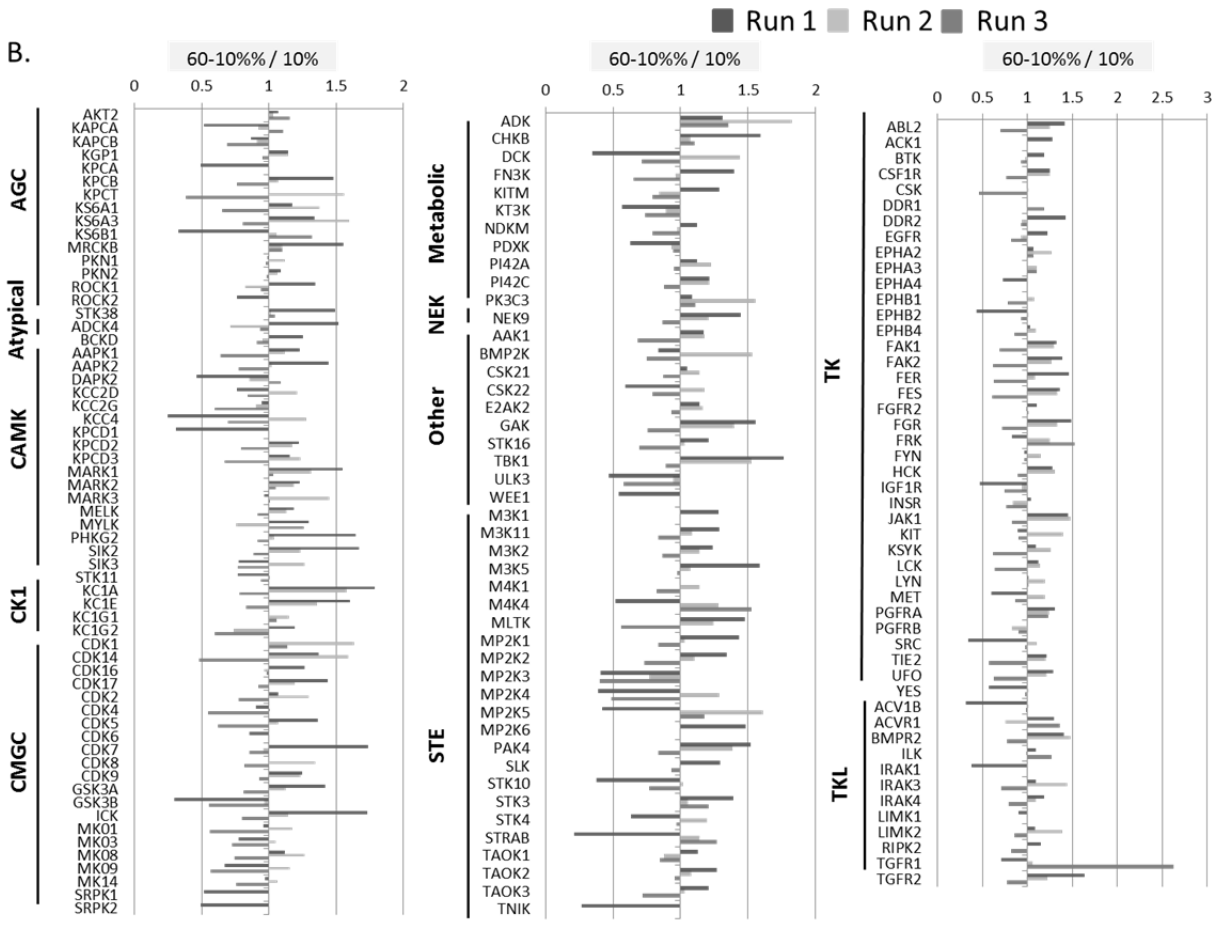


Figure 4.8. Measures of glucose intolerance were not altered by diet. A. Plasma insulin and glucose (B.) levels were measured in 6 h fasted mice at time points indicated. C. Homeostasis model assessment of insulin resistance (HOMA_{IR}) was calculated. (N=12 10%, N=12 60%; N=13 60-10%).

Figure 4.9

A.





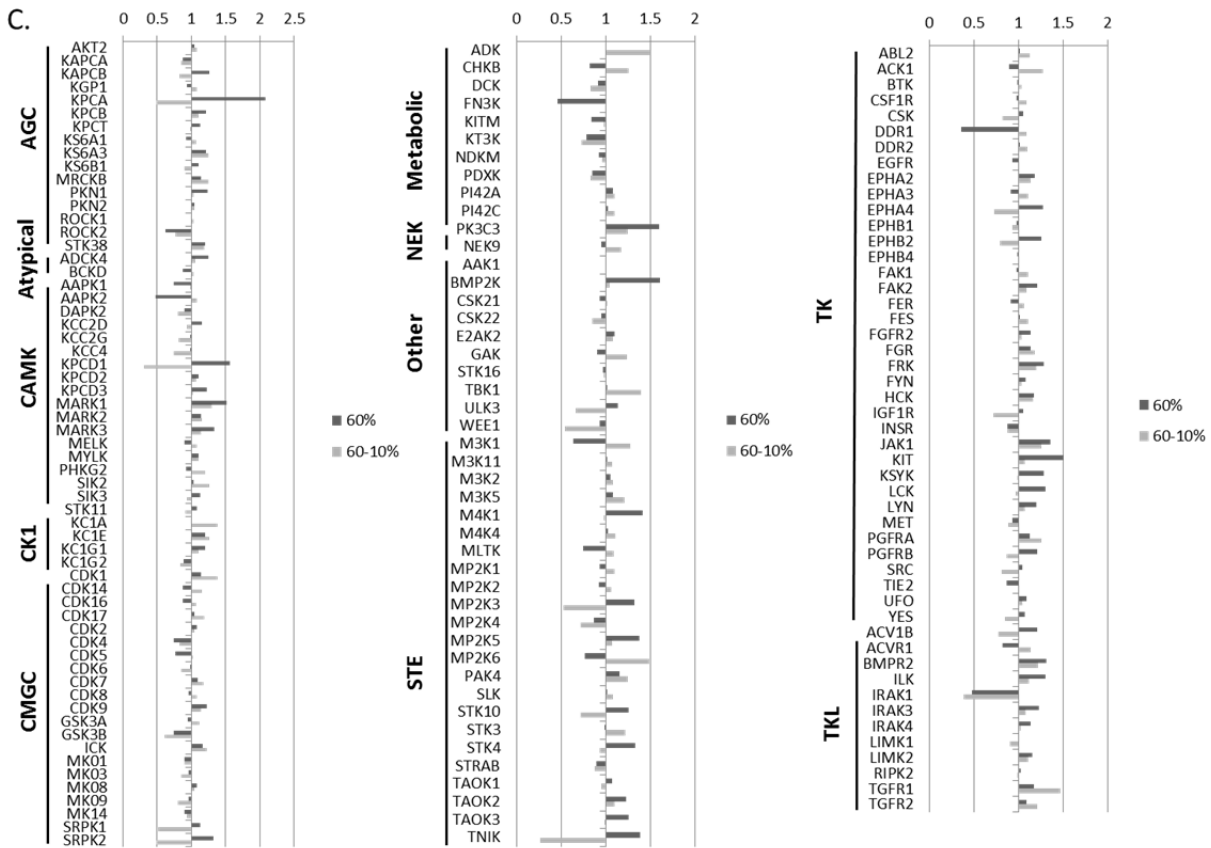


Figure 4.9. Kinome profiling reveals significant regulation of pathways by HFD that are reversed with weight loss. A&B. Quantitative comparison of kinases in unaffected mammary tissues from mice using MIB/MS was conducted. Legend indicates three iTRAQ runs with 2-4 samples pooled per group per run. The graphs indicates quantitative changes in kinase activity as a ratio of mice fed 60% (A) or 60-10% (B) diet relative to mice fed 10% diet group. Ratio <1 denotes decreased kinase activity and >1 increased kinase activity. Kinase families are indicated (AGC: Containing PKA, PKG, PKC families; CAMK: Calcium/calmodulin-dependent protein kinase; CK1: Casein kinase 1; CMGC: Containing CDK, MAPK, GSK3, CLK families; STE: Homologs of yeast Sterile 7, Sterile 11, Sterile 20 kinases; TK: Tyrosine kinase; TKL: Tyrosine kinase-like). C. Mean kinase activity is reported for mice fed 60% diet (dark grey) or 60-10% diet (light grey) compared to mice on 10% diet group. Error bars are not indicated for clarity. Statistically significant comparisons are reported in Figure 4.5D.

Table 4.1. Adiposity predicts BBC latency in C3(1)-Tag mice. Adiposity as determined by MRI of mice from 3 groups were stratified by quartiles. Quartile 1 includes the 25% mice with the lowest adiposity, while quartile 4 has the 25% mice with the highest adiposity.

Adiposity & Latency

<u>Weeks of age (weeks on diet)</u>	<u>Latency (weeks of age)</u>		<u>P VALUE</u>
	<u>Quartile 1</u>	<u>Quartile 4</u>	
8 (0)	17.29	16.35	0.08
11 weeks (3)	18.02	16.65	0.028
13 weeks (5)	17.84	16.50	0.046
15 weeks (7)	17.76	16.37	0.035
At sacrifice (varies)	17.60	16.32	0.012

Table 4.1. Adiposity of all the mice from 3 groups were stratified by quartiles. Quartile 1 includes the 25% mice with the lowest adiposity, while Quartile 4 has the 25% mice with the highest adiposity. Before diet started (8 weeks of age) no difference was found in latency between Quartile 1 and 4. At 11, 13 and 15 weeks of age (i.e. 3, 5, and 7 weeks on diet) and at sacrifice, Quartile 4 had significantly shorter latency compared to Quartile 1 (P=0.028, 0.046, 0.035, 0.012 respectively).

Table 4.2. Mice with higher body weight have shorter latency. Body weight of all the mice from 3 groups were stratified by quartiles. Quartile 1 includes the 25% mice with the lowest bodyweight, while quartile 4 has the 25% mice with the highest body weight.

Body Weight & Latency

	Latency (weeks of age)		
<u>Weeks of age (Weeks on diet)</u>	<u>Quartile 1</u>	<u>Quartile 4</u>	<u>P VALUE</u>
8 (0)	16.65	16.52	0.85
11 weeks (3)	17.05	16.60	0.47
13 weeks (5)	17.59	16.29	0.033
15 weeks (7)	17.75	16.07	0.0074
At sacrifice (varies)	16.59	16.57	0.98

Table 4.2. Body weight of all the mice from 3 groups was stratified by quartiles. Quartile 1 includes the 25% mice with the lowest bodyweight, while Quartile 4 has the 25% mice with the highest body weight. Before diet started (8 weeks of age) no difference was found in latency between Quartile 1 and 4. At 13 and 15 weeks of age (i.e. 5, and 7 weeks on diet), Quartile 4 had significantly shorter latency compared to Quartile 1 (P=0.033, 0.0074 respectively).

Table 4.3. Activated kinases regulated by high fat diet exposure and weight loss induced by diet switch. Proteomic analysis of activated kinases was conducted using MIB and MS/MS in unaffected mammary glands isolated at 15 weeks of age. Mean fold regulation of N=3 runs with 2-4 samples pooled per run. * Less than 3 measures were detectable.

	Kinase Family	Gene	Uniprot	Name	Avg. fold
High fat diet-regulated (> 1.5 and < 0.5)	AGC	<i>Prkca</i>	KPCA	Protein kinase C alpha type	2.09
	Other	<i>Bmp2k</i>	BMP2K	BMP-2-inducible protein kinase	1.61
	Metabolic	<i>Pik3c3</i>	PK3C3	Phosphatidylinositol 3-kinase catalytic subunit type 3	1.60
	CAMK	<i>Prkd1</i>	KPCD1	Serine/threonine-protein kinase D1	1.56
	CAMK	<i>Mark1</i>	MARK1	Serine/threonine-protein kinase MARK1	1.52
	TK	<i>Kit</i>	KIT	Mast/stem cell growth factor receptor Kit	1.50
	CAMK	<i>Prkaa2</i>	AAPK2	5'-AMP-activated protein kinase catalytic subunit alpha-2	0.48
	TKL	<i>Irak1</i>	IRAK1	Interleukin-1 receptor-associated kinase 1	0.48
	Metabolic	<i>Fn3k</i>	FN3K	Fructosamine-3-kinase	0.46
	TK	<i>Ddr1</i>	DDR1	Epithelial discoidin domain-containing receptor 1	0.36*
Weight loss-regulated (> 1.25 and < 0.5)	Metabolic	<i>Adk</i>	ADK	Adenosine kinase	1.50
	TKL	<i>Tgfr1</i>	TGFR1	TGF-beta receptor type-1	1.46
	Other	<i>Tbk1</i>	TBK1	Serine/threonine-protein kinase TBK1	1.39
	CMGC	<i>Cdk1</i>	CDK1	Cyclin-dependent kinase 1	1.39
	CK1	<i>Csnk1a1</i>	KC1A	Casein kinase I isoform alpha	1.38
	CAMK	<i>Mark1</i>	MARK1	Serine/threonine-protein kinase MARK1	1.30
	CAMK	<i>Sik2</i>	SIK2	Serine/threonine-protein kinase SIK2	1.26
	CK1	<i>Csnk1e</i>	KC1E	Casein kinase I isoform epsilon	1.26
	TK	<i>Pdgfra</i>	PGFRA	Platelet-derived growth factor receptor alpha	1.26
	Metabolic	<i>Chkb</i>	CHKB	Choline/ethanolamine kinase	1.26
	TK	<i>Jak1</i>	JAK1	Tyrosine-protein kinase JAK1	1.25
	AGC	<i>Cdc42bpb</i>	MRCKB	Serine/threonine-protein kinase MRCK beta	1.25
	Metabolic	<i>Pik3c3</i>	PK3C3	Serine/threonine-protein kinase	1.25

			MRCK beta	
AGC	<i>Rps6ka3</i>	KS6A3	Ribosomal protein S6 kinase alpha-3	1.25
AGC	<i>Prkca</i>	KPCA	Protein kinase C alpha type	0.49*
CMGC	<i>Srpk2</i>	SRPK2	SRSF protein kinase 2	0.49*
TKL	<i>Irak1</i>	IRAK1	Interleukin-1 receptor-associated kinase 1	0.38*
CAMK	<i>Prkd1</i>	KPCD1	Serine/threonine-protein kinase D1	0.31*
STE	<i>Tnik</i>	TNIK	Traf2 and NCK-interacting protein kinase	0.27*

Table 4.3. Activated kinases regulated by high fat diet exposure and weight loss induced by diet switch. High fat diet (HFD) increased 6 kinases in the unaffected mammary glands to more than a 1.5 fold change when normalized to those of mice on 10% diet. Four kinases were decreased by HFD to less than a 0.5-fold change when normalized to those of mice on 10% diet. Fourteen kinases had a more than 1.25-fold increase in the unaffected mammary glands after weight loss. Five kinases were decreased to less than a 0.5-fold change by weight loss when normalized to those of mice on 10% diet (No error bar here because these kinases were only detected in one run).

Table 4. Activated kinases regulated by weight loss induced by diet switch compared to high fat diet exposure. Proteomic analysis of activated kinases was conducted using MIB and MS/MS in unaffected mammary glands isolated at 15 weeks of age. Mean fold regulation of N=3 runs with 2-4 samples pooled per run. n.d.: Not determined because less than 3 measures were detectable in downregulated kinases.

Kinase Family	Gene	Uniprot	Name	HFD	HFD-LFD	P
AGC	Prkca	KPCA	Protein kinase C alpha type	2.09	0.49	n.d.
CAMK	Prkd1	KPCD1	Serine/threonine-protein kinase D1	1.56	0.31	n.d.
STE	Map2k3	MP2K3	Dual specificity mitogen-activated protein kinase kinase 3	1.32	0.53	0.00
AGC	Prkacb	KAPCB	cAMP-dependent protein kinase catalytic subunit beta	1.27	0.82	0.00
Other	Ulk3	ULK3	Serine/threonine-protein kinase ULK3	1.13	0.66	0.03
TK	Pdgfra	PGFRA	Platelet-derived growth factor receptor alpha	1.12	1.26	0.01
Metabolic	Adk	ADK	Adenosine kinase	1.00	1.50	0.05
CAMK	Prkaa2	AAPK2	5'-AMP-activated protein kinase catalytic subunit alpha-2	0.48	1.08	0.04

Table 4.4. Activated kinases regulated by weight loss induced by diet switch compared to high fat diet exposure. Kinases in the unaffected mammary glands that were significantly different between mice in the 60% group and 60%-10% group (N=2 or 4 samples were pulled together per group for a total protein content of 2.5mg for one run of MIB. N=3 runs).

CHAPTER V: SYNTHESIS

Overview of research findings

We examined the effect of high fat diet and alcohol consumption in the onset and progression of varied disease states to determine how certain exposures altered the microenvironment. We reported for the first time that there is an augmented inflammatory response in adipose tissue after the combined challenge of ethanol and burn injury. Binge drinking not only leads to many forms of injuries, such as increased susceptibility to infection, it also leads to adipose tissue inflammation. Adipose tissue inflammation with macrophage infiltration contributes to insulin resistance in obese individuals. Therefore, the role of adipose tissue inflammation and insulin resistance after alcohol exposure, and especially associated with burn injury, warrants further investigation.

We also focused our research on controlling adipose inflammation through the novel approach of restricting macrophage metabolism with the goal of further understanding effects on inflammation. Data presented herein supports findings that demonstrated that manipulating substrate metabolism by deleting FATP1 in macrophages affected their metabolic and inflammatory phenotype. We reported that macrophage-specific FATP1 plays an important role in controlling overall white adipose mass, as well as macrophage infiltration and inflammation, lipid peroxidation, and NLRP3 inflammasome activation in white adipose. Alteration of the adipose tissue was associated with systematic changes in body weight and glucose tolerance. Therefore, we demonstrated that manipulating macrophage metabolism is a unique approach to

controlling local composition of the adipose microenvironment, which has important effects systemically in diet-induced obesity.

In our third study, data supports the contribution of HFD exposure to the microenvironment and systemic biology associated with the onset of BBC. We demonstrated in a unique mouse model of BBC that HFD-induced changes to body composition and leptin levels, akin to obesity, led to increased tumor aggressiveness, premalignant hyperplasia, and DCIS, as well as elevation of kinases known to be regulated by obesity and novel findings. The reversibility of these obesity-associated effects was demonstrated by a diet switch-induced weight loss that delayed tumor onset, reduced hyperplasia and DCIS, as well as reduced leptin levels in plasma and certain kinases in the mammary gland. Thus, high fat diet-induced changes to the pre-neoplastic microenvironment are not immutable, and demonstrate that weight loss prior to tumor onset could reduce BBC tumor burden.

Through varied disease models exposed to alcohol or high fat diet, we have proved that lifestyle factors contribute to disease onset and progression through alterations to the microenvironment. In other words, the sequence of our genes is like the keys on the piano; it is the context that makes the music.

Direction for Future research

Obesity and alcohol abuse often co-exist, but few studies have investigated their combined deleterious effects on human health. Obesity and alcohol exposures can individually alter immune responses and induce immunosuppression, but their combined effects on systemic inflammation and immune defenses are largely unknown. It has been reported that obese individuals were at a greater risk for mortality/morbidity compared with healthy weight

individuals due to defects in immune regulation during the influenza 2009-2010 pandemic²⁴⁸.

Considering the prevalence of obesity in the US and high rate of emergency events after alcohol consumption⁷, future studies should focus on whether alcohol and obesity-mediated disease processes are synergistic and if they can be controlled by manipulating underlying inflammation. We can test future studies by putting the mice on high fat diet to induce obesity before alcohol consumption and burn as described in our study.

The role of lipid metabolism, especially fatty acids released from adipocytes in obesity²⁴⁹, is poorly understood and necessitates further study. One disadvantage of our study on FATP1 is the effect of radiation associated with BMT on weight gain and adiposity. Mice didn't gain as much weight as those without radiation. The relative reduced amount of adipose tissue caused by radiation may affect the adipokines, blood glucose concentrations, and the inflammatory response. In future studies, macrophage specific FATP1 knockout mice will be created using LysM-cre to further explore the mechanisms of how macrophages contribute to increased white adipose mass and glucose intolerance.

Finally, future work should also focus on the mechanism of how obesity affects activated kinase expression in the microenvironment of mammary glands. The exact signaling pathways of kinases in tumor growth need to be further explored in specific kinase or their receptor knockout murine models or what type of cells. The activation of these kinases in high fat diet exposure may be due to growth factors, inflammatory mediators, or metabolites secreted from cells uniquely regulated in obesity. Since BBC has been characterized by unique epithelial-stroma interactions, the role of cells in the microenvironment of mammary glands, like cancer-associated adipocytes, cancer-associated fibroblasts, and macrophages, on kinase activation associated with carcinogenesis remains to be determined.

Public Health significance

With dramatic increases in obesity worldwide, widespread alcohol consumption, the additive effect of these exposures is an especially significant and urgent global health challenge. About 4% and 7% of new cases of cancer in man and women, respectively, were due to obesity in the US in 2007²⁵⁰. Excess body weight contributes to as many as 1 out of 5 of all cancer-related deaths²⁵¹. A meta-analysis indicated that women who drank about 3 drinks per day had 1.5 times the risk of developing breast cancer as nondrinkers²⁵². The data generated from our study will provide important information about underlying biochemical mechanisms that will inform strategies to provide the most effective treatment strategies for alcohol and obesity-mediated pathology. Furthermore, understanding the metabolism associated with immune cells that contribute to obesity associated dysfunction is central to developing novel therapeutic targets for obesity and related diseases like diabetes.

Considering obesity is a contributing factor in at least half of basal-like breast cancers, this aggressive subtype of breast cancer may be preventable through lifestyle interventions. Given that basal-like breast cancer is most prevalent in young African American women, targeted prevention may help reduce mortality disparities. Our study tested the reversibility of obesity-associated risk using dietary interventions, leading to identification of mechanistically-based strategies for prevention of obesity-associated BBC.

REFERENCES

- 1 Yoon, P. W., Bastian, B., Anderson, R. N., Collins, J. L. & Jaffe, H. W. Potentially preventable deaths from the five leading causes of death--United States, 2008-2010. *MMWR. Morbidity and mortality weekly report* **63**, 369-374 (2014).
- 2 Lichtenstein, P. *et al.* Environmental and heritable factors in the causation of cancer--analyses of cohorts of twins from Sweden, Denmark, and Finland. *The New England journal of medicine* **343**, 78-85, doi:10.1056/NEJM200007133430201 (2000).
- 3 Peto, J. Cancer epidemiology in the last century and the next decade. *Nature* **411**, 390-395, doi:10.1038/35077256 (2001).
- 4 Kolonel, L. N., Altshuler, D. & Henderson, B. E. The multiethnic cohort study: exploring genes, lifestyle and cancer risk. *Nature reviews. Cancer* **4**, 519-527, doi:10.1038/nrc1389 (2004).
- 5 Gonzales, K. *et al.* Alcohol-attributable deaths and years of potential life lost--11 States, 2006-2010. *MMWR. Morbidity and mortality weekly report* **63**, 213-216 (2014).
- 6 MacLeod, J. B. & Hungerford, D. W. Alcohol-related injury visits: do we know the true prevalence in U.S. trauma centres? *Injury* **42**, 922-926 (2011).
- 7 Gentilello, L. M. *et al.* Alcohol interventions in a trauma center as a means of reducing the risk of injury recurrence. *Annals of surgery* **230**, 473-480; discussion 480-473 (1999).
- 8 Albright, J. M., Kovacs, E. J., Gamelli, R. L. & Schermer, C. R. Implications of formal alcohol screening in burn patients. *Journal of burn care & research : official publication of the American Burn Association* **30**, 62-69, doi:10.1097/BCR.0b013e3181921f31 (2009).
- 9 Bird, M. D. & Kovacs, E. J. Organ-specific inflammation following acute ethanol and burn injury. *Journal of leukocyte biology* **84**, 607-613, doi:10.1189/jlb.1107766 (2008).
- 10 Jung, M. K. *et al.* Alcohol exposure and mechanisms of tissue injury and repair. *Alcoholism, clinical and experimental research* **35**, 392-399, doi:10.1111/j.1530-0277.2010.01356.x (2011).
- 11 McGill, V., Kowal-Vern, A., Fisher, S. G., Kahn, S. & Gamelli, R. L. The impact of substance use on mortality and morbidity from thermal injury. *The Journal of trauma* **38**, 931-934 (1995).
- 12 Ogden, C. L., Carroll, M. D. & Flegal, K. M. Prevalence of obesity in the United States. *Jama* **312**, 189-190, doi:10.1001/jama.2014.6228 (2014).
- 13 Sundaram, S., Johnson, A. R. & Makowski, L. Obesity, metabolism and the microenvironment: Links to cancer. *Journal of carcinogenesis* **12**, 19, doi:10.4103/1477-3163.119606 (2013).

- 14 Denis, G. V. & Obin, M. S. 'Metabolically healthy obesity': origins and implications. *Molecular aspects of medicine* **34**, 59-70, doi:10.1016/j.mam.2012.10.004 (2013).
- 15 Xu, H. *et al.* Chronic inflammation in fat plays a crucial role in the development of obesity-related insulin resistance. *The Journal of clinical investigation* **112**, 1821-1830, doi:10.1172/JCI19451 (2003).
- 16 Weisberg, S. P. *et al.* Obesity is associated with macrophage accumulation in adipose tissue. *The Journal of clinical investigation* **112**, 1796-1808, doi:10.1172/JCI19246 (2003).
- 17 Neels, J. G. & Olefsky, J. M. Inflamed fat: what starts the fire? *The Journal of clinical investigation* **116**, 33-35, doi:10.1172/JCI27280 (2006).
- 18 Johnson, A. R., Milner, J. J. & Makowski, L. The inflammation highway: metabolism accelerates inflammatory traffic in obesity. *Immunological reviews* **249**, 218-238, doi:10.1111/j.1600-065X.2012.01151.x (2012).
- 19 Lacy-Hulbert, A. & Moore, K. J. Designer macrophages: oxidative metabolism fuels inflammation repair. *Cell Metab* **4**, 7-8, doi:S1550-4131(06)00204-X [pii] 10.1016/j.cmet.2006.06.001 (2006).
- 20 Vats, D. *et al.* Oxidative metabolism and PGC-1beta attenuate macrophage-mediated inflammation. *Cell Metab* **4**, 13-24 (2006).
- 21 Tannahill, G. M. *et al.* Succinate is an inflammatory signal that induces IL-1beta through HIF-1alpha. *Nature* **496**, 238-242, doi:10.1038/nature11986 (2013).
- 22 Sampey, B. P., Freerman, A.J., Zhang, J., Kuan, P-F., Galanaki, J.A., O'Connell, T.M., Ilkayeva, O.R., Muehlbauer, M.J., Stevens, R.D., Newgard, C.B., Brauer, H.A., Troester, M.A., Makowski, L. Metabolomic Profiling Reveals Mitochondrial-Derived Lipid Biomarkers that Drive Obesity-Associated Inflammation. *PLoS One* **in press** (2012).
- 23 Sampey, B. P. *et al.* Cafeteria diet is a robust model of human metabolic syndrome with liver and adipose inflammation: comparison to high-fat diet. *Obesity (Silver Spring)* **19**, 1109-1117, doi:10.1038/oby.2011.18 (2011).
- 24 Makowski, L. *et al.* Lack of macrophage fatty-acid-binding protein aP2 protects mice deficient in apolipoprotein E against atherosclerosis. *Nat Med* **7**, 699-705 (2001).
- 25 Makowski, L., Brittingham, K. C., Reynolds, J. M., Suttles, J. & Hotamisligil, G. S. The fatty acid-binding protein, aP2, coordinates macrophage cholesterol trafficking and inflammatory activity. Macrophage expression of aP2 impacts peroxisome proliferator-activated receptor gamma and IkappaB kinase activities. *J Biol Chem* **280**, 12888-12895 (2005).
- 26 Makowski, L. & Hotamisligil, G. S. The role of fatty acid binding proteins in metabolic syndrome and atherosclerosis. *Curr Opin Lipidol* **16**, 543-548 (2005).

- 27 Makowski, L. & Hotamisligil, G. S. Fatty acid binding proteins--the evolutionary crossroads of inflammatory and metabolic responses. *J Nutr* **134**, 2464S-2468S (2004).
- 28 Siegel, R. L., Miller, K. D. & Jemal, A. Cancer statistics, 2015. *CA: a cancer journal for clinicians* **65**, 5-29, doi:10.3322/caac.21254 (2015).
- 29 Prat, A. & Perou, C. M. Deconstructing the molecular portraits of breast cancer. *Molecular oncology* **5**, 5-23, doi:10.1016/j.molonc.2010.11.003 (2011).
- 30 Yang, X. R. *et al.* Differences in risk factors for breast cancer molecular subtypes in a population-based study. *Cancer epidemiology, biomarkers & prevention : a publication of the American Association for Cancer Research, cosponsored by the American Society of Preventive Oncology* **16**, 439-443, doi:10.1158/1055-9965.EPI-06-0806 (2007).
- 31 Millikan, R. C. *et al.* Epidemiology of basal-like breast cancer. *Breast cancer research and treatment* **109**, 123-139, doi:10.1007/s10549-007-9632-6 (2008).
- 32 Bissell, M. J., Kenny, P. A. & Radisky, D. C. Microenvironmental regulators of tissue structure and function also regulate tumor induction and progression: the role of extracellular matrix and its degrading enzymes. *Cold Spring Harbor symposia on quantitative biology* **70**, 343-356, doi:10.1101/sqb.2005.70.013 (2005).
- 33 Song, G. *et al.* Effects of tumor microenvironment heterogeneity on nanoparticle disposition and efficacy in breast cancer tumor models. *Clinical cancer research : an official journal of the American Association for Cancer Research* **20**, 6083-6095, doi:10.1158/1078-0432.CCR-14-0493 (2014).
- 34 Mokdad, A. H., Marks, J. S., Stroup, D. F. & Gerberding, J. L. Actual causes of death in the United States, 2000. *Jama* **291**, 1238-1245, doi:10.1001/jama.291.10.1238 (2004).
- 35 Bouchery, E. E., Harwood, H. J., Sacks, J. J., Simon, C. J. & Brewer, R. D. Economic costs of excessive alcohol consumption in the U.S., 2006. *American journal of preventive medicine* **41**, 516-524, doi:10.1016/j.amepre.2011.06.045 (2011).
- 36 Woerle, S., Roeber, J. & Landen, M. G. Prevalence of alcohol dependence among excessive drinkers in New Mexico. *Alcoholism, clinical and experimental research* **31**, 293-298, doi:10.1111/j.1530-0277.2007.00305.x (2007).
- 37 First, M. B. Diagnostic and statistical manual of mental disorders, 5th edition, and clinical utility. *The Journal of nervous and mental disease* **201**, 727-729, doi:10.1097/NMD.0b013e3182a2168a (2013).
- 38 Lieber, C. S. ALCOHOL: its metabolism and interaction with nutrients. *Annual review of nutrition* **20**, 395-430, doi:10.1146/annurev.nutr.20.1.395 (2000).
- 39 Best, C. A. & Laposata, M. Fatty acid ethyl esters: toxic non-oxidative metabolites of ethanol and markers of ethanol intake. *Frontiers in bioscience : a journal and virtual library* **8**, e202-217 (2003).

- 40 Nagy, L. E. Molecular aspects of alcohol metabolism: transcription factors involved in early ethanol-induced liver injury. *Annual review of nutrition* **24**, 55-78, doi:10.1146/annurev.nutr.24.012003.132258 (2004).
- 41 Driscoll, T. R., Harrison, J. A. & Steenkamp, M. Review of the role of alcohol in drowning associated with recreational aquatic activity. *Injury prevention : journal of the International Society for Child and Adolescent Injury Prevention* **10**, 107-113 (2004).
- 42 McDonald, A. J., 3rd, Wang, N. & Camargo, C. A., Jr. US emergency department visits for alcohol-related diseases and injuries between 1992 and 2000. *Archives of internal medicine* **164**, 531-537, doi:10.1001/archinte.164.5.531 (2004).
- 43 Schermer, C. R., Moyers, T. B., Miller, W. R. & Bloomfield, L. A. Trauma center brief interventions for alcohol disorders decrease subsequent driving under the influence arrests. *The Journal of trauma* **60**, 29-34, doi:10.1097/01.ta.0000199420.12322.5d (2006).
- 44 Spies, C. D. *et al.* Intensive care unit stay is prolonged in chronic alcoholic men following tumor resection of the upper digestive tract. *Acta anaesthesiologica Scandinavica* **40**, 649-656 (1996).
- 45 Madan, A. K., Yu, K. & Beech, D. J. Alcohol and drug use in victims of life-threatening trauma. *The Journal of trauma* **47**, 568-571 (1999).
- 46 Jurkovich, G. J. *et al.* The effect of acute alcohol intoxication and chronic alcohol abuse on outcome from trauma. *Jama* **270**, 51-56 (1993).
- 47 Bonab, A. A. *et al.* Effect of simvastatin on burn-induced alterations in tissue specific glucose metabolism: implications for burn associated insulin resistance. *International journal of molecular medicine* **26**, 311-316 (2010).
- 48 Silver, G. M. *et al.* Adverse clinical outcomes associated with elevated blood alcohol levels at the time of burn injury. *Journal of burn care & research : official publication of the American Burn Association* **29**, 784-789, doi:10.1097/BCR.0b013e31818481bc (2008).
- 49 Carter, E. A., Burks, D., Fischman, A. J., White, M. & Tompkins, R. G. Insulin resistance in thermally-injured rats is associated with post-receptor alterations in skeletal muscle, liver and adipose tissue. *International journal of molecular medicine* **14**, 653-658 (2004).
- 50 Cree, M. G. & Wolfe, R. R. Postburn trauma insulin resistance and fat metabolism. *American journal of physiology. Endocrinology and metabolism* **294**, E1-9, doi:10.1152/ajpendo.00562.2007 (2008).
- 51 Marshall, J. C. Inflammation, coagulopathy, and the pathogenesis of multiple organ dysfunction syndrome. *Critical care medicine* **29**, S99-106 (2001).
- 52 Qin, Y. *et al.* Adipose Inflammation and Macrophage Infiltration After Binge Ethanol and Burn Injury. *Alcoholism, clinical and experimental research*, doi:10.1111/acer.12210 (2013).

- 53 Molina, P. E. Alcohol bingeing exacerbates adipose tissue inflammation following burn injury. *Alcoholism, clinical and experimental research* **38**, 33-35, doi:10.1111/acer.12296 (2014).
- 54 <http://www.who.int/mediacentre/factsheets/fs311/en/>.
- 55 Malik, V. S., Willett, W. C. & Hu, F. B. Global obesity: trends, risk factors and policy implications. *Nature reviews. Endocrinology* **9**, 13-27, doi:10.1038/nrendo.2012.199 (2013).
- 56 <http://www.cdc.gov/obesity/data/adult.html>.
- 57 Finkelstein, E. A. *et al.* The lifetime medical cost burden of overweight and obesity: implications for obesity prevention. *Obesity (Silver Spring)* **16**, 1843-1848, doi:10.1038/oby.2008.290 (2008).
- 58 Mosser, D. M. & Edwards, J. P. Exploring the full spectrum of macrophage activation. *Nature reviews. Immunology* **8**, 958-969, doi:10.1038/nri2448 (2008).
- 59 Liu, Y. C., Zou, X. B., Chai, Y. F. & Yao, Y. M. Macrophage polarization in inflammatory diseases. *International journal of biological sciences* **10**, 520-529, doi:10.7150/ijbs.8879 (2014).
- 60 Shi, C. & Pamer, E. G. Monocyte recruitment during infection and inflammation. *Nature reviews. Immunology* **11**, 762-774, doi:10.1038/nri3070 (2011).
- 61 Maciver, N. J. *et al.* Glucose metabolism in lymphocytes is a regulated process with significant effects on immune cell function and survival. *Journal of leukocyte biology* **84**, 949-957 (2008).
- 62 Jacobs, S. R. *et al.* Glucose uptake is limiting in T cell activation and requires CD28-mediated Akt-dependent and independent pathways. *J Immunol* **180**, 4476-4486 (2008).
- 63 Wieman, H. L., Wofford, J. A. & Rathmell, J. C. Cytokine stimulation promotes glucose uptake via phosphatidylinositol-3 kinase/Akt regulation of Glut1 activity and trafficking. *Mol Biol Cell* **18**, 1437-1446, doi:E06-07-0593 [pii] 10.1091/mbc.E06-07-0593 (2007).
- 64 Michalek, R. D. *et al.* Cutting edge: distinct glycolytic and lipid oxidative metabolic programs are essential for effector and regulatory CD4⁺ T cell subsets. *J Immunol* **186**, 3299-3303, doi:jimmunol.1003613 [pii] 10.4049/jimmunol.1003613 (2011).
- 65 Shi, L. Z. *et al.* HIF1alpha-dependent glycolytic pathway orchestrates a metabolic checkpoint for the differentiation of TH17 and Treg cells. *J Exp Med* **208**, 1367-1376, doi:jem.20110278 [pii] 10.1084/jem.20110278 (2011).

- 66 Vander Heiden, M. G., Cantley, L. C. & Thompson, C. B. Understanding the Warburg effect: the metabolic requirements of cell proliferation. *Science* **324**, 1029-1033, doi:10.1126/science.1160809 (2009).
- 67 Kim, J. W. & Dang, C. V. Cancer's molecular sweet tooth and the Warburg effect. *Cancer research* **66**, 8927-8930, doi:10.1158/0008-5472.CAN-06-1501 (2006).
- 68 Lumeng, C. N., Bodzin, J. L. & Saltiel, A. R. Obesity induces a phenotypic switch in adipose tissue macrophage polarization. *The Journal of clinical investigation* **117**, 175-184, doi:10.1172/JCI29881 (2007).
- 69 Odegaard, J. I. & Chawla, A. Alternative macrophage activation and metabolism. *Annual review of pathology* **6**, 275-297, doi:10.1146/annurev-pathol-011110-130138 (2011).
- 70 Schaffer, J. E. & Lodish, H. F. Expression cloning and characterization of a novel adipocyte long chain fatty acid transport protein. *Cell* **79**, 427-436 (1994).
- 71 Hirsch, D., Stahl, A. & Lodish, H. F. A family of fatty acid transporters conserved from mycobacterium to man. *Proceedings of the National Academy of Sciences of the United States of America* **95**, 8625-8629 (1998).
- 72 Pohl, J. *et al.* Fatty acid transporters in plasma membranes of cardiomyocytes in patients with dilated cardiomyopathy. *European journal of medical research* **5**, 438-442 (2000).
- 73 Binnert, C. *et al.* Fatty acid transport protein-1 mRNA expression in skeletal muscle and in adipose tissue in humans. *American journal of physiology. Endocrinology and metabolism* **279**, E1072-1079 (2000).
- 74 Hall, A. M., Smith, A. J. & Bernlohr, D. A. Characterization of the Acyl-CoA synthetase activity of purified murine fatty acid transport protein 1. *J Biol Chem* **278**, 43008-43013, doi:10.1074/jbc.M306575200 (2003).
- 75 Hall, A. M., Wiczler, B. M., Herrmann, T., Stremmel, W. & Bernlohr, D. A. Enzymatic properties of purified murine fatty acid transport protein 4 and analysis of acyl-CoA synthetase activities in tissues from FATP4 null mice. *J Biol Chem* **280**, 11948-11954, doi:10.1074/jbc.M412629200 (2005).
- 76 Stahl, A. *et al.* Identification of the major intestinal fatty acid transport protein. *Molecular cell* **4**, 299-308 (1999).
- 77 Wiczler, B. M. & Bernlohr, D. A. A novel role for fatty acid transport protein 1 in the regulation of tricarboxylic acid cycle and mitochondrial function in 3T3-L1 adipocytes. *Journal of lipid research* **50**, 2502-2513, doi:10.1194/jlr.M900218-JLR200 (2009).
- 78 Xu, N. *et al.* The FATP1-DGAT2 complex facilitates lipid droplet expansion at the ER-lipid droplet interface. *The Journal of cell biology* **198**, 895-911, doi:10.1083/jcb.201201139 (2012).

- 79 Guitart, M. *et al.* FATP1 localizes to mitochondria and enhances pyruvate dehydrogenase activity in skeletal myotubes. *Mitochondrion* **9**, 266-272, doi:10.1016/j.mito.2009.03.007 (2009).
- 80 Stahl, A., Evans, J. G., Pattel, S., Hirsch, D. & Lodish, H. F. Insulin causes fatty acid transport protein translocation and enhanced fatty acid uptake in adipocytes. *Dev Cell* **2**, 477-488, doi:S1534580702001430 [pii] (2002).
- 81 Maeda, N. *et al.* Diet-induced insulin resistance in mice lacking adiponectin/ACRP30. *Nat Med* **8**, 731-737, doi:10.1038/nm724 (2002).
- 82 Memon, R. A., Feingold, K. R., Moser, A. H., Fuller, J. & Grunfeld, C. Regulation of fatty acid transport protein and fatty acid translocase mRNA levels by endotoxin and cytokines. *The American journal of physiology* **274**, E210-217 (1998).
- 83 Frohnert, B. I., Hui, T. Y. & Bernlohr, D. A. Identification of a functional peroxisome proliferator-responsive element in the murine fatty acid transport protein gene. *J Biol Chem* **274**, 3970-3977 (1999).
- 84 Martin, G. *et al.* The human fatty acid transport protein-1 (SLC27A1; FATP-1) cDNA and gene: organization, chromosomal localization, and expression. *Genomics* **66**, 296-304, doi:10.1006/geno.2000.6191 (2000).
- 85 Forman, B. M. *et al.* 15-Deoxy-delta 12, 14-prostaglandin J2 is a ligand for the adipocyte determination factor PPAR gamma. *Cell* **83**, 803-812 (1995).
- 86 Choi, H., Kim, S. J., Park, S. S., Chang, C. & Kim, E. TR4 activates FATP1 gene expression to promote lipid accumulation in 3T3-L1 adipocytes. *FEBS letters* **585**, 2763-2767, doi:10.1016/j.febslet.2011.08.002 (2011).
- 87 Coe, N. R., Smith, A. J., Frohnert, B. I., Watkins, P. A. & Bernlohr, D. A. The fatty acid transport protein (FATP1) is a very long chain acyl-CoA synthetase. *J Biol Chem* **274**, 36300-36304 (1999).
- 88 Wu, Q. *et al.* FATP1 is an insulin-sensitive fatty acid transporter involved in diet-induced obesity. *Mol Cell Biol* **26**, 3455-3467, doi:26/9/3455 [pii] 10.1128/MCB.26.9.3455-3467.2006 (2006).
- 89 Garcia-Martinez, C. *et al.* Impact on fatty acid metabolism and differential localization of FATP1 and FAT/CD36 proteins delivered in cultured human muscle cells. *American journal of physiology. Cell physiology* **288**, C1264-1272, doi:10.1152/ajpcell.00271.2004 (2005).
- 90 Holloway, G. P. *et al.* Increasing skeletal muscle fatty acid transport protein 1 (FATP1) targets fatty acids to oxidation and does not predispose mice to diet-induced insulin resistance. *Diabetologia* **54**, 1457-1467, doi:10.1007/s00125-011-2114-8 (2011).

- 91 Wiczer, B. M., Lobo, S., Machen, G. L., Graves, L. M. & Bernlohr, D. A. FATP1 mediates fatty acid-induced activation of AMPK in 3T3-L1 adipocytes. *Biochemical and biophysical research communications* **387**, 234-238, doi:10.1016/j.bbrc.2009.06.114 (2009).
- 92 Liu, Q., Gauthier, M. S., Sun, L., Ruderman, N. & Lodish, H. Activation of AMP-activated protein kinase signaling pathway by adiponectin and insulin in mouse adipocytes: requirement of acyl-CoA synthetases FATP1 and Acs11 and association with an elevation in AMP/ATP ratio. *FASEB J* **24**, 4229-4239, doi:fj.10-159723 [pii] 10.1096/fj.10-159723 (2010).
- 93 Shashkin, P., Dragulev, B. & Ley, K. Macrophage differentiation to foam cells. *Current pharmaceutical design* **11**, 3061-3072 (2005).
- 94 Siegel, R., Naishadham, D. & Jemal, A. Cancer statistics, 2013. *CA: a cancer journal for clinicians* **63**, 11-30, doi:10.3322/caac.21166 (2013).
- 95 Chugh, R. & Baker, L. Nonepithelial malignancies of the breast. *Oncology (Williston Park)* **18**, 665-673; discussion 673-666 (2004).
- 96 Grenier, J., Delbaldo, C., Zelek, L. & Piedbois, P. [Phyllodes tumors and breast sarcomas: a review]. *Bulletin du cancer* **97**, 1197-1207, doi:10.1684/bdc.2010.1174 (2010).
- 97 Adem, C., Reynolds, C., Ingle, J. N. & Nascimento, A. G. Primary breast sarcoma: clinicopathologic series from the Mayo Clinic and review of the literature. *British journal of cancer* **91**, 237-241, doi:10.1038/sj.bjc.6601920 (2004).
- 98 Morrow, M., Schnitt, S. J. & Norton, L. Current management of lesions associated with an increased risk of breast cancer. *Nature reviews. Clinical oncology*, doi:10.1038/nrclinonc.2015.8 (2015).
- 99 Ottini, L. Male breast cancer: a rare disease that might uncover underlying pathways of breast cancer. *Nature reviews. Cancer* **14**, 643 (2014).
- 100 Hulka, B. S. & Moorman, P. G. Breast cancer: hormones and other risk factors. *Maturitas* **38**, 103-113; discussion 113-106 (2001).
- 101 McPherson, K., Steel, C. M. & Dixon, J. M. ABC of breast diseases. Breast cancer-epidemiology, risk factors, and genetics. *BMJ* **321**, 624-628 (2000).
- 102 Siegel, R., Naishadham, D. & Jemal, A. Cancer statistics, 2012. *CA: a cancer journal for clinicians* **62**, 10-29, doi:10.3322/caac.20138 (2012).
- 103 Perou, C. M. & Borresen-Dale, A. L. Systems biology and genomics of breast cancer. *Cold Spring Harbor perspectives in biology* **3**, doi:10.1101/cshperspect.a003293 (2011).
- 104 Perou, C. M. *et al.* Molecular portraits of human breast tumours. *Nature* **406**, 747-752, doi:10.1038/35021093 (2000).

- 105 Comprehensive molecular portraits of human breast tumours. *Nature* **490**, 61-70, doi:10.1038/nature11412 (2012).
- 106 Prat, A. *et al.* Molecular characterization of basal-like and non-basal-like triple-negative breast cancer. *The oncologist* **18**, 123-133, doi:10.1634/theoncologist.2012-0397 (2013).
- 107 Bastien, R. R. *et al.* PAM50 breast cancer subtyping by RT-qPCR and concordance with standard clinical molecular markers. *BMC medical genomics* **5**, 44, doi:10.1186/1755-8794-5-44 (2012).
- 108 Nielsen, T. O. *et al.* A comparison of PAM50 intrinsic subtyping with immunohistochemistry and clinical prognostic factors in tamoxifen-treated estrogen receptor-positive breast cancer. *Clinical cancer research : an official journal of the American Association for Cancer Research* **16**, 5222-5232, doi:10.1158/1078-0432.CCR-10-1282 (2010).
- 109 Dalgin, G. S. *et al.* Portraits of breast cancer progression. *BMC bioinformatics* **8**, 291, doi:10.1186/1471-2105-8-291 (2007).
- 110 O'Brien, K. M. *et al.* Intrinsic breast tumor subtypes, race, and long-term survival in the Carolina Breast Cancer Study. *Clinical cancer research : an official journal of the American Association for Cancer Research* **16**, 6100-6110, doi:10.1158/1078-0432.CCR-10-1533 (2010).
- 111 Chia, S. K. *et al.* A 50-gene intrinsic subtype classifier for prognosis and prediction of benefit from adjuvant tamoxifen. *Clinical cancer research : an official journal of the American Association for Cancer Research* **18**, 4465-4472, doi:10.1158/1078-0432.CCR-12-0286 (2012).
- 112 Cheang, M. C. *et al.* Responsiveness of intrinsic subtypes to adjuvant anthracycline substitution in the NCIC.CTG MA.5 randomized trial. *Clinical cancer research : an official journal of the American Association for Cancer Research* **18**, 2402-2412, doi:10.1158/1078-0432.CCR-11-2956 (2012).
- 113 Schneider, B. P. *et al.* Triple-negative breast cancer: risk factors to potential targets. *Clinical cancer research : an official journal of the American Association for Cancer Research* **14**, 8010-8018, doi:10.1158/1078-0432.CCR-08-1208 (2008).
- 114 Badve, S. *et al.* Basal-like and triple-negative breast cancers: a critical review with an emphasis on the implications for pathologists and oncologists. *Modern pathology : an official journal of the United States and Canadian Academy of Pathology, Inc* **24**, 157-167, doi:10.1038/modpathol.2010.200 (2011).
- 115 Olopade, O. I. & Grushko, T. Gene-expression profiles in hereditary breast cancer. *The New England journal of medicine* **344**, 2028-2029, doi:10.1056/NEJM200106283442613 (2001).
- 116 Foulkes, W. D. *et al.* Germline BRCA1 mutations and a basal epithelial phenotype in breast cancer. *Journal of the National Cancer Institute* **95**, 1482-1485 (2003).
- 117 Sorlie, T. Molecular portraits of breast cancer: tumour subtypes as distinct disease entities. *Eur J Cancer* **40**, 2667-2675, doi:10.1016/j.ejca.2004.08.021 (2004).

- 118 Richardson, A. L. *et al.* X chromosomal abnormalities in basal-like human breast cancer. *Cancer cell* **9**, 121-132, doi:10.1016/j.ccr.2006.01.013 (2006).
- 119 Sorlie, T. *et al.* Distinct molecular mechanisms underlying clinically relevant subtypes of breast cancer: gene expression analyses across three different platforms. *BMC genomics* **7**, 127, doi:10.1186/1471-2164-7-127 (2006).
- 120 Carey, L. A. *et al.* Race, breast cancer subtypes, and survival in the Carolina Breast Cancer Study. *Jama* **295**, 2492-2502, doi:10.1001/jama.295.21.2492 (2006).
- 121 Gauthier, M. L. *et al.* Abrogated response to cellular stress identifies DCIS associated with subsequent tumor events and defines basal-like breast tumors. *Cancer cell* **12**, 479-491, doi:10.1016/j.ccr.2007.10.017 (2007).
- 122 Herschkowitz, J. I., He, X., Fan, C. & Perou, C. M. The functional loss of the retinoblastoma tumour suppressor is a common event in basal-like and luminal B breast carcinomas. *Breast cancer research : BCR* **10**, R75, doi:10.1186/bcr2142 (2008).
- 123 Whitfield, M. L., George, L. K., Grant, G. D. & Perou, C. M. Common markers of proliferation. *Nature reviews. Cancer* **6**, 99-106, doi:10.1038/nrc1802 (2006).
- 124 Bauer, K. R., Brown, M., Cress, R. D., Parise, C. A. & Caggiano, V. Descriptive analysis of estrogen receptor (ER)-negative, progesterone receptor (PR)-negative, and HER2-negative invasive breast cancer, the so-called triple-negative phenotype: a population-based study from the California cancer Registry. *Cancer* **109**, 1721-1728, doi:10.1002/cncr.22618 (2007).
- 125 Mullan, P. B. & Millikan, R. C. Molecular subtyping of breast cancer: opportunities for new therapeutic approaches. *Cellular and molecular life sciences : CMLS* **64**, 3219-3232, doi:10.1007/s00018-007-7389-z (2007).
- 126 Lund, M. J. *et al.* Race and triple negative threats to breast cancer survival: a population-based study in Atlanta, GA. *Breast cancer research and treatment* **113**, 357-370, doi:10.1007/s10549-008-9926-3 (2009).
- 127 Newman, B. *et al.* The Carolina Breast Cancer Study: integrating population-based epidemiology and molecular biology. *Breast cancer research and treatment* **35**, 51-60 (1995).
- 128 Huo, D. *et al.* Population differences in breast cancer: survey in indigenous African women reveals over-representation of triple-negative breast cancer. *Journal of clinical oncology : official journal of the American Society of Clinical Oncology* **27**, 4515-4521, doi:10.1200/JCO.2008.19.6873 (2009).
- 129 Thorner, A. R. *et al.* In vitro and in vivo analysis of B-Myb in basal-like breast cancer. *Oncogene* **28**, 742-751, doi:10.1038/onc.2008.430 (2009).
- 130 Weinstein, J. N. *et al.* The Cancer Genome Atlas Pan-Cancer analysis project. *Nature genetics* **45**, 1113-1120, doi:10.1038/ng.2764 (2013).

- 131 Kavanaugh, C. & Green, J. E. The use of genetically altered mice for breast cancer prevention studies. *J Nutr* **133**, 2404S-2409S (2003).
- 132 Maroulakou, I. G., Anver, M., Garrett, L. & Green, J. E. Prostate and mammary adenocarcinoma in transgenic mice carrying a rat C3(1) simian virus 40 large tumor antigen fusion gene. *Proceedings of the National Academy of Sciences of the United States of America* **91**, 11236-11240 (1994).
- 133 Green, J. E. *et al.* The C3(1)/SV40 T-antigen transgenic mouse model of mammary cancer: ductal epithelial cell targeting with multistage progression to carcinoma. *Oncogene* **19**, 1020-1027, doi:10.1038/sj.onc.1203280 (2000).
- 134 Sorlie, T. *et al.* Gene expression patterns of breast carcinomas distinguish tumor subclasses with clinical implications. *Proceedings of the National Academy of Sciences of the United States of America* **98**, 10869-10874, doi:10.1073/pnas.191367098 (2001).
- 135 Herschkowitz, J. I. *et al.* Identification of conserved gene expression features between murine mammary carcinoma models and human breast tumors. *Genome biology* **8**, R76, doi:10.1186/gb-2007-8-5-r76 (2007).
- 136 Calle, E. E., Rodriguez, C., Walker-Thurmond, K. & Thun, M. J. Overweight, obesity, and mortality from cancer in a prospectively studied cohort of U.S. adults. *The New England journal of medicine* **348**, 1625-1638, doi:10.1056/NEJMoa021423 (2003).
- 137 Flegal, K. M. & Kalantar-Zadeh, K. Overweight, mortality and survival. *Obesity (Silver Spring)* **21**, 1744-1745, doi:10.1002/oby.20588 (2013).
- 138 Howell, A., Chapman, M. & Harvie, M. Energy restriction for breast cancer prevention. *Recent results in cancer research. Fortschritte der Krebsforschung. Progres dans les recherches sur le cancer* **181**, 97-111 (2009).
- 139 Key, T. J., Verkasalo, P. K. & Banks, E. Epidemiology of breast cancer. *The lancet oncology* **2**, 133-140, doi:10.1016/S1470-2045(00)00254-0 (2001).
- 140 Iwamoto, T. & Pusztai, L. Predicting prognosis of breast cancer with gene signatures: are we lost in a sea of data? *Genome medicine* **2**, 81, doi:10.1186/gm202 (2010).
- 141 Kwan, M. L. *et al.* Epidemiology of breast cancer subtypes in two prospective cohort studies of breast cancer survivors. *Breast cancer research : BCR* **11**, R31, doi:10.1186/bcr2261 (2009).
- 142 Phipps, A. I., Malone, K. E., Porter, P. L., Daling, J. R. & Li, C. I. Body size and risk of luminal, HER2-overexpressing, and triple-negative breast cancer in postmenopausal women. *Cancer epidemiology, biomarkers & prevention : a publication of the American Association for Cancer Research, cosponsored by the American Society of Preventive Oncology* **17**, 2078-2086, doi:10.1158/1055-9965.EPI-08-0206 (2008).

- 143 Toft, D. J. & Cryns, V. L. Minireview: Basal-like breast cancer: from molecular profiles to targeted therapies. *Mol Endocrinol* **25**, 199-211, doi:10.1210/me.2010-0164 (2011).
- 144 Yang, X. R. *et al.* Associations of breast cancer risk factors with tumor subtypes: a pooled analysis from the Breast Cancer Association Consortium studies. *Journal of the National Cancer Institute* **103**, 250-263, doi:10.1093/jnci/djq526 (2011).
- 145 Cleary, M. P. Impact of Obesity on Development and Progression of Mammary Tumors in Preclinical Models of Breast Cancer. *Journal of mammary gland biology and neoplasia*, doi:10.1007/s10911-013-9300-x (2013).
- 146 Dogan, S. *et al.* Effects of high-fat diet and/or body weight on mammary tumor leptin and apoptosis signaling pathways in MMTV-TGF- α mice. *Breast cancer research : BCR* **9**, R91, doi:10.1186/bcr1840 (2007).
- 147 Khalid, S. *et al.* Evidence for a tumor promoting effect of high-fat diet independent of insulin resistance in HER2/Neu mammary carcinogenesis. *Breast cancer research and treatment* **122**, 647-659, doi:10.1007/s10549-009-0586-8 (2010).
- 148 Dunlap, S. M. *et al.* Dietary energy balance modulates epithelial-to-mesenchymal transition and tumor progression in murine claudin-low and basal-like mammary tumor models. *Cancer Prev Res (Phila)* **5**, 930-942, doi:10.1158/1940-6207.CAPR-12-0034 (2012).
- 149 Ford, N. A., Dunlap, S. M., Wheatley, K. E. & Hursting, S. D. Obesity, independent of p53 gene dosage, promotes mammary tumor progression and upregulates the p53 regulator microRNA-504. *PLoS One* **8**, e68089, doi:10.1371/journal.pone.0068089 (2013).
- 150 Sundaram, S. *et al.* Role of HGF in obesity-associated tumorigenesis: C3(1)-T mice as a model for human basal-like breast cancer. *Breast cancer research and treatment*, doi:10.1007/s10549-013-2741-5 (2013).
- 151 http://www.who.int/nutrition/topics/5_population_nutrient/en/index15.html.
- 152 Carpenter, C. L., Ross, R. K., Paganini-Hill, A. & Bernstein, L. Effect of family history, obesity and exercise on breast cancer risk among postmenopausal women. *International journal of cancer. Journal international du cancer* **106**, 96-102, doi:10.1002/ijc.11186 (2003).
- 153 Bernstein, L., Henderson, B. E., Hanisch, R., Sullivan-Halley, J. & Ross, R. K. Physical exercise and reduced risk of breast cancer in young women. *Journal of the National Cancer Institute* **86**, 1403-1408 (1994).
- 154 Huang, Z. *et al.* Dual effects of weight and weight gain on breast cancer risk. *Jama* **278**, 1407-1411 (1997).
- 155 Michels, K. B., Terry, K. L., Eliassen, A. H., Hankinson, S. E. & Willett, W. C. Adult weight change and incidence of premenopausal breast cancer. *International journal of cancer. Journal international du cancer* **130**, 902-909, doi:10.1002/ijc.26069 (2012).

- 156 Harvie, M. *et al.* Association of gain and loss of weight before and after menopause with risk of postmenopausal breast cancer in the Iowa women's health study. *Cancer epidemiology, biomarkers & prevention : a publication of the American Association for Cancer Research, cosponsored by the American Society of Preventive Oncology* **14**, 656-661, doi:10.1158/1055-9965.EPI-04-0001 (2005).
- 157 Pallavi, R., Giorgio, M. & Pelicci, P. G. Insights into the beneficial effect of caloric/dietary restriction for a healthy and prolonged life. *Frontiers in physiology* **3**, 318, doi:10.3389/fphys.2012.00318 (2012).
- 158 Fabian, C. J. *et al.* Favorable modulation of benign breast tissue and serum risk biomarkers is associated with >10 % weight loss in postmenopausal women. *Breast cancer research and treatment* **142**, 119-132, doi:10.1007/s10549-013-2730-8 (2013).
- 159 Colman, R. J. *et al.* Caloric restriction delays disease onset and mortality in rhesus monkeys. *Science* **325**, 201-204, doi:10.1126/science.1173635 (2009).
- 160 Dirx, M. J., Zeegers, M. P., Dagnelie, P. C., van den Bogaard, T. & van den Brandt, P. A. Energy restriction and the risk of spontaneous mammary tumors in mice: a meta-analysis. *International journal of cancer. Journal international du cancer* **106**, 766-770, doi:10.1002/ijc.11277 (2003).
- 161 Pape-Ansorge, K. A., Grande, J. P., Christensen, T. A., Maihle, N. J. & Cleary, M. P. Effect of moderate caloric restriction and/or weight cycling on mammary tumor incidence and latency in MMTV-Neu female mice. *Nutrition and cancer* **44**, 162-168, doi:10.1207/S15327914NC4402_07 (2002).
- 162 Murphy, E. A. *et al.* Benefits of exercise training on breast cancer progression and inflammation in C3(1)SV40Tag mice. *Cytokine* **55**, 274-279, doi:10.1016/j.cyto.2011.04.007 (2011).
- 163 Sundaram, S. *et al.* Obesity-mediated regulation of HGF/c-Met is associated with reduced basal-like breast cancer latency in parous mice. *PLoS One* **9**, e111394, doi:10.1371/journal.pone.0111394 (2014).
- 164 Camp, J. T. *et al.* Interactions with fibroblasts are distinct in Basal-like and luminal breast cancers. *Molecular cancer research : MCR* **9**, 3-13, doi:10.1158/1541-7786.MCR-10-0372 (2011).
- 165 Troester, M. A. *et al.* Activation of host wound responses in breast cancer microenvironment. *Clinical cancer research : an official journal of the American Association for Cancer Research* **15**, 7020-7028, doi:10.1158/1078-0432.CCR-09-1126 (2009).
- 166 Meyers, M. O. *et al.* Impact of breast cancer molecular subtypes on locoregional recurrence in patients treated with neoadjuvant chemotherapy for locally advanced breast cancer. *Annals of surgical oncology* **18**, 2851-2857, doi:10.1245/s10434-011-1665-8 (2011).

- 167 Kyndi, M. *et al.* Estrogen receptor, progesterone receptor, HER-2, and response to postmastectomy radiotherapy in high-risk breast cancer: the Danish Breast Cancer Cooperative Group. *Journal of clinical oncology : official journal of the American Society of Clinical Oncology* **26**, 1419-1426, doi:10.1200/JCO.2007.14.5565 (2008).
- 168 Graveel, C. R. *et al.* Met induces diverse mammary carcinomas in mice and is associated with human basal breast cancer. *Proceedings of the National Academy of Sciences of the United States of America* **106**, 12909-12914, doi:10.1073/pnas.0810403106 (2009).
- 169 Casbas-Hernandez, P. *et al.* Role of HGF in epithelial-stromal cell interactions during progression from benign breast disease to ductal carcinoma in situ. *Breast cancer research : BCR* **15**, R82, doi:10.1186/bcr3476 (2013).
- 170 Xu, K. *et al.* Lunatic fringe deficiency cooperates with the Met/Caveolin gene amplicon to induce basal-like breast cancer. *Cancer cell* **21**, 626-641, doi:10.1016/j.ccr.2012.03.041 (2012).
- 171 Sampey, B. P. *et al.* Metabolomic profiling reveals mitochondrial-derived lipid biomarkers that drive obesity-associated inflammation. *PLoS One* **7**, e38812, doi:10.1371/journal.pone.0038812 (2012).
- 172 Sun, X. *et al.* Normal breast tissue of obese women is enriched for macrophage markers and macrophage-associated gene expression. *Breast cancer research and treatment* **131**, 1003-1012, doi:10.1007/s10549-011-1789-3 (2012).
- 173 Howe, L. R., Subbaramaiah, K., Hudis, C. A. & Dannenberg, A. J. Molecular pathways: adipose inflammation as a mediator of obesity-associated cancer. *Clinical cancer research : an official journal of the American Association for Cancer Research* **19**, 6074-6083, doi:10.1158/1078-0432.CCR-12-2603 (2013).
- 174 Arendt, L. M. *et al.* Obesity promotes breast cancer by CCL2-mediated macrophage recruitment and angiogenesis. *Cancer research* **73**, 6080-6093, doi:10.1158/0008-5472.CAN-13-0926 (2013).
- 175 Bell, L. N. *et al.* Adipose tissue production of hepatocyte growth factor contributes to elevated serum HGF in obesity. *American journal of physiology. Endocrinology and metabolism* **291**, E843-848, doi:10.1152/ajpendo.00174.2006 (2006).
- 176 Coussens, L. M. & Werb, Z. Inflammation and cancer. *Nature* **420**, 860-867, doi:10.1038/nature01322 (2002).
- 177 Zheng, Q. *et al.* Leptin deficiency suppresses MMTV-Wnt-1 mammary tumor growth in obese mice and abrogates tumor initiating cell survival. *Endocrine-related cancer* **18**, 491-503, doi:10.1530/ERC-11-0102 (2011).
- 178 Thorell, A., Nygren, J. & Ljungqvist, O. Insulin resistance: a marker of surgical stress. *Current opinion in clinical nutrition and metabolic care* **2**, 69-78 (1999).

- 179 Marshall, J. C. Complexity, chaos, and incomprehensibility: parsing the biology of critical illness. *Critical care medicine* **28**, 2646-2648 (2000).
- 180 Johnson, A. R., Milner, J.J., Makowski, L. The inflammation highway: metabolism accelerates inflammatory traffic in obesity. *Immunologic Reviews* **249**, 218-238 (2012).
- 181 Faunce, D. E. *et al.* Neutrophil chemokine production in the skin following scald injury. *Burns : journal of the International Society for Burn Injuries* **25**, 403-410 (1999).
- 182 Li, X., Akhtar, S., Kovacs, E. J., Gamelli, R. L. & Choudhry, M. A. Inflammatory response in multiple organs in a mouse model of acute alcohol intoxication and burn injury. *Journal of burn care & research : official publication of the American Burn Association* **32**, 489-497, doi:10.1097/BCR.0b013e3182223c9e (2011).
- 183 Zahs, A. *et al.* Inhibition of Long Myosin Light Chain Kinase Activation Alleviates Intestinal Damage after Binge Ethanol Exposure and Burn Injury. *American journal of physiology. Gastrointestinal and liver physiology*, doi:10.1152/ajpgi.00157.2012 (2012).
- 184 Bird, M. D., Morgan, M. O., Ramirez, L., Yong, S. & Kovacs, E. J. Decreased pulmonary inflammation after ethanol exposure and burn injury in intercellular adhesion molecule-1 knockout mice. *Journal of burn care & research : official publication of the American Burn Association* **31**, 652-660, doi:10.1097/BCR.0b013e3181e4c58c (2010).
- 185 Zahs, A., Bird, M. D., Ramirez, L., Choudhry, M. A. & Kovacs, E. J. Anti-IL-6 Antibody Treatment but Not IL-6 Knockout Improves Intestinal Barrier Function and Reduces Inflammation After Binge Ethanol Exposure and Burn Injury. *Shock* **39**, 373-379, doi:10.1097/SHK.0b013e318289d6c6 (2013).
- 186 Chen, M. M. *et al.* Pulmonary inflammation after ethanol exposure and burn injury is attenuated in the absence of IL-6. *Alcohol* **47**, 223-229, doi:10.1016/j.alcohol.2013.01.004 (2013).
- 187 Zhong, W. *et al.* Chronic Alcohol Exposure Stimulates Adipose Tissue Lipolysis in Mice Role of Reverse Triglyceride Transport in the Pathogenesis of Alcoholic Steatosis. *The American journal of pathology*, doi:10.1016/j.ajpath.2011.11.017 (2012).
- 188 Kang, L. *et al.* Chronic ethanol-induced insulin resistance is associated with macrophage infiltration into adipose tissue and altered expression of adipocytokines. *Alcoholism, clinical and experimental research* **31**, 1581-1588, doi:ACER452 [pii] 10.1111/j.1530-0277.2007.00452.x (2007).
- 189 Bird, M. D. *et al.* Decreased pulmonary inflammation following ethanol and burn injury in mice deficient in TLR4 but not TLR2 signaling. *Alcoholism, clinical and experimental research* **34**, 1733-1741, doi:10.1111/j.1530-0277.2010.01260.x (2010).
- 190 Talukdar, S. *et al.* Neutrophils mediate insulin resistance in mice fed a high-fat diet through secreted elastase. *Nat Med*, doi:10.1038/nm.2885 (2012).

- 191 Nelson, S. & Kolls, J. K. Alcohol, host defence and society. *Nature reviews. Immunology* **2**, 205-209, doi:10.1038/nri744 (2002).
- 192 Thai, A. C., Yeo, P. P. & Cheah, J. S. Hypoglycaemia in diabetes mellitus. *Annals of the Academy of Medicine, Singapore* **14**, 354-359 (1985).
- 193 Biffl, W. L., Moore, E. E., Moore, F. A. & Peterson, V. M. Interleukin-6 in the injured patient. Marker of injury or mediator of inflammation? *Annals of surgery* **224**, 647-664 (1996).
- 194 Xu, A. *et al.* The fat-derived hormone adiponectin alleviates alcoholic and nonalcoholic fatty liver diseases in mice. *The Journal of clinical investigation* **112**, 91-100, doi:10.1172/JCI17797 (2003).
- 195 Sanchez, A. C., Davis, R. L. & Syapin, P. J. The Oct DNA motif participates in the alcohol inhibition of the inducible nitric oxide synthase gene promoter in rat C6 glioma cells. *Brain research* **1179**, 16-27, doi:10.1016/j.brainres.2007.08.047 (2007).
- 196 Oppeltz, R. F., Rani, M., Zhang, Q. & Schwacha, M. G. Gamma delta (gammadelta) T-cells are critical in the up-regulation of inducible nitric oxide synthase at the burn wound site. *Cytokine*, doi:10.1016/j.cyto.2012.07.003 (2012).
- 197 Babcock, G. F., Hernandez, L., Yadav, E., Schwemberger, S. & Dugan, A. The burn wound inflammatory response is influenced by midazolam. *Inflammation* **35**, 259-270, doi:10.1007/s10753-011-9313-9 (2012).
- 198 Elgazar-Carmon, V., Rudich, A., Hadad, N. & Levy, R. Neutrophils transiently infiltrate intra-abdominal fat early in the course of high-fat feeding. *Journal of lipid research* **49**, 1894-1903, doi:M800132-JLR200 [pii] 10.1194/jlr.M800132-JLR200 (2008).
- 199 Milner, J. J. & Beck, M. A. The impact of obesity on the immune response to infection. *The Proceedings of the Nutrition Society*, 1-9, doi:10.1017/S0029665112000158 (2012).
- 200 Rendon, J. L., Li, X., Akhtar, S. & Choudhry, M. A. Interleukin-22 modulates gut epithelial and immune barrier functions following acute alcohol exposure and burn injury. *Shock* **39**, 11-18, doi:10.1097/SHK.0b013e3182749f96 (2013).
- 201 Kavanaugh, M. J. *et al.* Effect of acute alcohol ingestion prior to burn injury on intestinal bacterial growth and barrier function. *Burns : journal of the International Society for Burn Injuries* **31**, 290-296, doi:10.1016/j.burns.2004.09.021 (2005).
- 202 Magnotti, L. J. & Deitch, E. A. Burns, bacterial translocation, gut barrier function, and failure. *The Journal of burn care & rehabilitation* **26**, 383-391 (2005).
- 203 Messingham, K. A., Faunce, D. E. & Kovacs, E. J. Alcohol, injury, and cellular immunity. *Alcohol* **28**, 137-149 (2002).

- 204 Choudhry, M. A. *et al.* Ethanol exacerbates T cell dysfunction after thermal injury. *Alcohol* **21**, 239-243 (2000).
- 205 Messingham, K. A., Fontanilla, C. V., Colantoni, A., Duffner, L. A. & Kovacs, E. J. Cellular immunity after ethanol exposure and burn injury: dose and time dependence. *Alcohol* **22**, 35-44 (2000).
- 206 Faunce, D. E., Gregory, M. S. & Kovacs, E. J. Acute ethanol exposure prior to thermal injury results in decreased T-cell responses mediated in part by increased production of IL-6. *Shock* **10**, 135-140 (1998).
- 207 Turnbaugh, P. J. *et al.* An obesity-associated gut microbiome with increased capacity for energy harvest. *Nature* **444**, 1027-1031, doi:10.1038/nature05414 (2006).
- 208 Shi, H. *et al.* TLR4 links innate immunity and fatty acid-induced insulin resistance. *The Journal of clinical investigation* **116**, 3015-3025, doi:10.1172/JCI28898 (2006).
- 209 Addolorato, G., Capristo, E., Greco, A. V., Stefanini, G. F. & Gasbarrini, G. Energy expenditure, substrate oxidation, and body composition in subjects with chronic alcoholism: new findings from metabolic assessment. *Alcoholism, clinical and experimental research* **21**, 962-967 (1997).
- 210 Yasuhara, S. *et al.* Adipocyte apoptosis after burn injury is associated with altered fat metabolism. *Journal of burn care & research : official publication of the American Burn Association* **27**, 367-376, doi:10.1097/01.BCR.0000216777.94365.47 (2006).
- 211 Duffy, S. L., Lagrone, L., Herndon, D. N. & Mileski, W. J. Resistin and postburn insulin dysfunction. *The Journal of trauma* **66**, 250-254, doi:10.1097/TA.0b013e31815ebad4 (2009).
- 212 Emanuele, N. V. *et al.* Ethanol potentiates the acute fatty infiltration of liver caused by burn injury: prevention by insulin treatment. *Journal of burn care & research : official publication of the American Burn Association* **30**, 482-488, doi:10.1097/BCR.0b013e3181a28df3 (2009).
- 213 Kang, L. & Nagy, L. E. Chronic ethanol feeding suppresses beta-adrenergic receptor-stimulated lipolysis in adipocytes isolated from epididymal fat. *Endocrinology* **147**, 4330-4338, doi:10.1210/en.2006-0120 (2006).
- 214 Shulga, N., Hoek, J. B. & Pastorino, J. G. Elevated PTEN levels account for the increased sensitivity of ethanol-exposed cells to tumor necrosis factor-induced cytotoxicity. *J Biol Chem* **280**, 9416-9424, doi:10.1074/jbc.M409505200 (2005).
- 215 Suganami, T. *et al.* Role of the Toll-like receptor 4/NF-kappaB pathway in saturated fatty acid-induced inflammatory changes in the interaction between adipocytes and macrophages. *Arterioscler Thromb Vasc Biol* **27**, 84-91, doi:01.ATV.0000251608.09329.9a [pii] 10.1161/01.ATV.0000251608.09329.9a (2007).

- 216 Colantoni, A. *et al.* Dose-dependent effect of ethanol on hepatic oxidative stress and interleukin-6 production after burn injury in the mouse. *Alcoholism, clinical and experimental research* **24**, 1443-1448 (2000).
- 217 Emanuele, M. A., Emanuele, N. V., Gamelli, R. L., Kovacs, E. J. & LaPaglia, N. Effects of insulin on hepatic inflammation induced by ethanol and burn injury in a murine model of critical illness. *Journal of burn care & research : official publication of the American Burn Association* **28**, 490-499, doi:10.1097/BCR.0B013E318053DAED (2007).
- 218 Tang, H. *et al.* Ethanol-induced oxidative stress via the CYP2E1 pathway disrupts adiponectin secretion from adipocytes. *Alcoholism, clinical and experimental research* **36**, 214-222, doi:10.1111/j.1530-0277.2011.01607.x (2012).
- 219 Sebastian, B. M. *et al.* Identification of a cytochrome P4502E1/Bid/C1q-dependent axis mediating inflammation in adipose tissue after chronic ethanol feeding to mice. *J Biol Chem* **286**, 35989-35997, doi:10.1074/jbc.M111.254201 (2011).
- 220 Faunce, D. E., Gregory, M. S. & Kovacs, E. J. Effects of acute ethanol exposure on cellular immune responses in a murine model of thermal injury. *Journal of leukocyte biology* **62**, 733-740 (1997).
- 221 Murdoch, E. L., Brown, H. G., Gamelli, R. L. & Kovacs, E. J. Effects of ethanol on pulmonary inflammation in postburn intratracheal infection. *Journal of burn care & research : official publication of the American Burn Association* **29**, 323-330, doi:10.1097/BCR.0b013e3181667599 (2008).
- 222 Freerman, A. J. *et al.* Metabolic reprogramming of macrophages: glucose transporter 1 (GLUT1)-mediated glucose metabolism drives a proinflammatory phenotype. *J Biol Chem* **289**, 7884-7896, doi:10.1074/jbc.M113.522037 (2014).
- 223 Wu, C. *et al.* BioGPS: an extensible and customizable portal for querying and organizing gene annotation resources. *Genome biology* **10**, R130 (2009).
- 224 Wen, H., Miao, E. A. & Ting, J. P. Mechanisms of NOD-like receptor-associated inflammasome activation. *Immunity* **39**, 432-441, doi:10.1016/j.immuni.2013.08.037 (2013).
- 225 Devries-Seimon, T. *et al.* Cholesterol-induced macrophage apoptosis requires ER stress pathways and engagement of the type A scavenger receptor. *The Journal of cell biology* **171**, 61-73, doi:10.1083/jcb.200502078 (2005).
- 226 Chait, A. & Bornfeldt, K. E. Diabetes and atherosclerosis: is there a role for hyperglycemia? *Journal of lipid research* **50 Suppl**, S335-339, doi:10.1194/jlr.R800059-JLR200 (2009).
- 227 Kanter, J. E. *et al.* Diabetes promotes an inflammatory macrophage phenotype and atherosclerosis through acyl-CoA synthetase 1. *Proceedings of the National Academy of Sciences of the United States of America* **109**, E715-724, doi:10.1073/pnas.1111600109 (2012).

- 228 Kim, J. K. *et al.* Inactivation of fatty acid transport protein 1 prevents fat-induced insulin resistance in skeletal muscle. *The Journal of clinical investigation* **113**, 756-763, doi:10.1172/JCI18917 (2004).
- 229 Han, C. Y. *et al.* NADPH Oxidase-derived Reactive Oxygen Species Increases Expression of Monocyte Chemotactic Factor Genes in Cultured Adipocytes. *J Biol Chem* **287**, 10379-10393, doi:10.1074/jbc.M111.304998 (2012).
- 230 Masters, S. L. *et al.* Activation of the NLRP3 inflammasome by islet amyloid polypeptide provides a mechanism for enhanced IL-1beta in type 2 diabetes. *Nature immunology* **11**, 897-904, doi:10.1038/ni.1935 (2010).
- 231 Wen, H., Ting, J. P. & O'Neill, L. A. A role for the NLRP3 inflammasome in metabolic diseases--did Warburg miss inflammation? *Nature immunology* **13**, 352-357, doi:10.1038/ni.2228 (2012).
- 232 Donath, M. Y. Targeting inflammation in the treatment of type 2 diabetes: time to start. *Nature reviews. Drug discovery* **13**, 465-476, doi:10.1038/nrd4275 (2014).
- 233 Boni-Schnetzler, M. & Donath, M. Y. How biologics targeting the IL-1 system are being considered for the treatment of type 2 diabetes. *British journal of clinical pharmacology* **76**, 263-268, doi:10.1111/j.1365-2125.2012.04297.x (2013).
- 234 Hanefeld, M., Pistrosch, F., Koehler, C. & Chiasson, J. L. Conversion of IGT to type 2 diabetes mellitus is associated with incident cases of hypertension: a post-hoc analysis of the STOP-NIDDM trial. *Journal of hypertension* **30**, 1440-1443, doi:10.1097/HJH.0b013e328354663c (2012).
- 235 Stanley, T. L. *et al.* TNF-alpha antagonism with etanercept decreases glucose and increases the proportion of high molecular weight adiponectin in obese subjects with features of the metabolic syndrome. *The Journal of clinical endocrinology and metabolism* **96**, E146-150, doi:10.1210/jc.2010-1170 (2011).
- 236 Solomon, D. H. *et al.* Association between disease-modifying antirheumatic drugs and diabetes risk in patients with rheumatoid arthritis and psoriasis. *Jama* **305**, 2525-2531, doi:10.1001/jama.2011.878 (2011).
- 237 Antohe, J. L. *et al.* Diabetes mellitus risk in rheumatoid arthritis: reduced incidence with anti-tumor necrosis factor alpha therapy. *Arthritis care & research* **64**, 215-221, doi:10.1002/acr.20657 (2012).
- 238 Erbay, E., Cao, H. & Hotamisligil, G. S. Adipocyte/macrophage fatty acid binding proteins in metabolic syndrome. *Curr Atheroscler Rep* **9**, 222-229 (2007).
- 239 Furuhashi, M. *et al.* Treatment of diabetes and atherosclerosis by inhibiting fatty-acid-binding protein aP2. *Nature* **447**, 959-965, doi:10.1038/nature05844 (2007).

- 240 Murphy, A. J. *et al.* ApoE regulates hematopoietic stem cell proliferation, monocytosis, and monocyte accumulation in atherosclerotic lesions in mice. *The Journal of clinical investigation* **121**, 4138-4149, doi:10.1172/JCI57559 (2011).
- 241 Chen, Y. C., Colvin, E. S., Maier, B. F., Mirmira, R. G. & Fueger, P. T. Mitogen-inducible gene 6 triggers apoptosis and exacerbates ER stress-induced beta-cell death. *Mol Endocrinol* **27**, 162-171, doi:10.1210/me.2012-1174 (2013).
- 242 Sundaram, S. *et al.* Role of HGF in obesity-associated tumorigenesis: C3(1)-TAg mice as a model for human basal-like breast cancer. *Breast cancer research and treatment* **142**, 489-503, doi:10.1007/s10549-013-2741-5 (2013).
- 243 Li, L. O. *et al.* Overexpression of rat long chain acyl-coa synthetase 1 alters fatty acid metabolism in rat primary hepatocytes. *J Biol Chem* **281**, 37246-37255, doi:10.1074/jbc.M604427200 (2006).
- 244 Othy, S. *et al.* Effect of IVIg on human dendritic cell-mediated antigen uptake and presentation: role of lipid accumulation. *Journal of autoimmunity* **39**, 168-172, doi:10.1016/j.jaut.2012.05.013 (2012).
- 245 Milner, J. J. *et al.* Diet-induced obese mice exhibit altered heterologous immunity during a secondary 2009 pandemic H1N1 infection. *J Immunol* **191**, 2474-2485, doi:10.4049/jimmunol.1202429 (2013).
- 246 Bhatt, A. P. *et al.* Dysregulation of fatty acid synthesis and glycolysis in non-Hodgkin lymphoma. *Proceedings of the National Academy of Sciences of the United States of America* **109**, 11818-11823, doi:10.1073/pnas.1205995109 (2012).
- 247 Edin, M. L. *et al.* Endothelial expression of human cytochrome P450 epoxygenase CYP2C8 increases susceptibility to ischemia-reperfusion injury in isolated mouse heart. *FASEB J* **25**, 3436-3447, doi:10.1096/fj.11-188300 (2011).
- 248 Milner, J. J. *et al.* Obesity Increases Mortality and Modulates the Lung Metabolome during Pandemic H1N1 Influenza Virus Infection in Mice. *J Immunol* **194**, 4846-4859, doi:10.4049/jimmunol.1402295 (2015).
- 249 Xu, X. *et al.* Obesity activates a program of lysosomal-dependent lipid metabolism in adipose tissue macrophages independently of classic activation. *Cell Metab* **18**, 816-830, doi:10.1016/j.cmet.2013.11.001 (2013).
- 250 <http://www.cancer.gov/about-cancer/causes-prevention/risk/obesity/obesity-fact-sheet#q3>.
- 251 <http://www.cancer.org/cancer/cancercauses/dietandphysicalactivity/bodyweightandcancer/risk/body-weight-and-cancer-risk-effects>.
- 252 Hamajima, N. *et al.* Alcohol, tobacco and breast cancer--collaborative reanalysis of individual data from 53 epidemiological studies, including 58,515 women with breast cancer and

95,067 women without the disease. *British journal of cancer* **87**, 1234-1245,
doi:10.1038/sj.bjc.6600596 (2002).